4

MATHEMATICAL SIMULATION AND EXPERIMENTAL RESEARCH IN CONTINUOUS PROCESSING OF ENERGETICS

Grant No. N00014-89-J-3208, DARPA (ARPA) URI
as managed by ONR

FINAL REPORT

To: Dr. Richard S. Miller, Code 4435
Program Manager
Propulsion and Energetic Materials
Office of Naval Research
800 N. Quincy Street
Arlington, VA 22217

From: Prof. Dilhan M. Kalyon
Highly Filled Materials Institute
Stevens Institute of Technology
Castle Point
Hoboken, NJ 07030

Date: Oct. 27, 1993

TABLE OF CONTENTS

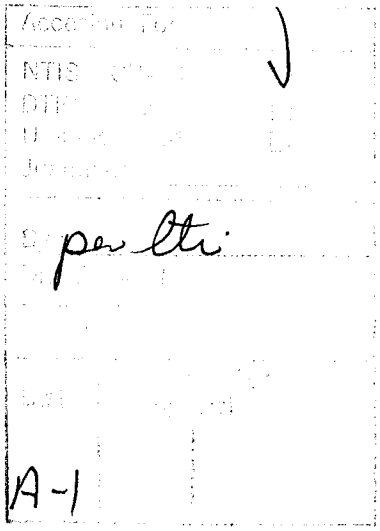

I. INTRODUCTION

In a proposal to DARPA dated March 27, 1989, the following objectives were proposed for research in the field of processing of energetics:

1. To expand the source codes which are being developed for SDIO (BMDO)/IST in the area of co-rotating twin screw extrusion of highly filled suspensions to processing of energetics in other continuous processors including single screw extruders and oscillating shaft continuous kneaders.

2. To expand the source codes which are being developed for SDIO (BMDO)/IST in the area of co-rotating twin screw extrusion to incorporate system components like dies. The simulation is to be relevant to energetic suspensions which are generally viscoplastic.

3. To verify the numerical findings with experimental data.

4. To develop an in-house x-ray based diagnostic technique to determine the mixing state of highly filled suspensions.

As will be shown in the following, the objectives (1-2) were met in conjunction with viscoplastic fluid model (Herschel-Bulkley fluid) and the simulation for single screw extrusion could be verified with experimental data (objective 3). New x-ray techniques were also developed to analyze the degree of mixing distributions to satisfy objective 4.

II. RESULTS

2.1 Simulation of Single Screw Extrusion Process

A non-isothermal model of the single screw extrusion processing of generalized Newtonian fluids was developed. Various temperature dependent forms of generalized Newtonian fluid constitutive equation representing the viscoplastic Herschel-Bulkley fluid and its simplifications including Bingham Plastic, Power law of Ostwald-de Waele and Newtonian fluids are applicable. The model includes the generally ignored transverse convection terms of the equation

of energy. The importance of keeping the transverse convection terms in the analysis is demonstrated by applying the model and comparison of findings to available experimental results involving the transverse flow temperature distributions in single screw extruders. The numerical instabilities, arising principally from the convection terms, generally encountered in high Peclet number extrusion flows, could be eliminated by the use of the Streamline Upwind/Petrov-Galerkin formulation. The model is sufficiently general to accommodate Navier's wall slip at the wall boundary condition commonly encountered during the processing of energetic suspensions.

Complete manuscripts which summarize these results are included in Appendix I.

1. A. Lawal and D. M. Kalyon, "A Non-isothermal Model of Single Screw Extrusion Processing of Viscoplastic Materials Subject to Wall Slip," *Society of Plastics Engineers ANTEC Technical Papers, 38* (1992) 2158-2161.

2. A. Lawal and D. M. Kalyon, "Incorporation of Wall Slip in Non-isothermal Modeling of Single Screw Extrusion Processing," *Proceedings of the First International Conference on Transport Phenomena in Processing,* S. Guceri, ed., Technomic Publ. Co. (1992) 985-996.

3. Z. Ji, A. Gotsis and D. M. Kalyon, "Single Screw Extrusion Processing of Highly Filled Suspensions Including Wall Slip," *Society of Plastics Engineers, ANTEC Technical Papers, 36* (1990) 160-163.

4. A. Lawal and D. M. Kalyon, "A Non-isothermal Model of Single Screw Extrusion of Generalized Newtonian Fluids," accepted for publication in *Numerical Heat Transfer,* December 1992.

2.2 Simulation of Oscillatory Kneaders

The oscillatory kneading flow was simulated in conjunction with the discontinuous cavity flow. Tools of dynamics were applied to this flow in conjunction with Generalized Newtonian Fluids, which are viscoplastic i.e., obey Herschel-Bulkley constitutive equation.

The two-dimensional rectangular-cavity flow generated by either continuous or discontinuous translation of one or two walls is an important model flow in efforts to simulate mixing occurring in all types of continuous processors including oscillatory kneaders. In this numerical study, the role of the viscoplasticity of the General Newtonian Fluids in affecting their mixing behavior in the discontinuous, isothermal and creeping cavity flow is investigated.

To study mixing effectiveness, various tools of dynamics including path line tracking, Poincare´ sections and Lyapunov exponents were employed along with the numerical visualization of the deformations of discrete blobs of passive tracers. The time evolution of the state of mixing represented by the fractional coverage of the cavity area by the passive tracer, and influenced by the development of chaotic mixing regions, is shown to be very different for viscoplastic fluids in comparison to Newtonian and shear thinning fluids. Typical results are shown in Figures 1 and 2, where the pathlines followed by the melt particles in regular motion and the Poincare' section for conditions which lesd into chaotic dynamics and mixing are shown.

2.3 Die Flows

Our source codes, which utilize the Finite Element Method were modified to allow the simulation of die flows. The methods developed allowed the incorporation of the rotation of the screw tip immediately preceding the flow channel. These yet-to-be-published capabilities are very important especially for energetic materials i.e., viscoplastic suspensions which exhibit yield stress. In the enclosed Figure 3 the typical development of the residence time distributions (pathlines followed by melt particles) in a slit die are shown.

Depending on the initial location, some melt particles move at high rates, while others take longer to go through the slit die. The role played by the inclusion of the rotation of the screws is indicated in the helical flow at the entrance to the die. The source code prepared under DARPA (ARPA) funding has already been used in applications in other DoD programs, especially in the design of an on-line rheometer. The U.S. Government has been provided with a non-exclusive license on this invention.

2.4 Development of X-ray Based Diagnostic Techniques to Determine the Mixing State in Highly Filled Suspensions

One of the most challenging aspects of any mixing operation, where two or more identifiable components are brought together, is the characterization of the state of the mixture i.e., the degree of mixedness or the "goodness" of mixing. In the non-diffusive mixing of a viscous polymeric binder with solid components, the complete description of the state of the mixture would require the

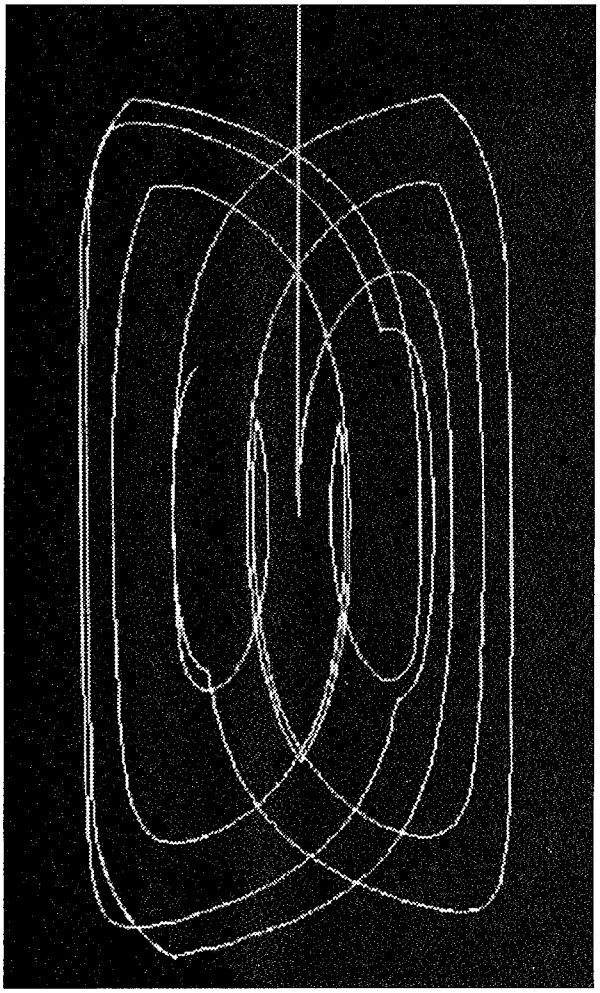

FIG. 1

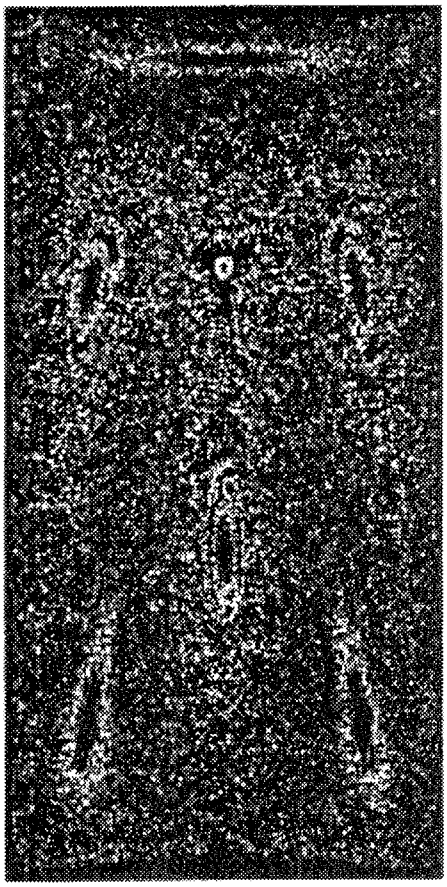

FIG. 2.—Poincaré section of 296 points.

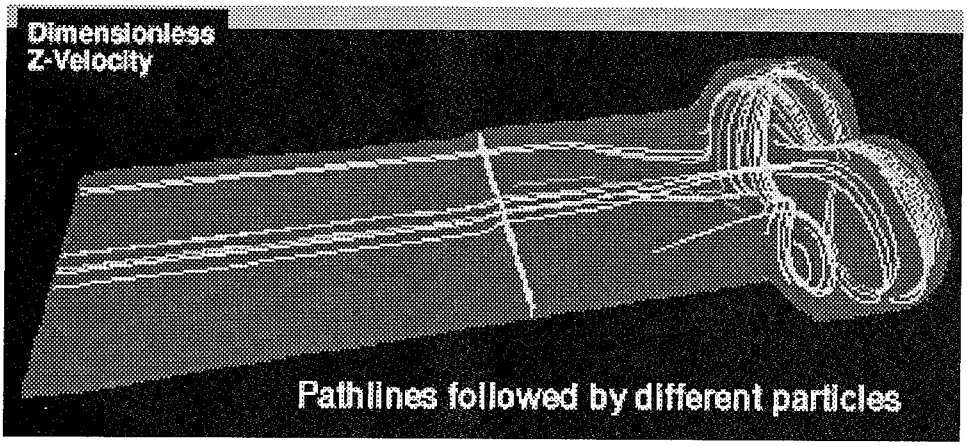

FIG. 3.—The FEM-based source codes developed at SIT include the capabilities to merge modeling of die flows with flow in the twin screw extruder. Here, the velocity distribution and the pathlines followed by different particles close to the entry to the die and at the die are shown.

specification of the sizes, shapes, orientations and the positions of the ultimate particles of the components.

Direct measurement techniques can provide detailed information on the process and the development of the microstructure of the energetic composite. The simplest technique which can be utilized to determine the mechanisms of mixing in a batch or continuous mixer is the injection of a dye into a transparent fluid and then to follow the distribution and the interfacial area growth of the non-diffusive tracer. Such techniques were used earlier to analyze the mixing mechanisms occurring in tangential and partially-full co-rotating twin screw extruders. Ottino and co-workers have employed the flow visualization technique to investigate the mechanisms of mixing in various time dependent flows, which may be governed by chaotic dynamics. On the other hand, White and co-workers have followed the spatial distribution of color incorporated elastomers to gain insight into the mixing occurring in internal mixers. The dispersive mixing aspects, in conjunction with simple shear flows, where the imposed stresses can be monitored, were also characterized employing the cone and plate flow of a transparent oil containing carbon black agglomerates.

If the materials of interest are opaque or if transparent barrel sections cannot be built i.e., as typical for inert suspensions which emulate the behavior of energetic suspensions or for energetic suspensions, the mechanisms of mixing can be studied through "post-mortem" analysis. In this technique, generally a distinguishable tracer is added into a mixer in a step or pulse fashion. Upon a certain duration of mixing the mixture is systematically removed from the mixer and sectioned to allow the investigation of distributive and dispersive mixing aspects. Tadmor and co-workers have used this technique for probing the mechanisms of laminar mixing occurring in co-rotating disk processors and to follow dispersive mixing of rubber and carbon black formulations. Gokbora has utilized pigmented polyethylene granules to investigate the state of mixedness occurring in single screw extrusion processing. Kalyon and co-workers have employed color incorporated thermoplastic elastomers, followed by computerized image analysis, to investigate the distributive mixing of thermoplastic elastomers in the regular flighted and kneading disc elements of twin screw extruders.

On the other hand, the rapid advent of imaging and sensing technology has facilitated the introduction of various powerful techniques, including the magnetic resonance imaging and x-ray based techniques, to the analyses of opaque mixtures. Kalyon, Sinton and co-workers have employed magnetic resonance imaging, wide-angle x-ray diffraction and x-ray radioscopy to characterize the amount of air entrained into composite suspensions with elastomeric binders during extrusion processing, which is related principally to the degree of fill profile in the extruder. In conjunction with our DARPA (ARPA) funding the energy dispersive x-ray and wide angle x-ray diffraction techniques were adapted and developed for the characterization of goodness of mixing in concentrated suspensions.

EXPERIMENTAL PROCEDURES MATERIAL PROCESSING AND SAMPLE PREPARATION

The concentrated suspension of the preliminary demonstration study consisted of a polymeric matrix and 76.5 volume percent of solids. The matrix was hydroxyl terminated polybutadiene (HTPB) i.e., a commonly used binder in energetics. The fillers were aluminum (Al) and ammonium sulfate (AS) in powder form (commonly used simulants for energetics). Ammonium sulfate was bimodal in particle size with seventy five percent coarse particles and twenty-five percent fine particles. The mean particle sizes of the coarse and fine fractions of ammonium sulfate were 200 and 20 microns, respectively. An APV MP50 twin screw extruder with a screw length-to-diameter ratio of 15 was employed for processing of the suspension samples.

CHARACTERIZATION OF MIXING INDICES

Various mixing indices which characterize the goodness of mixing of the suspension samples were determined on the basis of the relative volume-fraction measurements of the two filler materials by three principal analytical methods: scanning electron microscopy (SEM), electron-probe energy-dispersive x-ray analysis (EDX) and wide-angle x-ray diffractometry (XRD). Mixing indices were determined at different scales of examination by varying the sample area through alteration of the size of the electron and x-ray probes by several orders of

magnitude. The ratio of the volume fractions of the two fillers, aluminum (Al) and ammonium sulfate (AS), ϕ_{Al}/ϕ_{AS} , was utilized as a measure of degree mixedness of the sample.

If one makes N measurements of concentration c_i of one of the components, then the mean concentration is

$$\bar{c} = \frac{1}{N} \sum_{i=1}^{N} c_i \qquad (1)$$

where $\bar{c}$ should not differ significantly from ϕ, the overall concentration of the component, unless a faulty sampling technique is used. The difference between $\bar{c}$ and ϕ decreases as the finite number, N, of the characterized samples is increased. The measured concentration values of the minor component also depend on the sample size. These values approach the overall concentration of the minor component ϕ as the sample size is increased.

A basic measure of the homogeneity of a mixture is the extent to which the concentration in various regions of the volume of the mixture differ from the mean concentration. The variance, s^2, arising from the individual concentration, c_i, measurements, provides such an index to quantitatively assess the degree of mixedness. The variance is given by

$$s^2 = \frac{1}{(N-1)} \sum_{i=1}^{N} (c_i - \bar{c})^2 \qquad (2)$$

A small variance value implies that most of the samples yield concentration, c_i values which are close to the mean $\bar{c}$ of all samples, thus suggesting a homogeneous system. The maximum variance occurs if the components are completely segregated. Maximum variance is given by

$$s_o^2 = \bar{c}(1-\bar{c}) \qquad (3)$$

If the variance is normalized to its maximum value the resulting parameter is called the intensity of segregation, I_{seg}. This is given by

$$I_{seg} = \frac{s^2}{s_o^2} = \frac{s^2}{\bar{c}(1-\bar{c})} \qquad (4)$$

Intensity of segregation, I_{seg}, is another important index in evaluating goodness of mixing or distribution. The intensity of segregation ranges from unity, for completely segregated system, to zero, for a homogeneous system.

In the demonstration, the mean, variance and intensity of segregation of the relative concentration fractions of the two fillers, aluminum and ammonium sulfate, ϕ_{Al}/ϕ_{AS}, were determined to assess the goodness of mixing. The overall value of the relative volume concentration fraction of aluminum and ammonium sulfate, ϕ_{Al}/ϕ_{AS}, was 0.20 ± 0.02, as specified during processing.

ANALYTICAL TECHNIQUES

Electron microscopy coupled with energy-dispersive x-ray analysis is a powerful tool in the characterization of microstructure and the corresponding elemental distribution in the multi-phase materialss. Here the two techniques were utilized in synergy to obtain both qualitative and quantitative information on the state of mixedness. First the spatial distribution of the filler particles was determined by secondary-electron microscopic analysis. In order to distinguish the aluminum and ammonium sulfate particles from each other, elemental mappings of aluminum and sulfur were carried out with energy-dispersive x-ray analysis at the same locations, where the secondary-electron images were taken. The identity of each particle in the SEM images was thus determined for further evaluation.

The energy-dispersive x-ray analyzer employs a solid state detector to acquire the total spectrum of characteristic x rays from 0.75 to 20 keV (or more). Large number of x-ray photons can be counted at all energy levels with the aid of a multi-channel analyzer. This allows for the rapid evaluation of numerous elements in the sample. The intensity of the characteristic x-radiation is proportional to the concentration of the particular element in the sampling

volume. Intensity values, therefore, can be utilized for quantitative analysis. In this study the relative atomic fractions of the two elements aluminum and sulfur were measured by energy-dispersive x-ray analysis. Variation of the relative atomic fractions of the two elements was utilized to assess the degree of distributive mixedness. Standard samples were prepared by mixing controlled amounts of aluminum and ammonium sulfate powders in order to calibrate the measured values. According to this calibration the relative atomic fraction proportionality factor $k_{R.at.}$ was 1.21, i.e.,

$$N_{Al} / N_S = 1.21 \quad \phi_{Al}^{at.} / \phi_S^{at.} \tag{5}$$

where $\phi_{Al}^{at.}$ and $\phi_S^{at.}$ refer to the atomic concentrations of aluminum and sulfur. The relative weight fraction and relative volume fraction values for aluminum and ammonium sulfate components were then calculated from the relative atomic fraction of aluminum and sulfur. The conversion factor from relative atomic to relative weight fraction was 4.898 and from relative atomic to relative volume fraction was 7.47. Molecular and crystal structure parameters of the two components were used in determining these conversion factors. Finally, the relative volume fraction proportionality factor $k_{R.vol.}$ was 9.04, i.e.,

$$N_{Al} / N_S = 9.04 \quad \phi_{Al}^{vol} / \phi_{AS}^{vol} \tag{6}$$

Energy-dispersive x-ray measurements were carried-out by using a series of successively smaller probe sizes, at sites chosen systematically, by utilizing a grid system. A JOEL 840 (40Å resolution) scanning electron microscope with Tractor Northern TN 5500 energy-dispersive x-ray analysis system was used in these studies. The window thickness was 7.5 microns. The probe sizes in these experiments were set at 80 mm^2, 9 mm^2, 1 mm^2, 0.1 mm^2 and 0.01 mm^2 to determine the distributive mixing index, i.e., intensity of segregation, as a function of the scale of examination.

X-ray diffractometry has been successfully applied for both qualitative and quantitative phase analysis in multi phase materials. The particular advantage of x-ray diffraction analysis is that it discloses the presence of a substance, as that substance actually exists in the sample, and not in terms of its constituent chemical elements. If the sample contains more than one compound or phase

that constitute the same chemical elements, all these compounds are disclosed by diffraction analysis. Quantitative analysis is also possible, because the intensity of the diffraction pattern of a particular phase in a mixture of phases depends on the concentration of that phase in the mixture. The relation between integrated intensity I_X and volume fraction ϕ_X of a phase is generally nonlinear since diffracted intensity depends strongly on the absorption coefficient of the mixture μ_m, which itself depends on the concentration. For a two-phase material, (that with absorption coefficients μ_1 and μ_2 for the two phases) the absorption coefficient for the mixture becomes:

$$\mu_m = \phi_1\mu_1 + \phi_2\mu_2. \qquad (7)$$

The integrated intensity from phase 1 is then given by:

$$I_1 = K_1\,\phi_1/\mu_m \qquad (8)$$

where K_1 is a constant that depends on the material and incident beam used but not on the concentration. The ratio of intensities from two phases 1 and 2, however, is independent of μ_m and varies linearly with concentration:

$$I_1/I_2 = (K_1/K_2)\,\phi_1/\phi_2 \qquad (9)$$

In this study the ratio relative volume fractions of aluminum and ammonium sulfate, ϕ_{Al}/ϕ_{AS}, was calculated from the integrated intensity ratio, I_{Al}/I_{AS}. These measurements were carried out utilizing particular crystal-planes of the two filler materials. Relatively high number of crystal-plane reflections were evaluated in order to eliminate texture effects and to increase accuracy. Integrated intensities of the first two reflections (111 and 200) of aluminum and the first five reflections (002, 011, 102, 111 and 200) of ammonium sulfate were utilized for calculations. The value of the K_{Al}/K_{AS} constant was taken as 0.489 for (111) planes. This value was calculated according to the $I/I_{corundum}$ values listed by JCPDS. The contribution of the absorption of the matrix to the absorption coefficient of the mixture was less than 3 percent and, thus, it was negligible.

An automated GE wide-angle x-ray diffractometer was used for these studies. Nickel filtered Cu K_α radiation at 30 kV and 15 mA was used. The

scanning speed was one degree per minute. A 0.2 degree receiving slit was used in all runs. The X-ray probe size was varied by using 3 degree and 0.4 degree primary beam slits and a 8mm high window. The X-ray probe sizes used were 20mm x 8mm and 1mm x 8mm, respectively, at a Bragg angle, θ, of 20 degrees.

TYPICAL RESULTS AND DISCUSSION

In order to identify the aluminum and ammonium sulfate particles and to carry-out the quantitative analysis of mixing indices, the elemental mappings of aluminum and sulfur were carried-out using energy-dispersive x-ray analysis at the same locations of the scanning electron micrographs. These elemental mappings are shown in Figures 4b and 4c, respectively. As shown with connecting arrows in Figure 4, EDX technique can identify which particles are ammonium sulfate and which are aluminum.

The results of quantitative energy-dispersive x-ray analysis of the relative volume fractions of aluminum and ammonium sulfate, ϕ_{Al}/ϕ_{AS}, are given in Figure 5. The statistical analysis of the results are listed in Table I. The variance of the relative volume fraction, ϕ_{Al}/ϕ_{AS}, depends on the probe size. The largest probe size, 80 mm^2, as expected, gives rise to the minimum variation in the volumetric ratio. With the moderate probe sizes, which are in the 1 mm^2 to 10 mm^2 range, the variance of the volume ratio remained the same. At the relatively smaller probe sizes of 0.1 mm^2 and 0.01 mm^2, the deviation of the relative volume fraction of the two solid components from the mean increases considerably with decreasing probe size. The marked change in the variance of the relative volume fraction values between probe sizes 0.1 mm^2 to 1 mm^2 is in good agreement with the qualitative microstructural features observed in scanning electron microscopy. Clustering of the particles in 300 to 600 micron diameter regions should give rise to the observed scatter in the energy-dispersive x-ray analysis results. Probes smaller than 0.01 mm^2 in size were not used, as these would be in the same size range as the particle diameter of ammonium sulfate.

The 99% confidence intervals of the energy-dispersive x-ray analysis data determined according to Student's-t-distribution are also included in Table I. The mean of the data for all probe sizes is around 0.215-0.217. These mean values agree with the input volumetric ratio thus suggesting the absence of systematic

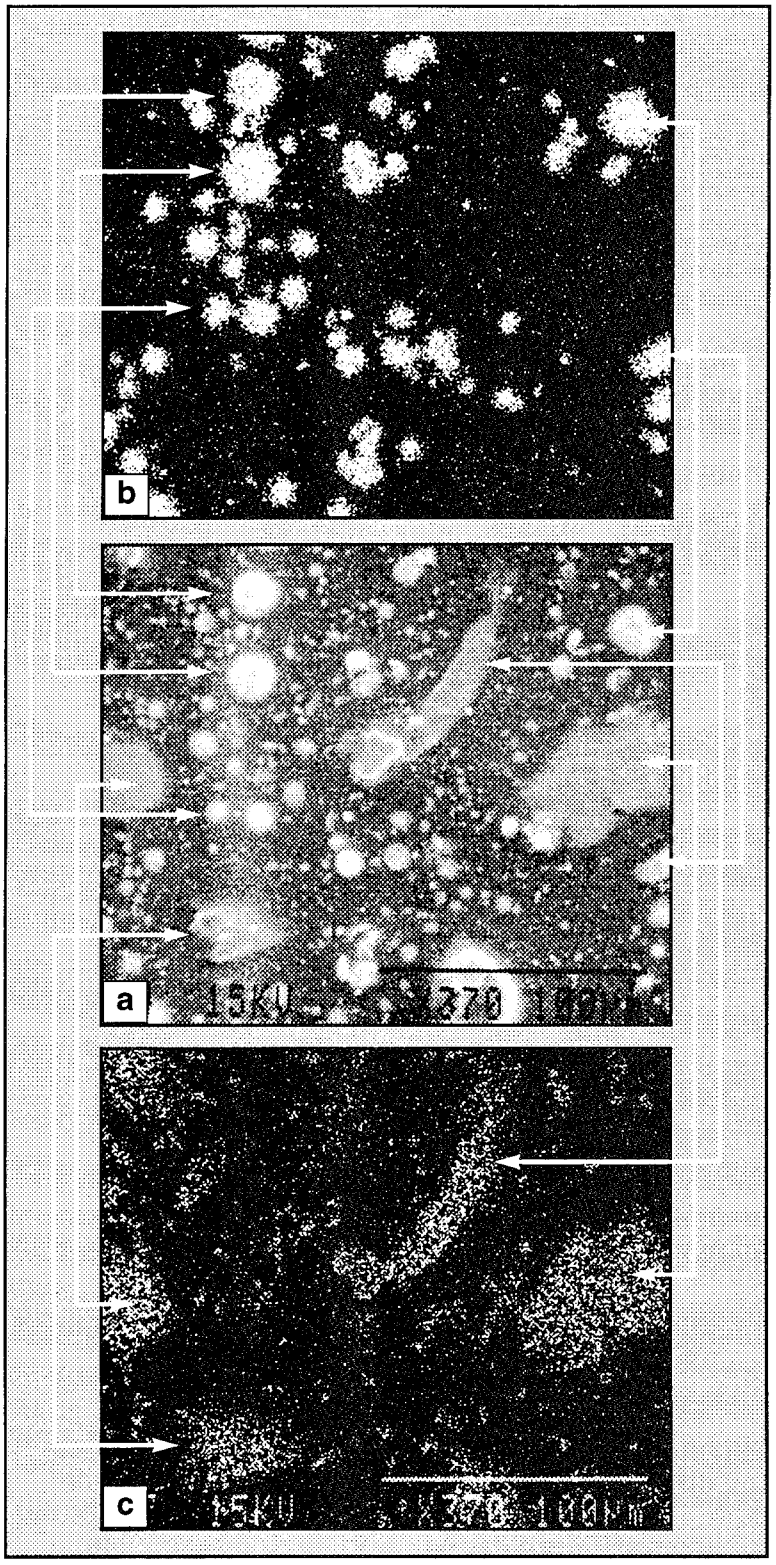

FIG. 4.— Microstructure and the matching elemental mappings of the filled suspension, taken by energy-dispersive x-ray analyzer: (a) scanning electron micrograph at 370X magnification, (b) matching aluminum mapping, (c) matching sulfur mapping.

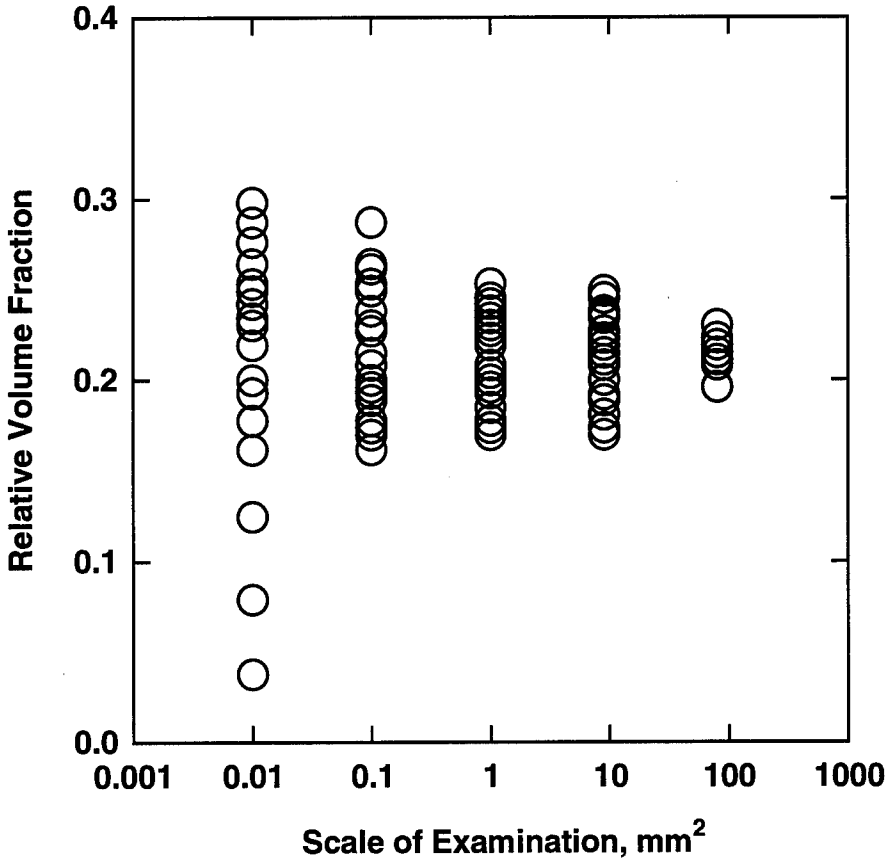

FIG. 5.— Variation of the relative volume fraction of the two solid components, aluminum and ammonium sulfate, at different locations of the mixture as a function of scale of examination of energy-dispersive x-ray analysis.

TABLE I

STATISTICAL PARAMETERS OF THE RELATIVE VOLUME FRACTIONS, Φ_{Al}/Φ_{AS}, FOR DIFFERENT EDX PROBE SIZES

Relative volume fraction, Φ_{Al}/Φ_{AS}, parameters	EDX Probe Size				
	80 mm^2	9 mm^2	1 mm^2	0.1 mm^2	0.01 mm^2
mean	0.216	0.215	0.217	0.217	0.216
standard deviation	0.007	0.024	0.025	0.034	0.069
99% confidence interval	±0.005	±0.014	±0.013	±0.018	±0.039
intensity of segregation	0.0003	0.0034	0.0037	0.0068	0.0281

errors. On the other hand, the standard deviation values increase from 0.007 at the probe size of 80 mm^2 to 0.07 at a probe size of 0.01 mm^2, indicating that the deviation from the mean increases by about one order of magnitude with the decrease in the probe size. The confidence intervals again reflect the same observation, with an increasing range around the mean as the probe size is reduced. Obviously, if the probe size were reduced further, one would probe only completely segregated regions, which would consist of either the aluminum or ammonium sulfate single particles. Which probe size (scale of examination) should be used for the characterization of the goodness of a given energetic mixture? The scale of examination should be selected depending on the application and the relevant ultimate properties of the mixture. For some applications in energetics the sample area may be as large or larger than the maximum probe size used in this analysis, i.e., 80 mm^2. However, for other applications it may be necessary to achieve a certain degree of mixedness at a smaller scale of examination.

The results of the quantitative x-ray diffraction analysis of relative volume fractions of aluminum and ammonium sulfate, by employing the relative integrated intensities, are given in Figure 6. The statistical analysis of the results are presented in Table II. With x-ray diffractometry, the mean of the relative volume fraction of aluminum in the solids, ϕ_{Al}/ϕ_{AS}, was determined as 0.216. The analysis was carried down to a probe size of 8 mm^2. Determination of the relative integrated intensity, I_{Al}/I_{AS}, values at smaller probe sizes was found to be complicated by the preferred crystallographic orientation exhibited by the ammonium sulfate particles. This preferred orientation was especially evident with 002, 200, or 202 planes. As seen in Figure 4, the ammonium sulfate particles exhibit relatively flat and angular surfaces, which can be preferentially oriented during processing. Since the samples are taken from random locations and at random orientations from the extruded suspension, a variety of preferred orientation characteristics were observed during x-ray diffractometry.

The x-ray diffractometry analysis also indicates that the various values of deviation from the mean increase with decreasing scale of examination. However, there are differences between the wide angle x-ray diffraction and energy-dispersive x-ray analysis data that emanate from the applicable depth of penetration. The electron beam used in energy-dispersive x-ray analysis is

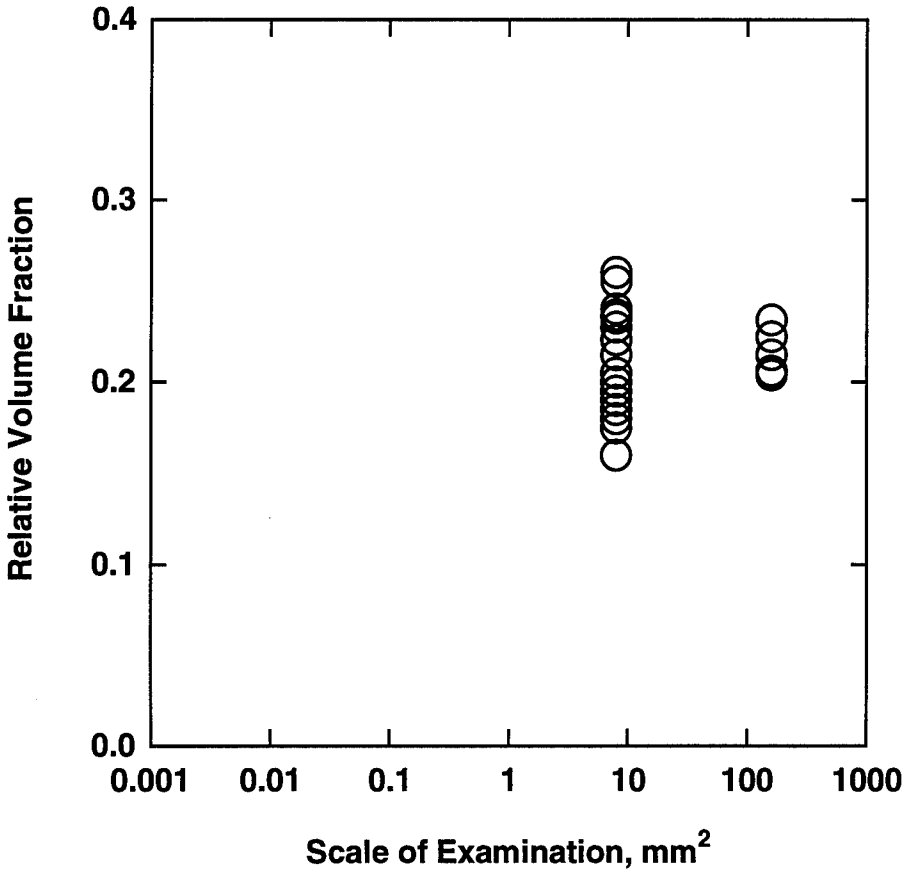

FIG. 6.— Variation of the relative volume fraction of the two solid components, aluminum and ammonium sulfate, at different locations of the mixture as a function of scale of examination of x-ray diffractometry.

TABLE II

STATISTICAL PARAMETERS OF THE RELATIVE VOLUME FRACTIONS, Φ_{Al}/Φ_{AS}, FOR DIFFERENT XRD PROBE SIZES

Relative volume fraction, Φ_{Al}/Φ_{AS}, parameters	XRD Probe Size	
	160 mm^2	8 mm^2
mean	0.216	0.216
standard deviation	0.012	0.029
99% confidence interval	±0.012	±0.017
intensity of segregation	0.0009	0.0050

strongly absorbed at the surface and the x-ray photons that make it to the detector come mostly from the top few microns depth. This depth is smaller than the particle sizes of both solid components of the formulation. However, in the wide-angle x-ray diffraction measurements 95% of the information is derived from the top 50 to 100 microns of the suspension, depending on the filler type and the diffraction angle θ. The penetration depth can be estimated from:

$$x = 3\sin\theta / 2\mu_m \qquad (10)$$

The penetration depth obtained with the x-ray diffraction technique is greater than the electron probe measurements and, thus, x-ray diffraction results are more representative of the bulk.

The intensity of segregation index, I_{seg}, values were determined from the energy-dispersive x-ray and x-ray diffractometry data, as shown in Tables I and II. The intensity of segregation values increase with the decreasing scale of examination in both techniques. The intensity values obtained with energy-dispersive x-ray analysis and x-ray diffraction are close, indicating that both techniques are capable of characterizing the degree of distributive mixedness of the solid ingredients, thus fulfilling the objective of our DARPA proposal.

A comprehensive manuscript which summarizes the results (R. Yazici and D. M. Kalyon, "Degree of Mixing Analyses of Concentrated Suspensions by Electron Probe and X-Ray Diffraction," accepted for publication in *Rubber Chem. and Techn.,* October 1992) is included in the Appendix .

CONCLUSION & ACKNOWLEDGMENTS

The URI funding allowed us to expand our simulation capabilities for continuous processors other than twin screw extruders and dies. Furthermore, the x-ray diffraction and energy-dispersive x-ray based techniques allowed us to develop quantitative techniques for the characterization of the degree of distributive mixing of concentrated suspensions including energetics, which had never been done before. The developed techniques will be used for DoD programs to analyze energetic samples during 1994. Furthermore, a significant probability

exists for the transfer of some of the characterization capabilities to the commercial sector also.

We are grateful to DARPA (ARPA) for this support which made our research in these areas possible and the continuing diligent guidance and encouragement of our Program Director, Dr. Richard S. Miller, of ONR.

APPENDIX

1. A. Lawal and D. M. Kalyon, "A Non-isothermal Model of Single Screw Extrusion Processing of Viscoplastic Materials Subject to Wall Slip," *Society of Plastics Engineers ANTEC Technical Papers, 38* (1992) 2158-2161.

2. A. Lawal and D. M. Kalyon, "Incorporation of Wall Slip in Non-isothermal Modeling of Single Screw Extrusion Processing," *Proceedings of the First International Conference on Transport Phenomena in Processing,* S. Guceri, ed., Technomic Publ. Co. (1992) 985-996.

3. Z. Ji, A. Gotsis and D. M. Kalyon, "Single Screw Extrusion Processing of Highly Filled Suspensions Including Wall Slip," *Society of Plastics Engineers, ANTEC Technical Papers, 36* (1990) 160-163.

4. A. Lawal and D. M. Kalyon, "A Non-isothermal Model of Single Screw Extrusion of Generalized Newtonian Fluids," accepted for publication in *Numerical Heat Transfer,* December 1992.

5. R. Yazici and D. M. Kalyon, "Degree of Mixing Analyses of Concentrated Suspensions by Electron Probe and X-Ray Diffraction," accepted for publication in *Rubber Chem. and Techn.,* October 1992)

Single Screw Extrusion Processing of Highly Filled Suspensions Including Wall Slip

Z. JI, A. D. GOTSIS, AND D. M. KALYON
Stevens Institute of Technology
Department of Chemistry and Chemical Engineering
Highly Filled Materials Institute
Castle Point
Hoboken, NJ 07030

1. INTRODUCTION

The single screw extruder is one of the most widely used machines in the plastics processing. In addition to its obvious solid conveying, melting and pressurization functions, it is also used for more specialized tasks involved in mixing or compounding [1-4]. The aim of the present study is to gain some fundamental insight into the dynamics of the flow during the mixing of suspensions in extruders. There are two complications arising from this specific flow problem. The first is connected to the solution of the set of differential equations that describe the problem in the complicated geometry of the extruders. The second complication is connected to the rheological behavior of the material. Since the morphology of the suspension changes during continuous mixing, the rheological behavior of the material also changes [5]. It is thus necessary to implement a shear viscosity that depends on the extent of mixing. Furthermore, highly filled suspensions have been found to slip at the walls of capillary and rotational rheometers [6]. The customary no-slip boundary conditions, thus, may not be used in the simulation of flows involving these materials. In fact the slip induced flow can become the dominant mode of flow under certain stress levels [6], to the degree that the true rheological behavior of the material becomes obscured.

Slip conditions have been used previously, as a numerical convenience, mostly in attempts to reduce mathematical singularities around the corners and in extrudate swell problems in conjunction with FEM and viscoelastic models [7,8]. Slip in pressure and drag induced isothermal flows of Newtonian fluids in single screw extruders was studied in [9] using simple 1-D and 2-D models and simplified analytical expressions. In the present paper, complicated 2-D problems are considered, for which no analytical solutions are available.

1.1 Slip at the Wall

The slip behavior of a suspension at the solid walls is characterized in terms of a "slip velocity". It is defined as the difference between the velocity of the solid wall surface (V_0) and the velocity of the layer of the fluid adjacent to the wall (u). The slip velocity is generally found to be proportional to the wall shear stress (τ_w) [6], as also found in the microstructural studies of solutions of dumb-bell models [7]. In general, the slip velocity can be given by [6]:

$$u_s = V_0 - u = \alpha(\tau_w - \tau_{cw})^m \tag{1}$$

where m is generally close to 1 and τ_{cw} is the value of the shear rate below which no slip occurs.

1.2 Constitutive Equation

A viscoplastic generalized Newtonian model with plastic viscosity η_0 and yield stress τ_y was used in this study. The viscosity function is given as [10]:

$$\eta = \eta_0 + \tau_y \frac{1 - \exp(-n\dot{\gamma})}{\dot{\gamma}} \tag{2}$$

where the viscosity coefficient η_0 depends on the specific energy input, according to the following equation:

$$\eta_0 = \frac{\eta_\infty}{[1-\exp(-\beta E_s)]} \tag{3}$$

and the specific energy input satisfies [11]:

$$\frac{DE_s}{Dt} = u_x\frac{\partial E_s}{\partial x} + u_y\frac{\partial E_s}{\partial y} + u_z\frac{\partial E_s}{\partial z} = \frac{1}{\rho}|\dot{\gamma}|\,|\tau| \tag{4}$$

where ρ is the density, $|\dot{\gamma}|$ is the second invariant of the strain rate, and $|\tau|$ is the second invariant of the stress.

The parameters η_0 and τ_y are also allowed to change with temperature with an Arrhenius type of relationship:

$$\eta_0(T) = \eta_0(T_0)\exp[-\beta'_T(T-T_0)]$$
$$\tau_y(T) = \tau_y(T_0)\exp[-\beta''_T(T-T_0)] \tag{5}$$

where T_0 is a reference temperature and β'_T and β''_T are material parameters.

2. THE FINITE ELEMENT MODEL OF SINGLE SCREW EXTRUSION

The treatment and the assumptions of the classical theory of single screw extruders [1-4] was used in the present article. In this theory, the channel-like domains that are formed between the screw and the barrel may be unwound to form a single straight channel [1,2]. Then, the barrel may be assumed to move with respect to the screw with an axial and a cross-channel velocity components, corresponding to the helical angle of the screw flight. When these assumptions are made, a constitutive equation of the Generalized Newtonian Fluid type is used and the inertia terms and the gravity are neglected. Furthermore, following the conventional lubrication assumption, the changes of velocities in the down channel direction, z, are neglected, upon comparison to those in x- and y- directions. However, due to the viscous energy dissipation, the viscosity varies along the channel. Thus, at every section along the channel, the velocity distributions depend on the down channel distance z. In all these treatments, the continuity equation and the linear momentum equations are solved.

$$\frac{\partial u_x}{\partial x} + \frac{\partial u_y}{\partial y} = 0 \tag{6}$$

$$\frac{\partial}{\partial x}(\eta\frac{\partial u_x}{\partial x}) + \frac{\partial}{\partial y}(\eta\frac{\partial u_x}{\partial y}) = -\frac{\partial P}{\partial x} \tag{7}$$

$$\frac{\partial}{\partial x}(\eta\frac{\partial u_y}{\partial x}) + \frac{\partial}{\partial y}(\eta\frac{\partial u_y}{\partial y}) = -\frac{\partial P}{\partial y} \tag{8}$$

$$\frac{\partial}{\partial x}(\eta\frac{\partial u_z}{\partial x}) + \frac{\partial}{\partial y}(\eta\frac{\partial u_z}{\partial y}) = -\frac{\partial P}{\partial z} \tag{9}$$

where the $\vec{u}$ is velocity vector and P is the pressure.

The penalty/Galerkin Finite Element Method was used in the present work to discretize equations (6)-(9). Details of this technique were given in [11]. A penalty factor of 10^8 times the shear viscosity was used in the calculations.

The slip law in eq. (1) is a combination of the force boundary condition and velocity condition in the tangential direction of the boundary surface. However, the normal velocity on the same surface is an essential. They are quite difficult to couple with FEM at the same boundary. To solve the problem, we present here a universal transformation of the essential condition into a natural condition form by introducing another penalty factor. To do so, we first write both the slip condition (here we use the value m=1 in eq. 1) and the specified velocity condition as :

$$S = S_{cw} + \frac{(\vec{V}_0 - \vec{u})\cdot\vec{\tau}}{\alpha} \tag{10}$$

$$(\vec{V}_0 - \vec{u})\cdot\vec{n} = 0 \tag{11}$$

where $\vec{\tau}$ and $\vec{n}$ are the tangential and the normal vectors of the slip boundary, respectively. A penalty parameter γ_n is then introduced and eq. (11) is rewritten in analogy to eq. (10) for the normal component N of the stress vector at the slip boundary:

$$N = \frac{1}{\gamma_n}(\vec{V}_0 - \vec{u})\cdot\vec{n} \tag{12}$$

Eq. (12) transforms the essential condition (eq. 11) into the same form as eq. (10), and it becomes equivalent to eq. (11) at the limit of $\gamma_n \to 0$ because N is finite at the boundary. In practice, the penalty parameter γ_n takes a very small value. This transformation implies no specific material, nor specific geometry of the boundary of the flow domain and it is universal in this sense. Of course, any kind of non-linear form of this transformation is also applicable, as long as its limit is eq. (11).

The presence of the boundary conditions in the form of eq. (10) and (12) causes the need to modify the system global matrix by adding to the appropriate nodes the terms from these equations involving the unknown velocities. After the solution vector is found, the following equation will give the "slip velocity" at each point at the wall:

$$u_s = (\vec{V}_0 - \vec{u})\cdot\vec{\tau} \tag{13}$$

Non-isothermal calculation is implemented after the velocity on previous cross section are known. A stepwise continuation with respect to z-coordinate similar to Crank-Nicolson method is used with PEM to solve the energy equation which is read:

$$\rho u_x \frac{\partial T}{\partial x} + \rho u_y \frac{\partial T}{\partial y} + \rho u_z \frac{\partial T}{\partial z} = \frac{\partial}{\partial x}(k\frac{\partial T}{\partial x}) + \frac{\partial}{\partial y}(k\frac{\partial T}{\partial y}) + \frac{\partial}{\partial z}(k\frac{\partial T}{\partial z}) \quad (14)$$

$$+ \tau_{xx}\frac{\partial u_x}{\partial x} + \tau_{yy}\frac{\partial u_y}{\partial y} + \tau_{zz}\frac{\partial u_z}{\partial z} + \tau_{xy}(\frac{\partial u_x}{\partial y} + \frac{\partial u_y}{\partial x}) + \tau_{xz}\frac{\partial u_x}{\partial z} + \tau_{yz}\frac{\partial u_y}{\partial z}$$

where heat conduction along z is neglected. The same technique is applied to solve the equation for the specific energy input. The material was assumed to have an energy input value of E_o of $10^3 kJ/kg$ on the entry.

3. RESULTS AND DISCUSSION

The mesh in the calculations describing the x-y cross section of the channel formed in a single screw extruder is shown in Fig. 1. The operating conditions are given in Table I. The x and z components of the barrel velocity (V_{ox} and V_{oz}) that result from a 40 rpm rotational speed of the screw are 32 mm/sec and 102 mm/sec respectively. The rheological and thermal parameters in the present study for a test material are listed in Table II and have values typical of a concentrated suspension of a solid filler within a polymeric matrix [11]. Velocity, stress, temperature and specific energy profiles were calculated as a function of x, y and z.

The effect of the slip on the velocity profile is shown in Fig 2. Here the slip velocity is normalized over the barrel velocity, so that the graph shows the percent of slip at that wall. The amount of slip in the x direction(curve 1) is not affected by the rate of pressurization in the down channel direction, as it only reflects the shear stress τ_{xy} changing along x. In the central part of the channel, the slip is almost constant (about 28%), but it changes greatly near the tips. Calculations show that the slip along the screw surface is almost zero. The slip along z(curve 2 and 3) is affected by dP/dz reflecting the changes of τ_{xy} along x. Again, in a greater portion of the central part of the channel, the slip is more uniform than that in x-direction ,with a smaller (about 15%) value, with much smaller value (less than 10%) for the slip in the screw surface(curve 4 and 5). However, near the two tips, the slip is decreased toward inside channel, which is in contrast to the slip in x and y directions.

z component velocity of the fluid with back flow in the channel in the form of isovels are shown in Fig. 3. Slip effect is clearly seen near the two tips. Inside the channel, the contours of the slip and no-slip are qualitatively same, but the slip reduces dramatically the magnitude. This, of course, will reduce the wall shear stress level, total stress level, and thus, the input energy and the temperature. If the contours of the stress invariant and the specific energy input were plotted here for both slip and no slip cases, the contours will show that slip makes these distributions more uniform than those with the no slip condition.

Temperature profiles in the flow channel are shown in Fig. 4. (a) is the case with the no wall slip case, and (b) is the slip case. The contour of T converges to 300 K on the barrel, the assumed temperature for the barrel. The specification of the temperature of the fluid in contact with the barrel as the boundary condition instead of the use of a wall-fluid heat transfer coefficient, may introduce some error to these calculations. The adiabatic conditions at the screw surface in combination with the long residence times result in high values of T there, especially in the no-slip case. The values of the temperature when slip is occurring are lower than those obtained with no slip at the wall, and the profile is more uniform.

The effect of the slip condition on the pressurization ability of the extruder and the dependence of the flow rate on the rotational speed are shown in Figures 5 and 6. The flow rate and the pressurization achieved are interdependent quantities in an extruder and these two figures should be examined together. As it should be expected the flow rate is reduced for the same rotational speed, when the material slips at the walls. Also, the pressurization obtained under the same flow rate is reduced by the slip. An empirical equation that fits the data reported here and relates the flow rate and the pressurization for such an extruder operating at Ω rpm, when the material slips at the wall with a coefficient α is given below:

$$Q = 0.2*10^{-4}\,(1 - 0.12*\alpha)\,\Omega - 0.07*10^{-4}\,(1 + 9*\alpha)\,\frac{\Delta P}{\Delta L} \qquad (m^3/sec) \quad (15)$$

By comparing the coefficients in the two terms, it can be seen from this equation that the effect of the wall slip is more pronounced on the effective loss of the pressurization ability of the extruder than on the decrease of the flow rate for a given rotational speed. In other words, for a desired pressurization rate the flow rate will decrease dramatically for high values of the slip coefficient, when the rpm remains the same.

4. CONCLUSIONS

A comprehensive mathematical model of the single screw extrusion process was developed using the Finite Element Method and a novel technique was introduced to incorporate the slip boundary condition at all walls. Furthermore, the shear viscosity material function was varied with the specific energy input. Both slip and specific energy input dependent rheological behavior are traits of the processing of highly filled suspensions. Thus, the presented techniques should be especially useful for predicting the processing behavior of such suspensions in single screw extruders.

The model was applied to a typical flow of highly filled suspensions in a single screw extruder. It was found that the accumulated energy affected the flow field to a greater degree in the initial stages of the flow. The changing nature of the viscosity was found, however, to have a profound effect on cumulative quantities such as specific energy input and temperature. On the other hand, the ability of the material to slip at the walls affects extensively the operating characteristics of the extruder, reducing the generated flow rate for a given pressure drop at the die downstream. On the other hand, the slip decreases the pressurization ability of the extruder. It reduces the energy that is accumulated on the material as it passes through the extruder, adversely affecting the mixing capabilities of the machine. It also reduces the temperature increase.

ACKNOWLEDGEMENTS

The authors would like to thank Dr. Yilmazer for his suggestions on the slip problem and Dr. Tsenoglou for his criticism on the viscosity models. This work was supported by the Office of Naval Research and DARPA, for which we are grateful.

REFERENCES

1. J. N. McKelvey, "Polymer Processing", Wiley, N. Y. (1962).
2. Z. Tadmor and I. Klein, "Engineering Principles of Plasticating Extrusion", R. E. Krieger Publ. Co., N.Y. (1978).
3. D.M. Kalyon, in"Encyclopedia of Engineering Materials", N Cheremisinoff ed. Dekker, New York 1989.
4. Z. Tadmor and C. Gogos, "Principles of Polymer Processing", Wiley , N.Y. (1980).
5. A.B. Payne, J.Appl.Polym.Sci., 9, 2273 (1985).
6. U. Yilmazer and D. Kalyon, J. Rheol. 33(8), (1989).
7. R.D Weason and T.C. Papanastasiou, J.Non-Newt.Fl.Mech, 24, (1988) 277-295.
8. N. Phan-Thien, J.Non-Newt.Fl.Mech, 24, (1988) 327-340.
9. T.C. Papanastasiou, J.Rheol., 31(5), (1987) 385-404.
10. H.E.H. Meijer, C.P.J.M. Verbrask, Polym.Eng.Sci. 28(11),
11. D. Kalyon, A.D. Gotsis, U. Yilmazer, C. Gogos, H. Sangani, B. Aral and C. Tsenoglou, Adv.Polym.Proc. 8(4) (1988) 337-353.
12. A.D. Gotsis, D. Kalyon, SPE ANTEC Technical papers 35 44-48, (1989). (1988) 758-772.

TABLE 1.

Operating Conditions and Geometry of the Extruder
Screw Diameter = 50.8 mm
Pitch = 50.8 mm
Screw Rotational Speed = 40 rpm
Inlet Temperature = 300 K
Barrel Temperature = 300 K
Full Channels

TABLE 2.

Rheological and Thermal Properties of the Test Material
$\eta_\infty = 14000\ Pa.s$ $\tau_y = 1100\ Pa$ $n = 50\ s$ $B = 5.*10^{-5}\ J/kg$ $B_T = 0$
$\alpha = 9.2*10^{-9}\ m/Pa.s$ $\tau_{crit} = 0\ Pa$
$\rho = 1400\ kg/m^3$ $C_p = 2000\ J/kg.K$ $k = 0.27\ W/m.K$

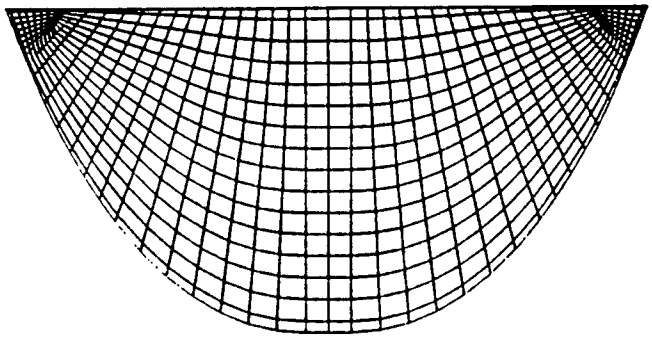

Figure 1

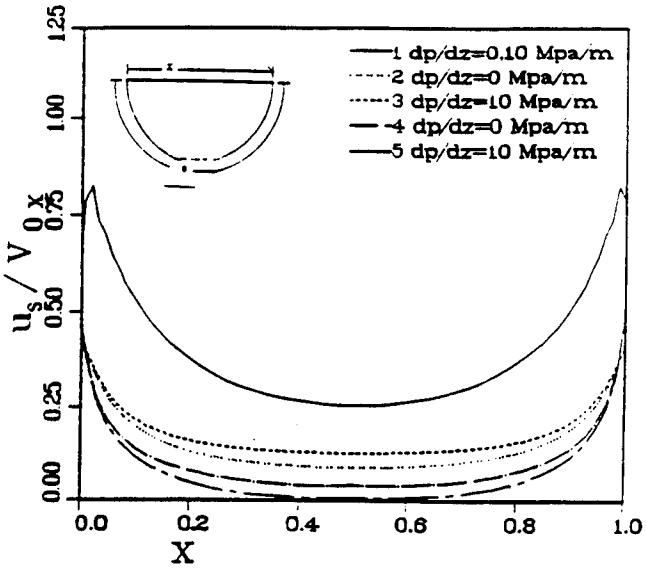

Figure 2

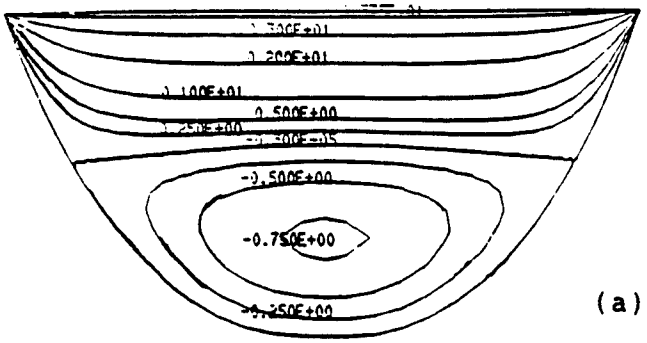

(a)

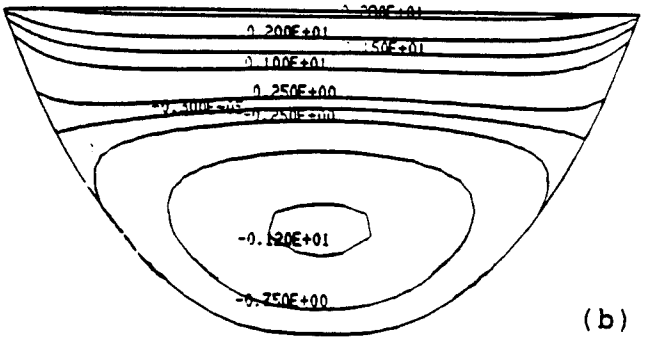

(b)

Figure 3

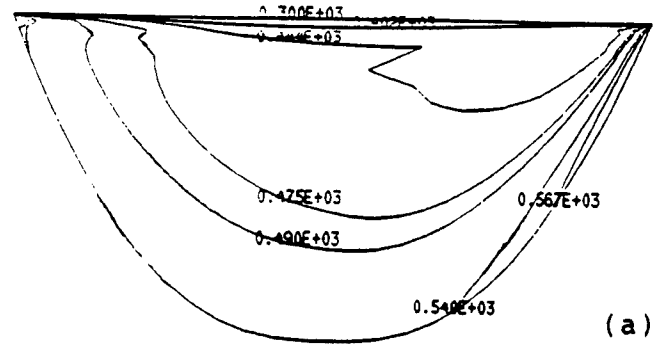

(a)

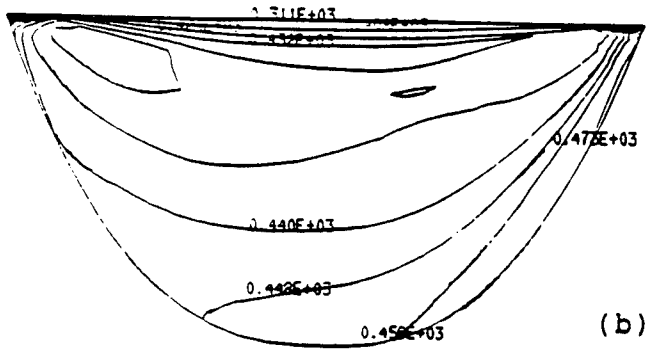

(b)

Figure 4

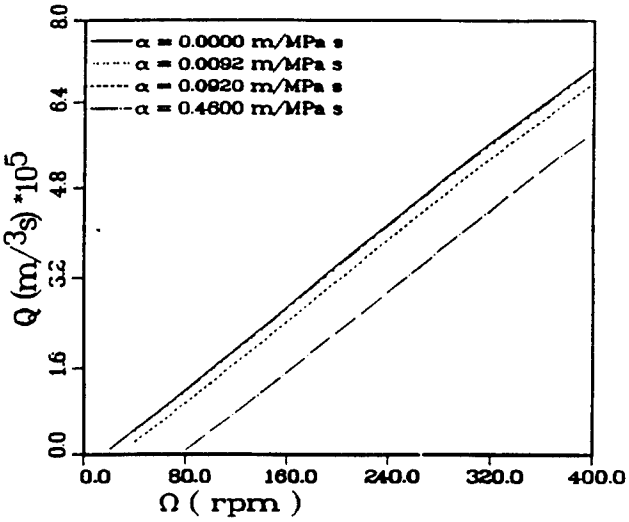

Figure 6

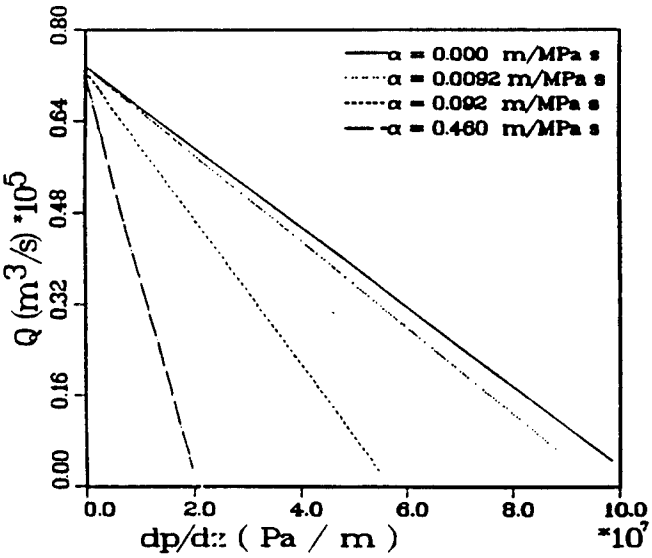

Figure 5

INCORPORATION OF WALL SLIP IN NON-ISOTHERMAL MODELING OF SINGLE SCREW EXTRUSION PROCESSING

by

Adeniyi Lawal and Dilhan M. Kalyon

Highly Filled Materials Institute
Stevens Institute of Technology

INTRODUCTION

The single screw extruder is one of the most widely used continuous processors for conveying of solids, melting, pressurization, blending, reactive extrusion and compounding of a wide variety of materials. The experimental and/or simulation based knowledge gained over the years has helped our understanding of the single screw extrusion process (1, 2), which in turn has led to the improvement in the design of this processing machine.

In the numerical simulation of the flow dynamics and heat transfer occurring in the single screw extrusion processing of a variety of complicated materials, including concentrated suspensions, three complications are manifest. The geometry of the extruder is complex. This can be effectively dealt with by using the finite element method in the solution of the conservation equations. The second complication is related to the rheological behavior of non-Newtonian materials. Besides exhibiting shear rate and temperature dependent material functions, many materials also exhibit viscoplasticity, i.e. they possess a limiting stress (yield stress) below which they experience little or no deformation and hence flow in a plug-like manner.

The third complication arises from the behavior of some viscoplastic materials at solid boundaries. Experimental evidence shows conclusively that various materials, including suspensions, gels and emulsions exhibit slip at the solid boundaries during flow and deformation (3-11). The implication is that the commonly employed no-slip condition of continuum mechanics is not applicable for a wide range of generally viscoplastic materials. Wall-slip in pressure flows, especially the capillary flow has received considerable attention. Mooney's (3) investigation of slip in capillary flow dates back to 1931. From available experimental data on viscometric flows, it is now generally accepted that the slip velocity in duct flows can be described by the Navier slip condition(12). A review of wall slip occurring at solid boundaries is available, Schowalter (13).

The numerical solution of flow and heat transfer of polymer melts is reviewed by Nakazawa et al. (14) along with finite element solution of non-isothermal cavity flows of Ostwald-de Waele model fluids. The generally encountered highly viscous nature of processed materials implies significant viscous dissipation effects in single screw extrusion. In the non-isothermal analysis of single screw extrusion, viscous dissipation and heat conduction in the direction of screw depth were the first effects to be considered (15). Subsequently, heat conduction in the other transverse direction (16) and more recently, heat convection in the down channel direction (17) were included in the solution of the equation of energy. Overall, most non-isothermal simulation studies of single screw extrusion have ignored the transverse convection terms, possibly due to the fact that when both the channel direction and the transverse convection terms are retained and become dominant, the commonly utilized standard Bubnov-Galerkin method as well as its equivalent in the finite difference based methods, produces oscillations in the numerical solution. This numerical difficulty has long been recognized in the finite difference and finite element literature. (18)

The standard technique for dealing with spurious oscillations associated with both spatial and temporal discretizations of first derivatives involves the addition of an artificial diffusion term into the numerical formulation (18). Artificial diffusion techniques for Galerkin finite element methods can be accomplished by using modified forms of weighting functions (Petrov-Galerkin) typically with test functions which are one degree higher than basis functions (19). The artificial diffusion term can also be incorporated by modifying the test functions by a perturbation, dependent upon the velocity field (20, 21), i.e. Streamline Upwind/Petrov-Galerkin (SUPG) method. For a parabolic problem, which may arise from time dependency (or in the case of steady state problems, from the existence of a predominant flow direction), the structure of SUPG method is only preserved if time-space elements are used(22).

In this study, we adopt an earlier developed method of incorporating the Navier slip condition for flows in complex geometries (23). This method has been successful in handling the slip condition under isothermal conditions. A modified Bingham plastic model (24) is used to characterize the rheological behavior of viscoplastic materials, which avoids the need to track yield surfaces. For the non-isothermal analysis in single screw extruders, the SUPG formulation is further developed leading to an easy to implement algorithm and oscillation free temperature solution. This model can be utilized to simulate the non-isothermal processing behavior of materials like concentrated suspensions, which exhibit viscoplasticity as well as wall slip.

ANALYSIS

Flow Equations

The governing equations of the flow in the single screw extruder are given by the general equations of conservation of mass and momentum, which are fully elliptic and three-dimensional. But the solution of the complete set of three-dimensional equations is unwarranted since experimental data indicate that certain simplifying assumptions (23) can be made which will render the equations parabolic and therefore amenable to stepwise integration in the z-direction (primary flow direction) from prescribed upstream conditions. Following the parabolic flow analysis and introducing the following dimensionless variables:

$$x = R_s x^* \quad y = R_s y^* \quad \overline{u} = R_s \omega \overline{u}^* \tag{1a}$$

$$\eta = \eta_o \eta^* \quad \alpha' = \frac{R_s}{\eta_o} \alpha^* \quad Q = R_s^3 \omega Q^* \tag{1b}$$

$$\overline{p} = \eta_o \omega \overline{p}^* \tag{1c}$$

the equations of conservation of mass and momentum become:

$$\frac{\partial u_x}{\partial x} + \frac{\partial u_y}{\partial y} = 0 \qquad (2)$$

$$\frac{\partial \overline{p}}{\partial x} = \frac{\partial}{\partial x}\left(2\eta \frac{\partial u_x}{\partial x}\right) + \frac{\partial}{\partial y}\left\{\eta\left(\frac{\partial u_x}{\partial y} + \frac{\partial u_y}{\partial x}\right)\right\} \qquad (3a)$$

$$\frac{\partial \overline{p}}{\partial y} = \frac{\partial}{\partial y}\left(2\eta \frac{\partial u_y}{\partial y}\right) + \frac{\partial}{\partial x}\left\{\eta\left(\frac{\partial u_x}{\partial y} + \frac{\partial u_y}{\partial x}\right)\right\} \qquad (3b)$$

$$\frac{dp_m}{dz} = \frac{\partial}{\partial x}\left(\eta \frac{\partial u_z}{\partial x}\right) + \frac{\partial}{\partial y}\left(\eta \frac{\partial u_z}{\partial y}\right) \qquad (3c)$$

where ω is the angular velocity of the screw and the asterisk (*) has been suppressed in the equations for convenience. The parabolic nature of these differential equations is preserved through p_m the mean viscous pressure which has been defined for the primary flow direction, z and is constant for any x-y plane. We assume that dp_m/dz is constant. Equations (3a-b) can now be handled separately from the channel direction equation (3c) and the penalty method is used in approximating the pressure $\overline{p}$. The procedure adopted in this study for the implementation of wall slip is well described in (23) and is therefore not repeated here.

For the modified Bingham plastic model (24), the viscosity η is given by:

$$\eta = \left[\eta_o + \frac{\tau_y(1 - \exp(-n'|\dot{\gamma}|))}{|\dot{\gamma}|}\right] \qquad (4)$$

where η_o is the viscosity coefficient, τ_y and n' are material parameters and $|\dot{\gamma}|$ is defined for our case, by:

$$|\dot{\gamma}|^2 = 2u_{x,x}^2 + 2u_{y,y}^2 + (u_{x,y} + u_{y,x})^2 + u_{z,x}^2 + u_{z,y}^2 \qquad (5)$$

Energy Equation and Boundary Conditions

By order-of-magnitude analysis, it can be demonstrated that in the single screw extruder, the transverse convection terms are not negligible. In fact, one of the transverse convection terms is generally comparable to the channel direction convection term. However, one can neglect heat conduction along the channel direction and assume steady state. With these assumptions, the energy equation reduces to:

$$u_x \frac{\partial T}{\partial x} + u_y \frac{\partial T}{\partial y} + u_z \frac{\partial T}{\partial z} = \frac{k}{\rho C_p}\left(\frac{\partial^2 T}{\partial x^2} + \frac{\partial^2 T}{\partial y^2}\right) + \frac{\eta \dot{\gamma}^2}{\rho C_p} \qquad (6)$$

where ρ is the density, C_p the specific heat and k is the thermal conductivity. The fluid enters the screw channel at a temperature T_o and the barrel temperature is designated as T_b, which is different from the entrance temperature. Variations in T_b in the channel direction are allowed. The screw surface is assumed to be adiabatic. Since the velocity distribution can be determined , this parabolic problem can be solved in a stepwise fashion along the channel direction z. Equation 6 was solved with the above specified boundary conditions in (23) using the Bubnov-Galerkin method, and the removal of oscillations in the temperature solution was attempted by a simple smoothing procedure. Here we implement the recently developed SUPG method (which has rarely been implemented in polymer processing simulation) by introducing weighting functions of the form:

$$\overline{W} = W + w \qquad (7)$$

where W is a continuous function of space and w is a discontinuous perturbation of W. The weak form of the energy equation is then given by:

$$\int_z^{z+\Delta z} \left[W\left(u_x \frac{\partial T}{\partial x} + u_y \frac{\partial T}{\partial y} + u_z \frac{\partial T}{\partial z}\right) + \frac{k}{\rho C_p}(\nabla W \cdot \nabla T) - \frac{W \eta \dot{\gamma}^2}{\rho C_p} \right] dD$$

$$+ \sum_i \int_{e_i} w \left[u_x \frac{\partial T}{\partial x} + u_y \frac{\partial T}{\partial y} + u_z \frac{\partial T}{\partial z} - \frac{k}{\rho C_p} \nabla \cdot \nabla T - \frac{\eta \dot{\gamma}^2}{\rho C_p} \right] d\Gamma_s \, dz = 0 \qquad (8)$$

where the last integral is over element interiors. The shape functions are chosen to satisfy the boundary conditions on the barrel and must therefore vanish there.

The shape functions for the temperature are similar to those used for velocity in that they are linear in the space coordinates but the weighting function W has a quadratic variation in the z-coordinate to improve accuracy, while still retaining the linear form in x and y (22). Since the thermal problem is parabolic, the integration in z in Eq. 8 can be carried out independent of the other two directions producing a part with known values of T (a source term) and the other containing values of T being sought. At this point, the solution procedure adopted for the velocity equations can then be applied.

Several approaches have been suggested in the literature for the definition of the perturbation function for SUPG. We have followed the method outlined by Hughes et al. [25]. In this analysis, an element in the arbitrary domain x,y, and z can be mapped into an isoparametric element of unit dimension in each of the transformed co-ordinates ξ, χ, and ζ. An element mesh parameter can then be defined as

$$h^e = \frac{2||u||}{b} \qquad (9)$$

where $||u||$ is the Euclidean norm of the velocities and b is given by

$$b^2 = \left(u_x \frac{\partial \xi}{\partial x} + u_y \frac{\partial \xi}{\partial y}\right)^2 + \left(u_x \frac{\partial \chi}{\partial x} + u_y \frac{\partial \chi}{\partial y}\right)^2 + \left(u_z \frac{\partial \zeta}{\partial z}\right)^2 \qquad (10)$$

Hughes et al. (25) have suggested that the perturbation function be taken as:

$$w = \frac{\sigma h^e \beta^e}{2||u||} u \cdot \nabla W \qquad (11)$$

where,

$$\beta^e = \coth \gamma^e - \frac{1}{\gamma^e} \qquad \text{and} \qquad \gamma^e = \frac{\rho C_p ||u|| h^e}{2k} \qquad (12a, b)$$

A value of $\sigma = 1$ was used by Hughes et al. (25). However, our numerical experimentation revealed that the value of σ is dependent on such factors as the element skewness and the flow and heat transfer parameters. Here it is recommended that σ be adjusted until the solution is oscillation free. For the range of parameters considered in this study, the values of σ were between 0.3 and 0.4 and furnished satisfactory results.

RESULTS AND DISCUSSION

For the finite element solution of the conservation equations, the domain is discretized by bilinear elements and the discretized equations for u_x , u_y , u_z , and T in matrix form were solved by standard techniques. The results to be presented (all in dimensionless form defined in Equations 1a-1c) were obtained based on the operating and processing conditions listed in Table 1. The operating conditions are in the range, which we typically utilize in our experiments on industrial scale extruders.

Table 1.

OPERATING AND PROCESSING CONDITIONS	
$\eta = 1.0$	Radius of barrel (R_s) = 2.54cm
$\tau_y = 0.05$	Helix angle $\phi = 17.61^\circ$
$n' = 80$	$\rho = 1400$ kg/m^3
$\alpha = 1.0$	$C_p = 2000$ J/kgK
Screw speed = 40 rpm	k = 0.27 W/mK

The effect of wall slip on the channel direction velocity u_z is illustrated in Figs. 1a-b for a positive pressure gradient ($dp_m/dz = 2.0$). The velocity distribution varies uniformly from the screw surface to the barrel for both conditions of wall stick (Fig. 1a) and wall slip. Wall slip greatly modulates the magnitude of the velocity with the maximum decreasing from 0.953 to 0.2097 upon wall slip. This is also true for other values of positive pressure gradient not reported here. As the value of dp_m/dz increases, a region of backflow appears, the strength and size of which increase with increased slip parameter. On the other hand, the wall slip enhances channel direction velocity for negative pressure gradient. The corresponding

dimensionless temperature distributions at a down channel location of z = 0.5 are presented in Figs. 2a-b. The effect of wall slip is essentially the shifting of the region of lowest temperature to approximately the center of the screw surface, thus ensuring that the fluid feels more uniformly the effect of the barrel temperature.

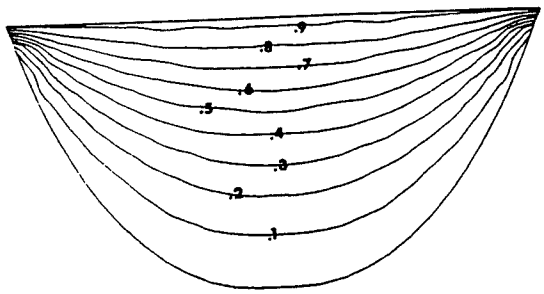

Figure 1a: Channel direction velocity distribution for wall stick condition (α = 0 and dp_m/dz = 2.0)

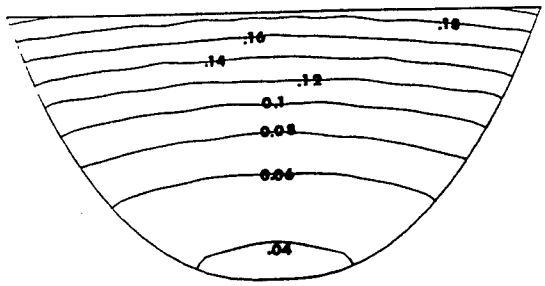

Figure 1b: Channel direction velocity distribution for wall slip condition (α = 1.0 and dp_m/dz = 2.0)

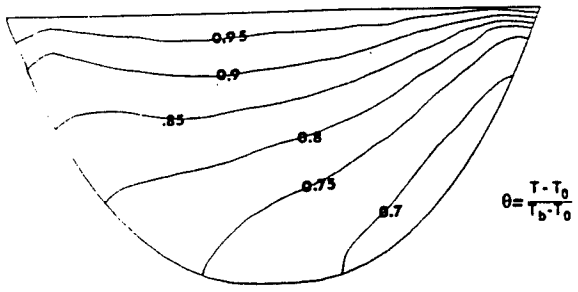

Figure 2a: Dimensionless temperature distribution at channel location z = 0.5 for wall stick condition

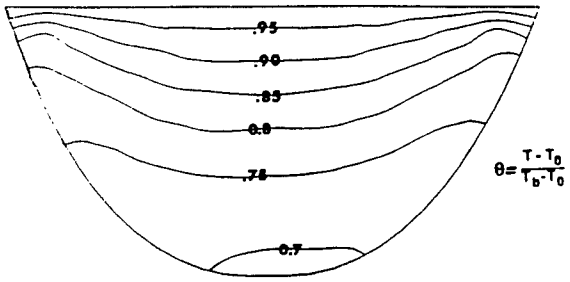

Figure 2b: Dimensionless temperature distribution at channel location z = 0.5 for wall slip condition (α = 1.0)

Fig. 3a displays the effect of wall slip parameter and pressure gradient on the xy-cross sectional wall slip velocity distribution. The region AB represents the barrel surface while BA is the screw surface. For the slip coefficient considered, i.e. 0.01 to 1 and for all values of dimensionless pressure gradient dp_m/dz, the slip velocity on the screw surface is effectively zero.

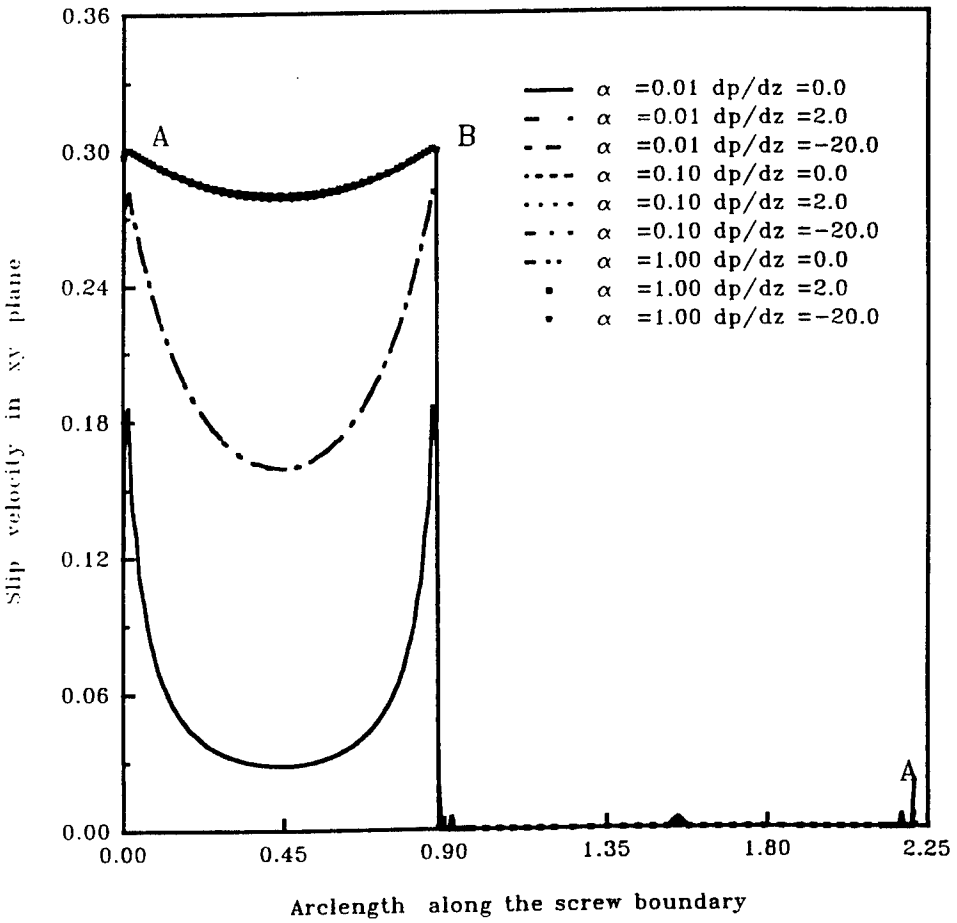

Figure 3a: Slip velocity distribution along the screw surface for different values of slip parameter and pressure drop

The maxima which occur at the two tips of the screw are due to the small gaps at those locations. On the barrel surface, the slip velocity increases as the slip parameter increases but exhibits no appreciable dependence on the pressure gradient, either positive or negative. On the other hand, the channel direction slip velocity is affected by both the slip parameter and the pressure gradient with a reversal in behavior occurring from a change from negative to positive pressure gradient (Fig 3b).

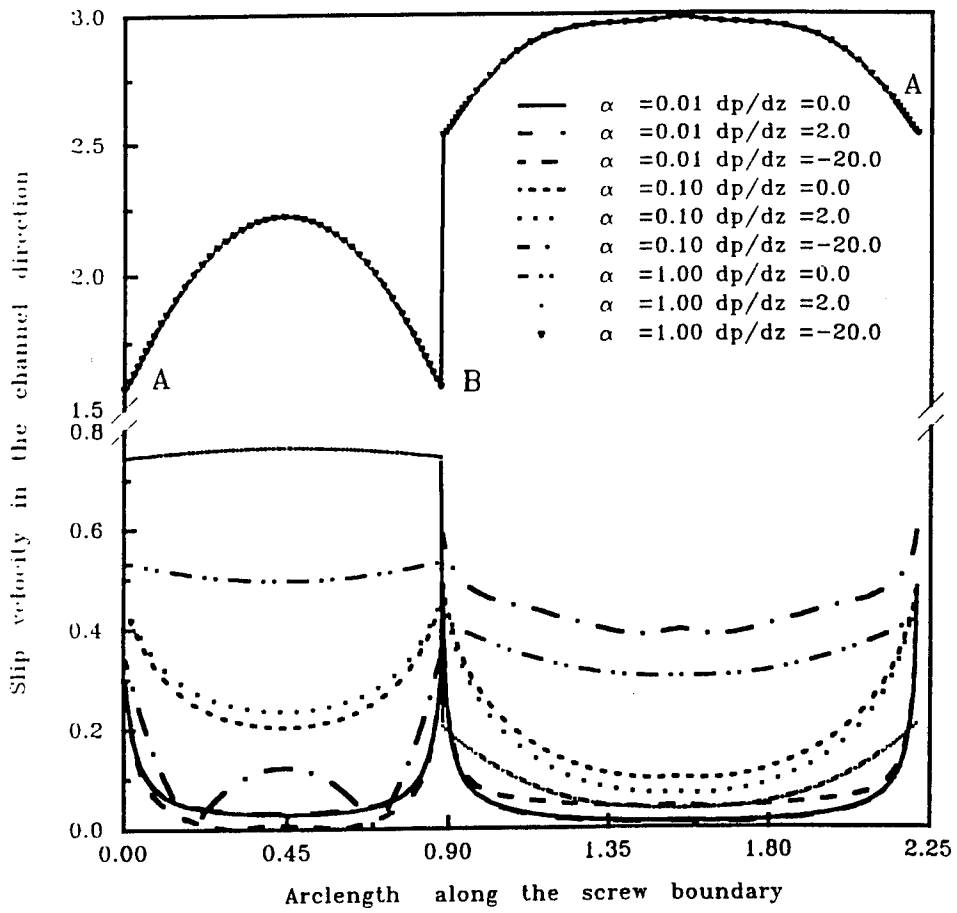

Figure 3b: Channel direction slip velocity along the screw surface for different values of slip parameter and pressure drop

Finally, in Fig.4, the effect of slip on the overall pressure drop versus the volume flow rate relationship is depicted for positive pressure gradient values. Generally, for the same pressure gradient, the flow rate is reduced by the occurrence of slip and the reverse is obtained for negative pressure gradients.

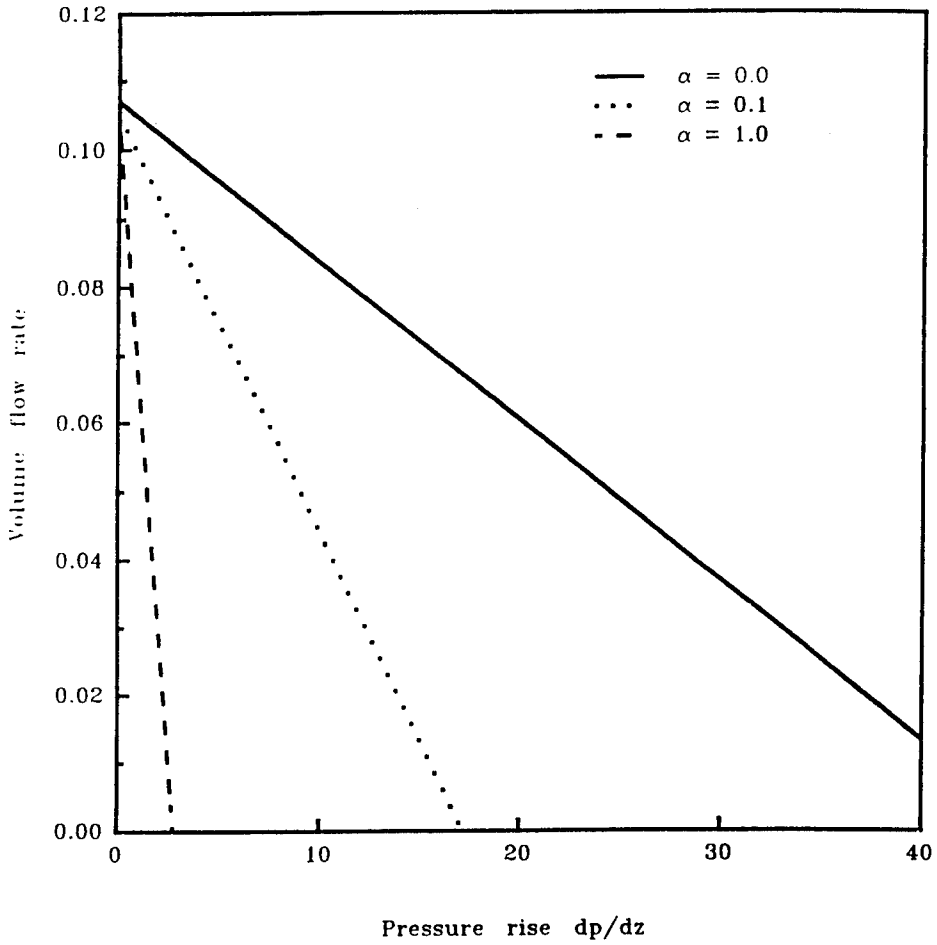

Figure 4: Pressure drop flow rate relationship for different values of slip parameter

CONCLUSION

A non-isothermal model of the single screw extrusion processing with wall slip has been developed using the Streamline Upwind/Petrov-Galerkin (SUPG) method. Wall slip reduces the capacity of pressurization and also tends to produce more uniform temperature distributions in the single screw channel. This model should generate a better predictive understanding of the single screw processing of viscoplastic materials subject to wall slip.

ACKNOWLEDGEMENTS

This study was sponsored by the Department of the Navy, Office of the Chief of Naval Research, for which we are grateful. The content of the information does not reflect the policy of the Government, and no official endorsement should be inferred.

REFERENCES

1. McKelvey, M.,"Polymer Processing," John Wiley, NY (1962).
2. Tadmor Z., and I. Klein, "Engineering Principles of Plasticating Extrusion, Robert Krieger Comp., NY (1978).
3. Mooney, M., *J. Rheology, 2* (1931) 210
4. Vand, V., *J. Phys. Colloid Chem., 52* (1948) 277.
5. Toms, B.*J. Colloid Sci, 4* (1949) 511.
6. Cox , R., and S. Mason, *Ann. Rev. Fluid Mech., 3,* (1971) 291.
7. Yoshimura, A., and R. K. Prud'homme, *J. Rheol., 32* (1988) 53.
8. Cohen, Y., and A. B. Metzner, *J. Rheol., 25* (1985) 67.
9. Ramamurthy, A. V., *J. Rheology, 30* (1986) 337.
10. Yilmazer, U., and D. Kalyon, *J. Rheol., 33* (1989) 1197.
11. Hatzikiriakos, S.G., and J.M. Dealy, *J. Rheol., 35* (1991) 497.
12. Silliman, W.T., and L.E. Scriven, *J. Comp. Phys., 34* (1980) 287.
13. Schowalter, W.R., *J. Non-Newtonian Fluid Mech., 29* (1988) 25.
14. Nakazawa, S., Pittman, J.F.T., and O.C. Zienkiewicz, in "Finite Elements in Fluids," Volume 4, R. H. Gallagher, D. H. Norrie, J.T. Oder and O.C. Zienkiewicz, eds. (New York: John Wiley and Sons), 1982.
15. Colwell, R.E., and K.R. Nickolls, *Ind. Eng. Chem., 51* (1959) 841.
16. Griffith, R.M., *Ind. Eng. Chem. Fundam., 1* (1960) 180.
17. Kwon, T.H. , Jaluria, Y., Karwe, M.V. and T. Sastrohartono, in: A. I. Isayev (ed.), *Modeling of Polymer Processing (Recent Developments)*, Hanser Publishers (1991) 77.
18. Heinrich, J. C., and O.C. Zienkiewicz in: T.J.R. Hughes (ed.), "Finite Elements for Convection Dominated Flow, " ASME Publ. AMD, 34 (1979) 105.
19. Westink, J.J., and D. Shea, *Int. J. Numer. Methods Eng., 28* (1989) 1077.
20. Hughes, T.J.R., and A.N. Brooks, in "Finite Elements Methods for Convection Dominated Flows," T.J.R. Huges, ed., ASME Publication AMD, (1979) 34.
21. Brooks, A.N., and T.J.R. Hughes, *Comp. Methods Appl. Mech. Eng., 32* (1982) 199.
22. Yu, C.C., and J.C. Heinrich, *Int. J. Num. Methods in Eng., 24* (1987)2201.
23. Ji, Z., Gotsis, A.D., and D.M. Kalyon, *SPE Antec Technical Papers,* (1990) 160.
24. Papanastasiou, T.C., *J. Rheol., 31* (1987) 385.
25. Hughes, T.J.R., Mallet, M., and A. Mizukami, Comp. Methods in *Appl. Mech. Eng., 54* (1986) 341.

A Non-Isothermal Model of Single Screw Extrusion Processing of Viscoplastic Materials Subject to Wall Slip

A. LAWAL AND D. M. KALYON
Stevens Institute of Technology
Highly Filled Materials Institute
Department of Chemistry and Chemical Engineering
Castle Point on the Hudson
Hoboken, NJ 07030, U.S.A.

INTRODUCTION

The single screw extruder is one of the most widely used continuous processors for conveying of solids, melting, pressurization, blending, reactive extrusion and compounding of a wide variety of materials. The experimental and/or simulation based knowledge gained over the years has helped our understanding of the single screw extrusion process (1, 2), which in turn has led to the improvement in the design of this processing machine.

In the numerical simulation of the flow dynamics and heat transfer occurring in the single screw extrusion processing of a variety of complicated materials, including concentrated suspensions, three complications are manifest. The geometry of the extruder is complex. This can be effectively dealt with by using the finite element method in the solution of the conservation equations. The second complication is related to the rheological behavior of non-Newtonian materials. Besides exhibiting shear rate and temperature dependent material functions, many materials also exhibit viscoplasticity, i.e. they possess a limiting stress (yield stress) below which they experience little or no deformation and hence flow in a plug-like manner.

The third complication arises from the behavior of some viscoplastic materials at solid boundaries. Experimental evidence shows conclusively that various materials, including suspensions, gels and emulsions exhibit slip at the solid boundaries during flow and deformation (3-11). The implication is that the commonly employed no-slip condition of continuum mechanics is not applicable for a wide range of generally viscoplastic materials. Wall-slip in pressure flows, especially the capillary flow has received considerable attention. Mooney's (3) investigation of slip in capillary flow dates back to 1931. From available experimental data on viscometric flows, it is now generally accepted that the slip velocity in duct flows can be described by the Navier slip condition(12). A review of wall slip occurring at solid boundaries is available, Schowalter (13).

The numerical solution of flow and heat transfer of polymer melts is reviewed by Nakazawa et al. (14) along with finite element solution of non-isothermal cavity flows of Ostwald-de Waele model fluids. The generally encountered highly viscous nature of processed materials implies significant viscous dissipation effects in single screw extrusion. In the non-isothermal analysis of single screw extrusion, viscous dissipation and heat conduction in the direction of screw depth were the first effects to be considered (15). Subsequently, heat conduction in the other transverse direction (16) and more recently, heat convection in the down channel direction (17) were included in the solution of the equation of energy. Overall, most non-isothermal simulation studies of single screw extrusion have ignored the transverse convection terms, possibly due to the fact that when both the channel direction and the transverse convection terms are retained and become dominant, the commonly utilized standard Bubnov-Galerkin method as well as its equivalent in the finite difference based methods, produces oscillations in the numerical solution. This numerical difficulty has long been recognized in the finite difference and finite element literature. (18)

The standard technique for dealing with spurious oscillations associated with both spatial and temporal discretizations of first derivatives involves the addition of an artificial diffusion term into the numerical formulation (18). Artificial diffusion techniques for Galerkin finite element methods can be accomplished by using modified forms of weighting functions (Petrov-Galerkin) typically with test functions which are one degree higher than basis functions (19). The artificial diffusion term can also be incorporated by modifying the test functions by a perturbation, dependent upon the velocity field (20, 21), i.e. Streamline Upwind/Petrov-Galerkin (SUPG) method. For a parabolic problem, which may arise from time dependency (or in the case of steady state problems, from the existence of a predominant flow direction), the structure of SUPG method is only preserved if time-space elements are used(22).

In this study, we adopt an earlier developed method of incorporating the Navier slip condition for flows in complex geometries (23). This method has been successful in handling the slip condition under isothermal conditions. A modified Bingham plastic model (24) is used to characterize the rheological behavior of viscoplastic materials, which avoids the need to track yield surfaces. For the non-isothermal analysis in single screw extruders, the SUPG formulation is further developed leading to an easy to implement algorithm and oscillation free temperature solution. This model can be utilized to simulate the non-isothermal processing behavior of materials like concentrated suspensions, which exhibit viscoplasticity as well as wall slip.

ANALYSIS

Flow Equations

The governing equations of the flow in the single screw extruder are given by the general equations of conservation of mass and momentum, which are fully elliptic and three-dimensional. But the solution of the complete set of three-dimensional equations is unwarranted since experimental data indicate that certain simplifying assumptions (23) can be made which will render the equations parabolic and therefore amenable to stepwise integration in the z-direction (primary flow direction) from prescribed upstream conditions. Following the parabolic flow analysis and introducing the following dimensionless variables:

$$x = R_s x^* \quad y = R_s y^* \quad \vec{u} = R_s \omega \vec{u}^* \tag{1a}$$

$$\eta = \eta_o \eta^* \quad \alpha' = \frac{R_s}{\eta_o}\alpha^* \quad Q = R_s^3 \omega Q^* \tag{1b}$$

$$\bar{p} = \eta_o \omega \bar{p}^* \tag{1c}$$

the equations of conservation of mass and momentum become:

$$\frac{\partial u_x}{\partial x} + \frac{\partial u_y}{\partial y} = 0 \tag{2}$$

$$\frac{\partial \bar{p}}{\partial x} = \frac{\partial}{\partial x}\left(2\eta \frac{\partial u_x}{\partial x}\right) + \frac{\partial}{\partial y}\left\{\eta\left(\frac{\partial u_x}{\partial y} + \frac{\partial u_y}{\partial x}\right)\right\} \quad (3a)$$

$$\frac{\partial \bar{p}}{\partial y} = \frac{\partial}{\partial y}\left(2\eta \frac{\partial u_y}{\partial y}\right) + \frac{\partial}{\partial x}\left\{\eta\left(\frac{\partial u_x}{\partial y} + \frac{\partial u_y}{\partial x}\right)\right\} \quad (3b)$$

$$\frac{dp_m}{dz} = \frac{\partial}{\partial x}\left(\eta \frac{\partial u_z}{\partial x}\right) + \frac{\partial}{\partial y}\left(\eta \frac{\partial u_z}{\partial y}\right) \quad (3c)$$

where ω is the angular velocity of the screw and the asterisk (*) has been suppressed in the equations for convenience. The parabolic nature of these differential equations is preserved through p_m the mean viscous pressure which has been defined for the primary flow directon, z and is constant for any x-y plane. We assume that dp_m / dz is constant . Equations (3a-b) can now be handled separately from the channel direction equation (3c) and the penalty method is used in approximating the pressure $\bar{p}$. The procedure adopted in this study for the implementation of wall slip is well described in (23) and is therefore not repeated here.

For the modified Bingham plastic model (24), the viscosity η is given by:

$$\eta = \left[\eta_o + \frac{\tau_y(1 - \exp(-n'|\dot{\gamma}|))}{|\dot{\gamma}|}\right] \quad (4)$$

where η_o is the viscosity coefficient, τ_y and n' are material parameters and $|\dot{\gamma}|$ is defined for our case, by:

$$|\dot{\gamma}|^2 = 2u_{x,x}^2 + 2u_{y,y}^2 + (u_{x,y} + u_{y,x})^2 + u_{z,x}^2 + u_{z,y}^2 \quad (5)$$

Energy Equation and Boundary Conditions

By order-of-magnitude analysis, it can be demonstrated that in the single screw extruder, the transverse convection terms are not negligible. In fact, one of the transverse convection terms is generally comparable to the channel direction convection term. However, one can neglect heat conduction along the channel direction and assume steady state.With these assumptions, the energy equation reduces to:

$$u_x \frac{\partial T}{\partial x} + u_y \frac{\partial T}{\partial y} + u_z \frac{\partial T}{\partial z} = \frac{k}{\rho C_p}\left(\frac{\partial^2 T}{\partial x^2} + \frac{\partial^2 T}{\partial y^2}\right) + \frac{\eta \dot{\gamma}^2}{\rho C_p} \quad (6)$$

where ρ is the density, C_p the specific heat and k is the thermal conductivity. The fluid enters the screw channel at a temperature T_o and the barrel temperature is designated as T_b, which is different from the entrance temperature. Variations in T_b in the channel direction are allowed. The screw surface is assumed to be adiabatic. Since the velocity distribution can be determined , this parabolic problem can be solved in a stepwise fashion along the channel direction z. Equation 6 was solved with the above specified boundary conditions in (23) using the Bubnov-Galerkin method, and the removal of oscillations in the temperature solution was attempted by a simple smoothing procedure. Here we implement the recently developed SUPG method (which has rarely been implemented in polymer processing simulation) by introducing weighting functions of the form:

$$\bar{W} = W + w \quad (7)$$

where W is a continuous function of space and w is a discontinuous perturbation of W. The weak form of the energy equation is then given by:

$$\int_z^{z+\Delta z} \left\{ \int \left[W\left(u_x \frac{\partial T}{\partial x} + u_y \frac{\partial T}{\partial y} + u_z \frac{\partial T}{\partial z}\right) + \frac{k}{\rho C_p}(\nabla W \cdot \nabla T) - \frac{W \eta \dot{\gamma}^2}{\rho C_p} \right] dD \right.$$

$$\left. + \sum_i \int_{e_i} w\left[u_x \frac{\partial T}{\partial x} + u_y \frac{\partial T}{\partial y} + u_z \frac{\partial T}{\partial z} - \frac{k}{\rho C_p} \nabla \cdot \nabla T - \frac{\eta \dot{\gamma}^2}{\rho C_p} \right] d\Gamma_s \right\} dz = 0 \quad (8)$$

where the last integral is over element interiors. The shape functions are chosen to satisfy the boundary conditions on the barrel and must therefore vanish there.

The shape functions for the temperature are similar to those used for velocity in that they are linear in the space coordinates but the weighting function W has a quadratic variation in the z-coordinate to improve accuracy, while still retaining the linear form in x and y (22). Since the thermal problem is parabolic, the integration in z in Eq. 8 can be carried out independent of the other two directions producing a part with known values of T (a source term) and the other containing values of T being sought. At this point, the solution procedure adopted for the velocity equations can then be applied.

Several approaches have been suggested in the literature for the definition of the perturbation function for SUPG. We have followed the method outlined by Hughes et al. [25]. In this analysis, an element in the arbitrary domain x,y, and z can be mapped into an isoparametric element of unit dimension in each of the transformed co-ordinates ξ, χ, and ζ. An element mesh parameter can then be defined as

$$h^e = \frac{2\|u\|}{b} \quad (9)$$

where $\|u\|$ is the Euclidean norm of the velocities and b is given by

$$b^2 = \left(u_x \frac{\partial \xi}{\partial x} + u_y \frac{\partial \xi}{\partial y}\right)^2 + \left(u_x \frac{\partial \chi}{\partial x} + u_y \frac{\partial \chi}{\partial y}\right)^2 + \left(u_z \frac{\partial \zeta}{\partial z}\right)^2 \quad (10)$$

Hughes et al. (25) have suggested that the perturbation function be taken as:

$$w = \frac{\sigma h^e \beta^e}{2\|u\|} \underset{\sim}{u} \cdot \nabla W \quad (11)$$

where,

$$\beta^e = \coth \gamma^e - \frac{1}{\gamma^e} \qquad \text{and} \qquad \gamma^e = \frac{\rho C_p \|u\| h^e}{2k} \quad (12a, b)$$

A value of $\sigma = 1$ was used by Hughes et al. (25). However, our numerical experimentation revealed that the value of σ is dependent on such factors as the element skewness and the flow and heat transfer parameters. Here it is recommended that σ be adjusted until the solution is oscillation free. For the range of parameters considered in this study, the values of σ were between 0.3 and 0.4 and furnished satisfactory results.

RESULTS AND DISCUSSION

For the finite element solution of the conservation equations, the domain is discretized by bilinear elements and the discretized equations for u_x , u_y , u_z , and T in matrix form were solved by standard techniques. The typical geometry of the single screw extruder used in this study is shown in Fig. 1. The results to be presented (all in dimensionless form defined in Equations 1a-1c) were obtained based on the operating and processing conditions listed in Table 1. The operating conditions are in the range, which we typically utilize in our experiments on industrial scale extruders.

The effect of wall slip on the channel direction velocity u_z is illustrated in Fig. 2 for a positive pressure gradient ($dp_m/dz = 2.0$). The velocity distribution varies uniformly from the screw surface to the barrel for both conditions of wall stick (Fig. 2a) and wall slip. Wall slip greatly modulates the magnitude of the velocity with the maximum decreasing from 0.953 to 0.2097 upon wall slip. This is also true for other values of positive pressure gradient not reported here. As the value of dp_m/dz increases, a region of backflow appears, the strength and size of which increase with increased slip parameter. On the other hand, the wall slip enhances channel direction velocity for negative pressure gradient. The corresponding dimensionless temperature distributions at a down channel location of z = 0.5 are presented in Figs 3a-b. The effect of wall slip is essentially the shifting of the region of lowest temperature to approximately the center of the screw surface, thus ensuring that the fluid feels more uniformly the effect of the barrel temperature.

Figure 4a displays the effect of wall slip parameter and pressure gradient on the xy-cross sectional wall slip velocity distribution. The region AB represents the barrel surface while BA is the screw surface. For the slip coefficient considered, i.e. 0.01 to 1 and for all values of dimensionless pressure gradient dp_m/dz, the slip velocity on the screw surface is effectively zero. The maxima which occur at the two tips of the screw are due to the small gaps at those locations. On the barrel surface, the slip velocity increases as the slip parameter increases but exhibits no appreciable dependence on the pressure gradient, either positive or negative. On the other hand, the channel direction slip velocity is affected by both the slip parameter and the pressure gradient with a reversal in behavior occurring from a change from negative to positive pressure gradient (Fig 4b). Finally, in Fig.5, the effect of slip on the overall pressure drop versus the volume flow rate relationship is depicted for positive pressure gradient values. Generally, for the same pressure gradient, the flow rate is reduced by the occurence of slip and the reverse is obtained for negative pressure gradients.

CONCLUSION

A non-isothermal model of the single screw extrusion processing with wall slip has been developed using the Streamline Upwind /Petrov-Galerkin (SUPG) method. Wall slip reduces the capacity of pressurization and also tends to produce more uniform temperature distributions in the single screw channel. This model should generate a better predictive understanding of the single screw processing of viscoplastic materials subject to wall slip.

ACKNOWLEDGEMENTS

This study was sponsored by the Department of the Navy, Office of the Chief of Naval Research, for which we are grateful. The content of the information does not reflect the policy of the Government, and no official endorsement should be inferred.

REFERENCES

1. McKelvey, M.,"Polymer Processing," John Wiley, NY (1962).
2. Tadmor Z., and I. Klein, "Engineering Principles of Plasticating Extrusion, Robert Krieger Comp., NY (1978).
3. Mooney, M., *J. Rheology, 2* (1931) 210
4. Vand, V., *J. Phys. Colloid Chem., 52* (1948) 277.
5. Toms, B.,*J. Colloid Scl, 4* (1949) 511.
6. Cox , R., and S. Mason, *Ann. Rev. Fluid Mech., 3,* (1971) 291.
7. Yoshimura, A., and R. K. Prud'homme, *J. Rheol., 32* (1988) 53.
8. Cohen, Y., and A. B. Metzner, *J. Rheol., 25* (1985) 67.
9. Ramamurthy, A. V., *J. Rheology, 30* (1986) 337.
10. Yilmazer, U., and D. Kalyon, *J. Rheol., 33* (1989) 1197.
11. Hatzikiriakos, S.G., and J.M. Dealy, *J. Rheol., 35* (1991) 497.
12. Silliman, W.T., and L.E. Scriven, *J. Comp. Phys., 34* (1980) 287.
13. Schowalter, W.R., *J. Non-Newtonian Fluid Mech., 29* (1988) 25.
14. Nakazawa, S., Pittman, J.F.T., and O.C. Zienkiewicz, in "Finite Elements in Fluids," Volume 4, R. H. Gallagher, D. H. Norrie, J.T. Oder and O.C. Zienkiewicz, eds. (New York: John Wiley and Sons), 1982.
15. Colwell, R.E., and K.R. Nickolls, *Ind. Eng. Chem., 51* (1959) 841.
16. Griffith, R.M., *Ind. Eng. Chem. Fundam., 1* (1960) 180.
17. Kwon, T.H. , Jaluria, Y., Karwe, M.V. and T. Sastrohartono, in: A. I. Isayev (ed.), *Modeling of Polymer Processing (Recent Developments)*, Hanser Publishers (1991) 77.
18. Heinrich, J. C., and O.C. Zienkiewicz in: T.J.R. Hughes (ed.), "Finite Elements for Convection Dominated Flow, " ASME Publ. AMD, 34 (1979) 105.
19. Westink, J.J., and D. Shea, *Int. J. Numer. Methods Eng., 28* (1989) 1077.
20. Hughes, T.J.R., and A.N. Brooks, in "Finite Elements Methods for Convection Dominated Flows," T.J.R. Huges, ed., ASME Publication AMD, (1979) 34.
21. Brooks, A.N., and T.J.R. Hughes, *Comp. Methods Appl. Mech. Eng., 32* (1982) 199.
22. Yu, C.C., and J.C. Heinrich, *Int. J. Num. Methods in Eng., 24* (1987)2201.
23. Ji, Z., Gotsis, A.D., and D.M. Kalyon, *SPE Antec Technical Papers,* (1990) 160.
24. Papanastasiou, T.C., *J. Rheol., 31* (1987) 385.
25. Hughes, T.J.R., Mallet, M., and A. Mizukami, Comp. Methods in *Appl. Mech. Eng., 54* (1986) 341.

Table 1.

OPERATING AND PROCESSING CONDITIONS	
η = 1.0	Radius of barrel (R_b) = 2.54cm
τ_y = 0.05	Helix angle ø = 17.61°
n' = 80	ρ = 1400 kg/m^3
α = 1.0	C_p = 2000 J/kgK
Screw speed = 40 rpm	k = 0.27 W/mK

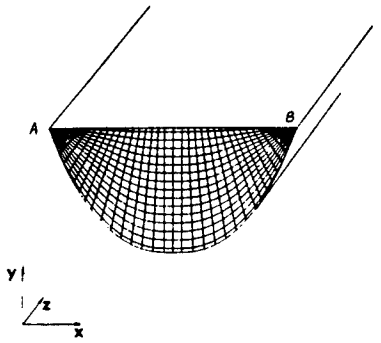

Figure 1: Finite element mesh for the computation of the velocity & temperature profiles.

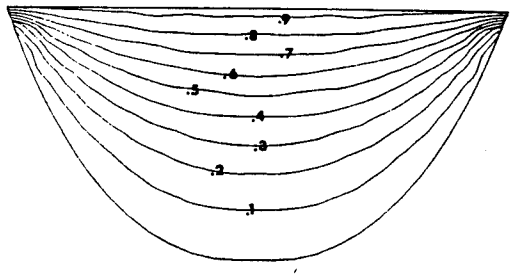

Figure 2a: Channel direction velocity distribution for wall stick condition (α =0 and dPm/dz=2.0)

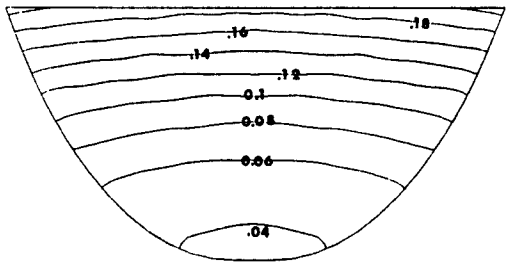

Figure 2b: Channel direction velocity distribution for wall slip condition (α=1.0 and dPm/dz= 2.0)

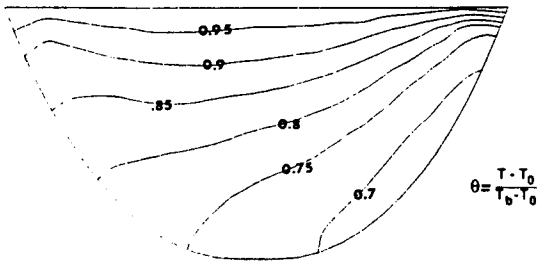

Figure 3a: Dimensionless temperature distribution at channel location z=0.5 for wall stick condition

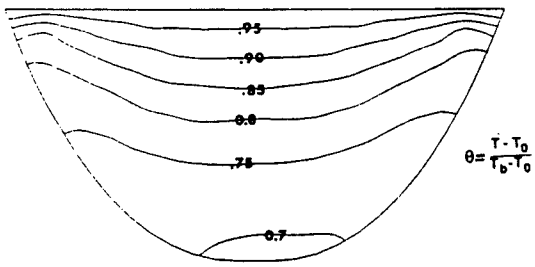

Figure 3b: Dimensionless temperature distribution at channel location z=0.5 for wall slip condition (α=1.0)

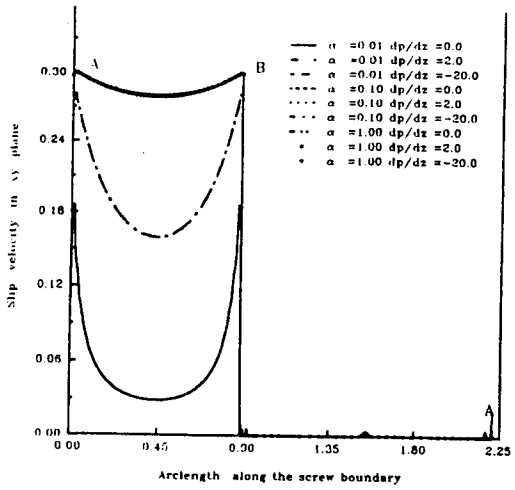

Figure 4a: Slip velocity distribution along the screw surface for different values of slip parameter and pressure drop

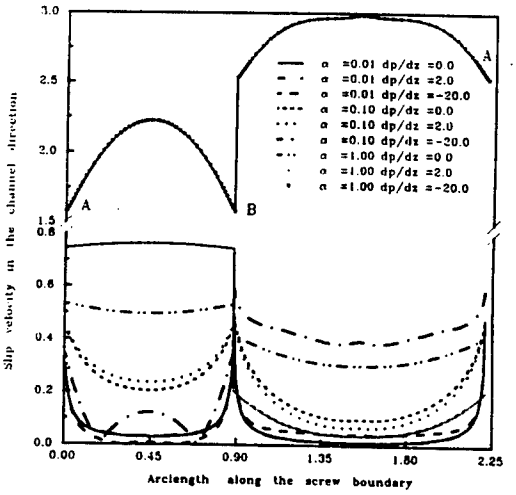

Figure 4b: Channel direction slip velocity along the screw surface for different values of slip parameter and pressure drop

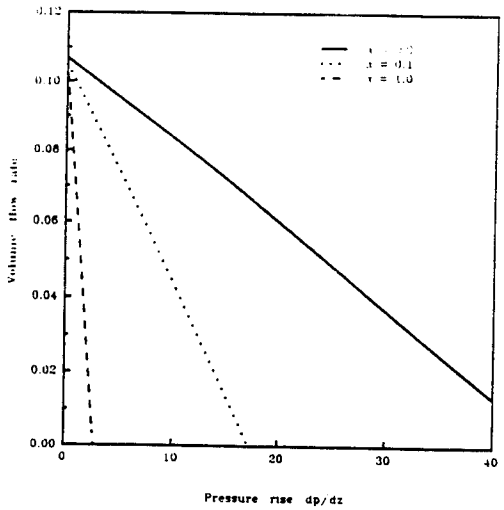

Figure 5: Pressure drop flow rate relationship for different values of slip parameter

A NON-ISOTHERMAL MODEL OF SINGLE SCREW EXTRUSION OF GENERALIZED NEWTONIAN FLUIDS

by

Adeniyi Lawal and Dilhan M. Kalyon

Highly Filled Materials Institute
Stevens Institute of Technology
Castle Point on the Hudson
Hoboken, NJ 07030

ABSTRACT

A non-isothermal model of the single screw extrusion processing of generalized Newtonian fluids is presented. Various temperature dependent forms of generalized Newtonian fluid constitutive equation representing the Herschel-Bulkley fluid and its simplifications including Bingham Plastic, Power law of Ostwald-de Waele and Newtonian fluids are applicable. The model includes the generally ignored transverse convection terms of the equation of energy. The importance of keeping the transverse convection terms in the analysis is demonstrated by applying the model and comparison of findings to experimental results involving the transverse flow temperature distributions in single screw extruders, available in the literature. The numerical instabilities, arising principally from the convection terms, generally encountered in high Peclet number extrusion flows could be eliminated by the use of the Streamline Upwind/Petrov-Galerkin formulation. The model is sufficiently general to accommodate Navier's wall slip at the wall boundary condition commonly encountered during the processing of gels, and concentrated suspensions.

INTRODUCTION

The single screw extruder is one of the most widely used continuous processors for conveying of solids, melting, pressurization, blending, reactive extrusion and compounding of a wide variety of materials. The experimental and/or simulation based knowledge gained over the years has helped our understanding of the single screw extrusion process and are summarized in various sources (1-5).

The numerical solution of flow and heat transfer of polymer melts is reviewed by Nakazawa et al. (6) along with the finite element solution of non-isothermal cavity flows of Ostwald-de Waele model fluids. The generally encountered highly viscous nature of processed materials implies significant viscous dissipation effects in single screw extrusion. Fenner investigated various solution methods available for the flow and deformation occurring in the single screw extruder and compared the findings against experimental results (2). The geometry of the single screw extruder is usually unwound in the channel direction and the curvature effects are neglected. Zamodits and Pearson (3) assumed the channel geometry to be rectangular but the effects of

the flight on the velocity distribution were ignored. Screw characteristic curves of volume flow rate versus pressure generated for different values of power law index were presented. Denson and Hwang, using the Finite Element Method, analyzed the flow in several actual channel geometries but the fluid was assumed to be Newtonian. An equation relating the throughput to the pressure rise was developed (5).

In the non-isothermal analysis of single screw extrusion, viscous dissipation and heat conduction in the direction of screw depth were the first effects to be considered (7). Subsequently, heat conduction in the transverse direction (8) and more recently, heat convection in the down channel direction (9) were included in the solution of the equation of energy. Overall, most non-isothermal simulation studies of single screw extrusion have ignored the transverse convection terms, possibly due to the fact that when both the channel direction and the transverse convection terms are retained and become dominant, the commonly utilized standard Bubnov-Galerkin method as well as its equivalent in the finite difference based methods (i.e. the central difference scheme), produces oscillations in the numerical solution. This numerical difficulty has long been recognized in the finite difference and finite element literature (10).

The standard technique for dealing with spurious oscillations associated with both spatial and temporal discretizations of first derivatives involves the addition of an artificial diffusion term in the numerical formulation (10). Artificial diffusion techniques for Galerkin finite element methods can be accomplished by using modified forms of weighting functions (Petrov-Galerkin) typically with test functions which are one degree higher than basis functions (11). The artificial diffusion term can also be incorporated by modifying the test functions by a perturbation, dependent upon the velocity field (12, 13), i.e. Streamline Upwind/Petrov-Galerkin (SUPG) method. For a parabolic problem, which may arise from time dependency (or in the case of steady state problems, from the existence of a predominant flow direction), the structure of SUPG method is only preserved if time-space elements are used (14). In the finite difference literature, the spurious oscillations are usually remedied by using a combination of central-difference and upwind-difference formulations for the first order derivatives (15), a procedure akin to the classical upwinding technique of the finite element method.

In the following, we present a new model of non-isothermal extrusion of generalized Newtonian fluids in single screw extruders. In the model, the generally ignored transverse convection terms of the equation of energy are included, in conjunction with the Streamline Upwind/Petrov-Galerkin formulation of the Finite Element Method. The modeling results are compared with the experimental results available in the literature to demonstrate the importance of keeping the transverse convection terms. The model also has the facility to include the Navier's wall slip boundary condition commonly encountered with a variety of fluids (16-22). Various simplifications of the Herschel-Bulkley viscoplastic fluid model, i.e., the Bingham Plastic, the Power-law fluid of Ostwald-de Waele and the Newtonian fluid can be accommodated.

ANALYSIS

Flow Equations

The governing equations of the flow in the single screw extruder are given by the general equations of conservation of mass and momentum, which are fully elliptic and three-dimensional. But the solution of the complete set of three-dimensional equations is unwarranted since experimental data indicate that certain simplifying assumptions can be made which will render the equations parabolic and therefore amenable to stepwise integration in the z-direction (primary flow direction) from prescribed upstream conditions. These assumptions are that:

(i) the inertia effect is negligible because of the highly viscous nature of the generally polymeric materials used in extrusion and the creeping nature of the resulting flow,
(ii) the flow is steady,
(iii) the screw channel can be unwound in a helical direction of the screw,
(iv) the velocity derivatives along the channel are small compared with those in the transverse directions except close to the entrance, and
(v) the barrel moves relative to the screw at an angle (i.e. the helix angle) to the down channel direction with a constant velocity given by the screw rotational speed and barrel diameter.

The parabolic flow analysis is followed and the following dimensionless variables are introduced:

$$x = R_s x^*, \; y = R_s y^*, \; z = R_s z^*, \; u = R_s \omega u^* \tag{1a}$$

$$\eta = m_o \omega^{n-1} \eta^*, \quad Q = R_s^3 \omega Q^* \tag{1b}$$

$$\bar{p} = m_o \omega^n \bar{p}^*, \quad p_m = m_o \omega^n p_m^* \tag{1c}$$

where R_s is the screw radius, ω is screw rotational speed, m_o and n are material parameters and Q is the volumetric flow rate. The equations of conservation of mass and momentum become:

$$\frac{\partial u_x}{\partial x} + \frac{\partial u_y}{\partial y} + \frac{\partial u_z}{\partial z} = 0 \tag{2}$$

$$\frac{\partial \bar{p}}{\partial x} = \frac{\partial}{\partial x}\left(2\eta \frac{\partial u_x}{\partial x}\right) + \frac{\partial}{\partial y}\left\{\eta\left(\frac{\partial u_x}{\partial y} + \frac{\partial u_y}{\partial x}\right)\right\} \tag{3a}$$

$$\frac{\partial \bar{p}}{\partial y} = \frac{\partial}{\partial y}\left(2\eta \frac{\partial u_y}{\partial y}\right) + \frac{\partial}{\partial x}\left\{\eta\left(\frac{\partial u_x}{\partial y} + \frac{\partial u_y}{\partial x}\right)\right\} \tag{3b}$$

$$\frac{dp_m}{dz} = \frac{\partial}{\partial x}\left(\eta \frac{\partial u_z}{\partial x}\right) + \frac{\partial}{\partial y}\left(\eta \frac{\partial u_z}{\partial y}\right) \tag{3c}$$

where the asterisk (*) denoting the dimensionless forms of the variables has been suppressed in the equations for convenience. The parabolic nature of these differential equations is preserved through p_m, the mean viscous pressure which has been defined for the primary flow direction, z, and is constant for any x-y plane. The down-channel direction pressure gradient, dp_m/dz, which is a function of the channel direction coordinate, z, for temperature dependent shear viscosity, is determined by the requirement that the conservation of mass constraint on the total volumetric flow rate is satisfied, i.e.:

$$Q - \int_D u_z dD = 0 \tag{4}$$

where Q is set by the specified inlet value of dp_m/dz. The pressure $\overline{p}$, is allowed to vary in the transverse directions in such a way that the continuity equation (Eq. 2) is satisfied. Even though u_z varies along the down-channel direction z, it is assumed in Eq. 2 that step sizes in z direction are so small that $\partial u_z/\partial z$ is negligible compared with the other two terms. Equations 3a-b can now be handled separately from the channel direction equation 3c and the penalty method is used in approximating the pressure $\overline{p}$.

Boundary Conditions and Implementation of Wall Slip

Applying Bubnov-Galerkin's method to Eqs. 3a-b leads to the following dimensionless residual equations:

$$\int_D \nabla\pi \cdot \underline{\underline{T}} dD - \int_{\Gamma_s} \pi(\mathbf{n} \cdot \underline{\underline{T}})\, d\Gamma_s = \mathbf{0} \qquad (5)$$

where π is the weighting function and $\underline{\underline{T}}$, the total stress tensor is as modified by the parabolic flow assumption. On the boundaries, the traction $\mathbf{n} \cdot \underline{\underline{T}}$ can be decomposed into the tangential and normal components to obtain:

$$\int_D \nabla\pi \cdot \underline{\underline{T}}\, dD - \int_{\Gamma_s} \pi(\mathbf{nt} : \underline{\underline{T}})\mathbf{t}\, d\Gamma_s - \int_{\Gamma_s} \pi(\mathbf{nn} : \underline{\underline{T}})\mathbf{n}\, d\Gamma_s = \mathbf{0} \qquad (6)$$

where **t** and **n** are respectively the unit tangent and unit outward normal vectors to the solid boundary. Eqs. 3a-b are required to be satisfied on the boundary. The conditions of wall slip and no material exchange between the fluid and the boundary in dimensionless form, can be expressed as:

$$\mathbf{t} \cdot (\mathbf{u} - \mathbf{u}_{solid}) = \beta^*(\mathbf{nt} : \underline{\underline{T}}) \qquad (7a)$$

$$\mathbf{n} \cdot (\mathbf{u} - \mathbf{u}_{solid}) = 0 \qquad (7b)$$

where $\mathbf{u}_s$ is the solid boundary velocity, **u** the fluid velocity, $\beta^* = (m_o\omega^{n-1}/R_s)\beta$ is the dimensionless Navier's slip coefficient, i.e., $\beta = 0$ gives no slip and $\beta = \infty$ is perfect slip. Eq. 7a is the Navier's slip condition as applicable to the two-dimensional transverse plane (23).

Referring now to Eq. 6, for the implementation of the boundary conditions, one observes that while the slip condition easily blends with it by providing the tangential component of the traction, the normal component presents a difficulty as it is not recoverable from the second condition Eq. 7b, which gives only the normal velocity. To resolve this, the essential condition of normal velocity is transformed into a mixed condition (24):

$$\mathbf{nt} : \underline{\underline{T}} = \frac{\mathbf{t} \cdot (\mathbf{u} - \mathbf{u}_{solid})}{\beta^*} \tag{8a}$$

$$\mathbf{nn} : \underline{\underline{T}} = \frac{\mathbf{n} \cdot (\mathbf{u} - \mathbf{u}_{solid})}{\lambda_s} \tag{8b}$$

where a new penalty parameter, λ_s, has been introduced. As $\lambda_s \rightarrow 0$, Eq. 8b becomes equivalent to Eq. 7b since the normal component of the traction must be finite at the boundary. In practice, a λ_s value in the range 10^{-10} - 10^{-18} produces a normal velocity difference of the same order of magnitude. Equations 8a-b are now substituted into Eq. 6 to give:

$$\int_D \nabla\pi \cdot \underline{\underline{T}} \, dD - \int_{\Gamma_s} \pi \frac{\mathbf{t} \cdot (\mathbf{u} - \mathbf{u}_{solid})}{\beta^*} \, \mathbf{t} \, d\Gamma_s - \int_{\Gamma_s} \pi \frac{\mathbf{n} \cdot (\mathbf{u} - \mathbf{u}_{solid})}{\lambda_s} \mathbf{n} \, d\Gamma_s = \mathbf{0} \tag{9}$$

For the channel direction momentum equation, the normal component of traction does not exist which makes the incorporation of wall slip by the Galerkin method straightforward. The components of $\mathbf{u}_{solid}$ on the screw root surface are all zero while on the barrel, the solid boundary velocity $\mathbf{u}_{solid}$, is given in dimensionless form as:

$$\mathbf{u}_{solid} = \mathbf{i} \sin\phi + \mathbf{k} \cos\phi \tag{10}$$

where ϕ is the helix angle of the screw and, $\mathbf{i}$ and $\mathbf{k}$ are unit vectors in x- and z-directions respectively.

Constitutive Model

The fluid is assumed to be a purely viscous fluid which can be characterized rheologically by the generalized Newtonian fluid constitutive relation:

$$\underline{\underline{T}} = -\eta(\dot{\gamma})\,\underline{\underline{\dot{\gamma}}} \tag{11}$$

where η is the shear viscosity material function, $\underline{\underline{\dot{\gamma}}}$ is the rate-of-deformation tensor, and $\dot{\gamma}$ is the deformation rate. The dependence of the shear viscosity material function on the deformation rate is assumed to follow the modified Herschel-Bulkley model, which for a temperature dependent viscosity is given by:

$$\eta = \left[m_o |\dot{\gamma}|^{n-1} + \frac{\tau_y (1 - \exp(-n_b |\dot{\gamma}|))}{|\dot{\gamma}|} \right] \exp(-c'(T - T_o)) \tag{12}$$

where n is a material parameter which governs the sensitivity of the fluid to deformation rate, τ_y, the apparent yield stress, n_b, a stress growth exponent, c′, the temperature coefficient of viscosity, with T_o, the entrance temperature as the reference temperature. The magnitude of the rate-of-deformation tensor $|\dot{\gamma}|$ is defined for our case, by:

$$|\dot{\gamma}|^2 = 2u_{x,x}^2 + 2u_{y,y}^2 + (u_{x,y} + u_{y,x})^2 + u_{z,x}^2 + u_{z,y}^2 \tag{13}$$

where comma indicates differentiation. If we introduce the following dimensionless variables:

$$|\dot{\gamma}| = \omega |\dot{\gamma}|^*, \tau_y = m_o \omega^n \tau_y^*, n_b = n_b^* / \omega \tag{14}$$

then Eq. 12, in dimensionless form, becomes:

$$\eta^* = \left[(|\dot{\gamma}|^*)^{n-1} + \frac{\tau_y^* (1 - \exp(-n_b^* |\dot{\gamma}|^*))}{|\dot{\gamma}|^*} \right] \exp(-c'(T - T_o)) \tag{15}$$

Various simplifications of the modified Herschel-Bulkley model include the Ostwald-de Waele power-law fluid ($\tau_y^* = 0$), the Newtonian fluid (n=1, $\tau_y^* = 0$), the modified Bingham plastic (Papanastasiou (25), (n=1)), and the classical Bingham plastic fluid above the yield point (n=1, $n_b^* = \infty$).

Energy Equation and Boundary Conditions

By an order-of-magnitude analysis of the energy equation, it can be demonstrated that in the single screw extruder, the importance of the transverse convection terms ($\rho C_p u_x \partial T/\partial x$, $\rho C_p u_y \partial T/\partial y$) relative to heat conduction in y-direction scales as $Pe\, u_x^* H^2/W$ where $Pe = \rho C_p \omega R_s^2/k$ is the Peclet number, and H and W are respectively, the dimensionless maximum depth and width of the screw channel. Polymeric liquids generally have low thermal conductivity and, moderately high values of ρ and C_p, hence high Peclet number. Therefore, the transverse convection term will be negligible only for small H and, large W (i.e. low aspect ratio geometries), and also for small helix angle. If the transverse convection term is compared with the down channel convection term, the transverse convection term will be negligible if the ratio $u_x^* z^* / u_z^* W$ is small, where u_x^* and u_z^* are dimensionless. From the continuity equation, and the choice of step size, u_z^* / z^* is small, hence transverse convection can be ignored only if W is very large or the helix angle very small, the same conditions as earlier obtained. Since these conditions are rarely used in the design and operation of realistic extruders, the transverse convection terms should be included in the energy equation for the analysis of extrusion flows.

By a similar analysis, the quantity $Pe\, u_z^* z^*$ governs the relative importance of the down channel convection to heat conduction in the down channel direction. Therefore, except for low volume flow rates, and the region very close to the entrance, one can neglect heat conduction in the down channel direction since the Peclet number is generally high. With these assumptions and the assumption of steady state conditions, using the dimensionless temperature $\theta = (T - T_o) / (T_b - T_o)$, the energy equation in dimensionless form becomes:

$$Pe\left(u_x\frac{\partial\theta}{\partial x}+u_y\frac{\partial\theta}{\partial y}+u_z\frac{\partial\theta}{\partial z}\right)=\left(\frac{\partial^2\theta}{\partial x^2}+\frac{\partial^2\theta}{\partial y^2}\right)+G\eta^*\left(|\dot\gamma|^*\right)^2 \qquad (16)$$

where $G=m_o\omega^{n-1}(\omega R_s)^2/k(T_b-T_o)$ is the Griffith number, (generally referred to as the Brinkmann number for the Newtonian fluid) and the asterisk (*) denoting the dimensionless forms has been suppressed for the velocity components and co-ordinates. The Griffith number indicates the relative importance of viscous dissipation effects to heat conduction.

The fluid enters the screw channel at a temperature T_o. The barrel temperature is designated as T_b, and is different from the entrance temperature. Variations in T_b along the channel direction are allowed. Although the model can be used in conjunction with any type of thermal boundary condition, we will restrict our demonstration here to the use of constant barrel temperature and adiabatic screw surface. Thus, in dimensionless form, the initial and boundary conditions become:

$$\begin{aligned} &\text{at } z = 0,\ \theta = 0 \\ &\text{on barrel surface } \theta = 1 \\ &\text{on screw surface } \partial\theta / \partial\mathbf{n} = \mathbf{0} \end{aligned} \qquad (17a\text{-}c)$$

where **n** is the unit vector normal to screw surface. Since the velocity distribution can be determined, this parabolic problem can be solved in a stepwise fashion along the channel direction, z. Equation 16 was solved with the above specified boundary conditions in (24) using the Bubnov-Galerkin method, and the removal of oscillations in the temperature solution was attempted by a simple smoothing procedure. Here we implement the recently developed SUPG method (12-14), (which has rarely been implemented in polymer extrusion simulation) by introducing weighting functions of the form:

$$\overline{W}^f = W^f + w^f \qquad (18)$$

where W^f is a continuous function of space and w^f is a discontinuous perturbation of W^f. The weighted residual form of the energy equation is then given by:

$$\int_z^{z+\Delta z}\left\{\int_D\left[\overline{w}^f Pe\left(u_x\frac{\partial\theta}{\partial x}+u_y\frac{\partial\theta}{\partial y}+u_z\frac{\partial\theta}{\partial z}\right)+\nabla\overline{w}^f\cdot\nabla\theta-\overline{w}^f G(|\dot{\gamma}|^*)^2\eta^*\right]dD\right.$$

$$\left.-\int_{\Gamma_s}\overline{w}^f(\nabla\theta\cdot\mathbf{n})d\Gamma_s\right\}dz=0 \qquad (19)$$

The shape functions are chosen to satisfy the boundary conditions on the barrel and must therefore vanish there.

Several approaches have been suggested in the literature for the definition of the perturbation function for SUPG. We have followed the method outlined by Hughes et al. (26). In this analysis, an element in the arbitrary domain x,y, and z can be mapped into an isoparametric element of unit dimension in each of the transformed serendipity coordinates ξ, χ, and ζ. An element mesh parameter can then be defined as

$$h^e = \frac{2||\mathbf{u}||}{b} \qquad (20)$$

where $||\mathbf{u}||$ is the Euclidean norm of the velocities and b is given by

$$b^2 = \left(u_x\frac{\partial\xi}{\partial x} + u_y\frac{\partial\xi}{\partial y}\right)^2 + \left(u_x\frac{\partial\chi}{\partial x} + u_y\frac{\partial\chi}{\partial y}\right)^2 + \left(u_z\frac{\partial\zeta}{\partial z}\right)^2 \qquad (21)$$

Hughes et al. (26) have suggested that the perturbation function be taken as:

$$w^f = \frac{\sigma h^e\varepsilon^e}{2||\mathbf{u}||}\mathbf{u}\cdot\nabla W^f \qquad (22)$$

where,

$$\varepsilon^e = \coth\gamma^e - \frac{1}{\gamma^e} \text{ and } \gamma^e = Pe||\mathbf{u}||h^e/2. \qquad (23a, b)$$

NUMERICAL SOLUTION

Flow Equations

For the finite element solution of the momentum equations, the domain is discretized by bilinear elements in x and y, and trial functions are chosen such that:

$$x^e = \sum_{i=1}^{Nod} x_i^e \pi_i^e(x,y) \qquad x_i^e, \pi_i^e \in D^e \qquad (24\ a, b)$$

where D^e is an element domain, Nod is the number of nodes per element, and π_i^e is the trial function with x^e representing the velocity vector. The discretized equations take the matrix form:

$$\underline{\underline{A}}\,\mathbf{x} = \mathbf{f} \qquad (25)$$

where $\underline{\underline{A}}$ is the stiffness matrix and **f** is a force vector resulting from specified nodal values or source term and the nodal unknowns are recovered from the vector **x**.

Energy Equation

The shape functions for the temperature are similar to those used for velocity in that they are linear in the space coordinates. The weighting function W^f has a trilinear dependence on the x-, y-, and z- coordinates. Since the thermal problem is parabolic, the integration in z in Eq. 16 can be carried out independent of the other two directions producing a part with known values of θ (source term) and the other containing values of θ being sought. At this point, the solution procedure adopted for the velocity equations can then be applied.

The element mesh parameter h^e , and the cell Peclet number γ^e in Eqs. 20 and 23 were evaluated based on the velocity at the centroid of the element. A value of $\sigma = 1$ in Eq. 22 was suggested by Hughes et al. (26). However, our numerical experimentation revealed that the value of σ is dependent on such factors as the element skewness and the flow and heat transfer parameters. Here it is recommended that σ be adjusted until the solution is oscillation free. For the range of parameters considered in this study, the values of σ were between 0.5 and 3.0 and furnished satisfactory results.

Solution Procedure

At the inlet of the channel, the temperature distribution is known, hence only the x-, y-, and z- velocity components are computed, based on a specified value of the inlet pressure gradient dp_m^*/dz^*. The Picard iteration (27) is then utilized for the shear rate dependent shear viscosity. After convergence, the volumetric flow rate is calculated. We proceed down the channel and as a first step, solve for the temperature distribution. With a viscosity distribution based on this temperature profile and the value of dp_m^*/dz^* at the previous channel location, for the second step, we solve for the velocity components and calculate the volumetric flow rate. A new value of dp_m^*/dz^* is obtained using the secant method with the residual taken as the difference between the calculated volumetric flow rate and that obtained at the inlet. This completes the second step which is repeated until convergence on account of shear rate dependent shear viscosity.

Subsequently, we solve for a new temperature distribution and go back to the second step since the shear viscosity material function is temperature dependent. This iterative procedure is continued until the volumetric flow rate constraint (Eq. 4) is satisfied and simultaneously, the Euclidean norms of the difference between successive iterates of $\mathbf{u}$, and θ are small, usually $\leq 10^{-3}$. Another step size is taken with the values of the variables at the previous channel location serving as the initial guesses. Convergence on the inner iteration for shear rate dependent shear viscosity is usually achieved in 4 to 8 iterations while the outer Picard iteration on account of the temperature coefficient of viscosity may require up to 10 iterations, with both values

depending on the channel location and the value of the temparature coefficient of viscosity. When the backflow is significant but not severe, the SUPG method provides reliable and accurate results when compared with the upwind marching scheme of finite difference but the required number of iterations goes up slightly. The allowable step size Δz, is dictated by the stability of the discretized temperature equation which is dependent on the thermal and flow parameters. The dimensionless step size used in this study is 1.0.

RESULTS AND DISCUSSION

The code was initially tested by comparison of the well-known results available in the literature for the square cavity flow of a Newtonian fluid in conjunction with the no-slip at the wall boundary condition. As indicated in Fig. 1a, excellent agreement was found between our results and the velocity profiles reported by Burggraf (28). Furthermore, the difference between our computed volume flow rate and that predicted by the empirical characteristic equation of Denson and Hwang (5) for a single screw extruder was less than 5% for a wide range of pressure rise values (Fig. 1b). In Fig. 1c, the temperature distribution along the center-line of the channel for a temperature dependent shear viscosity fluid as predicted numerically by Gopalakrishna et al. (29) for a parallel-plate geometry without the transverse convection terms, is compared with our computed results, also ignoring the transverse convection terms. It is observed that the agreement is indeed very good, the slight difference between the results can be attributed to the fact that our results are based on the actual geometry of the single screw extruder with the curvature included to give rise to slightly higher velocity gradients and consequently greater viscous dissipation effects than the simplified parallel plate based calculations of Gopalakrishna et al. (29). Other essential parts of the code have been similarly compared with numerical results available in the literature to arrive at an optimum element size distribution for accurate numerical predictions. However, experimental results are necessary to validate the model.

The only experimental study which was aimed at determining the temperature distribution in the extruder was carried out by Esseghir and Sernas (30,31), who obtained experimental results of temperature distribution along the center-line of the channel of a single screw extruder. The double flighted screw

element used had a diameter of 30.6mm, channel depth of $0.31R_S$, depth to width ratio of 0.40, a helix angle of 16.2° and a pitch of 28mm. There were three heat transfer sections along the axis of the barrel with the barrel temperature in each section maintained at a constant value. The fluid used was a corn syrup with a temperature dependent shear viscosity, the rheological and thermophysical properties of which were determined (30,31).

The first set of experimental temperature measurements chosen for comparison (Fig. 2) were obtained with the first barrel section maintained at 22°C, the same temperature as that of the fluid at the inlet of the extruder. The solid/fluid interface temperatures at the second and third sections were kept at 11.9°C. In the second set of temperature measurements, results of which are shown in Fig. 3a, the barrel wall temperatures for all the three heat transfer sections were maintained at 12.2°C, while the inlet temperature of the fluid was 20.3°C. On the basis of the geometrical parameters of the screw element, a finite element mesh was constructed. The required dimensionless parameters in the equations of conservation of mass, momentum, and energy were obtained from the operating conditions, thermophysical and rheological properties. For both experimental runs, the value of $Peu_x^* H^2/W$ was determined to be approximately 120, which suggests that transverse convection term may not be negligible. Figures 2 and 3a show the comparison between the predicted and experimental temperature distributions with the origin as the screw root when the transverse convection terms are included in the energy equation. The agreement is excellent and the differences are within typical experimental and numerical error ranges. Furthermore, the temperature distributions confirm that the adiabatic condition at the screw root is appropriate.

If the transverse convection terms in the equation of energy were neglected, Figs. 2 and 3a also indicate that the numerical predictions would be grossly in error. Therefore, this simple experiment demonstrates that the commonly employed assumption of negligible transverse convection in single screw extrusion may be inappropriate. Of course, for a sufficiently long extruder and, negligible viscous dissipation, as we approach the exit, all the temperature values will approach that at the wall. This explains why the difference in temperature values between the predictions with and without transverse convection terms in the second experiment at z^* of 48. is less than that for the

first experiment at z^* =20. When the model predictions are compared for the second experiment at z^* of 20., Fig. 3b shows a greater difference between the predicted temperature values with and without transverse convection terms. On the other hand, the corresponding experimental values of the total pressure generated in the extruder for the two experimental runs were 21.0 and 20.4 bars while the numerical predictions are 15.4 and 16.3 bars respectively. This agreement should be considered to be satisfactory noting that the experimental operating conditions and, the geometry of the extruder were such that the volume flow rate versus pressure gradient relationship exhibits a steep slope. A 5% experimental error in volume flow rate would account for the differences obtained and, errors of this magnitude in volume flow rate measurements are not unexpected considering the method of acquisition of the data (31).

Since the Peclet number (3500) for the experimental conditions used (30,31) is not high enough, the use of upwinding was not necessary. However, for high Peclet numbers, the use of upwinding may be necessary. For example, with the Peclet number at 28,000, Figs. 4a-b show that the temperature distributions obtained with and without the use of SUPG method are totally different. This value of Pe is based on the operating conditions and physical properties of Table 1, which are in the range we typically utilize in our own experiments on industrial scale extruders. The unwound screw channel profile is that of a screw element (Baker-Perkins 50.8mm machine) with a channel depth of $0.44R_S$ and depth to width ratio of 0.5. It is obvious that at this Peclet number, the numerical predictions without SUPG are inaccurate since the dimensionless temperature not only oscillates but also violates the physics of the problem which precludes a temperature value less than that at the inlet (θ_o = 0.0). Such negative values of temperature have also been reported elsewhere, (32), when the central difference scheme (the equivalent of Bubnov-Galerkin method) is implemented in the discretization of the convection terms of the energy equation. When the Peclet number is increased to 2.8×10^5, the temperature oscillations become more pronounced without the use of SUPG as evidenced from Figs. 5a-b. All the results to be presented in the next section pertain to the conditions in Table 1 and other necessary parameters are specified in the figures.

The model can be used to assess the importance of wall slip on development of temperature distributions in extrusion flows. The effects of the

slip parameter on the dimensionless temperature distribution are depicted in Figs. 6a-b. At the down channel location of $z^* = 20.0$, the value of the minimum dimensionless temperature within the channel decreases as the slip parameter, β^*, increases. Wall slip essentially reduces the local temperature. The corresponding channel direction velocity distributions are shown in Figs. 7a-b. For the same volume flow rate, as the slip parameter increases, the size and strength of the backflow region, and the maximum downchannel fluid velocity decrease.

The development of the dimensionless pressure gradient along the channel, presented in Fig. 8, shows that at any channel location, the pressure gradient generated decreases as the slip parameter increases for a fixed volume flow rate. Wall slip reduces the velocity gradients thereby reducing the pressure gradient. In addition, very close to the entrance region, the high velocity gradients result in an increase in the pressure gradient. Subsequently, a decrease in viscosity arising from the temperature rise accounts for the decrease of the pressure gradient down the channel.The effect of the velocity gradient reduction on the temperature development will be, as expected, to decrease the viscous dissipation effects and hence result in lower dimensionless bulk temperature. This is confirmed by the results in Fig. 9 which show a decreased value of dimensionless bulk temperature, θ_b, as the slip parameter increases, which was also suggested by the temperature profiles reported in Figs. 6a-b.

CONCLUSION

A non-isothermal model of the single screw extrusion processing of generalized Newtonian fluids which includes the transverse convection terms in the energy equation has been developed using the Streamline Upwind/Petrov-Galerkin (SUPG) method. The numerical predictions of the code are in excellent agreement with experimental temperature measurements and other numerical results available in the literature. The capabilities of the model were also demonstrated by investigating the effect of the wall slip boundary condition, commonly observed with a variety of materials including gels and concentrated suspensions. This model should provide a better predictive understanding of the single screw extrusion process.

ACKNOWLEDGMENTS

This study has been sponsored by the Department of the Navy, Office of the Chief of Naval Research, and partially by Exxon Education Foundation, for which we are grateful. The content of the information does not necessarily reflect the position or the policy of the Government. Portions of the FEM Source Code utilized were prepared by Dr. A. Gotsis and Dr. Z. Ji of HFMI.

REFERENCES

1. M. McKelvey, Polymer Processing, John Wiley, NY, 1962.
2. T. R. Fenner, "Melt Flow in Polymer Extrusion Equipment," Ph.D. Thesis, University of London, 1969.
3. H. J. Zamodits, and J. R. A. Pearson, Flow of polymer melts in extruders, Part 1., The effect of transverse flow and of a superposed steady temperature profile, *Trans. Soc. Rheol., Vol. 13*, pp. 357- 385, 1969.
4. Z. Tadmor, and I. Klein, Engineering Principles of Plasticating Extrusion, Robert Krieger Comp., NY, 1978.
5. C. D. Denson, and B. K. Hwang, The Influence of the Axial Pressure Gradient on Flow Rate for Newtonian Liquids in a Self Wiping, Co-Rotating Twin Screw Extruder, *Polym. Eng. Sci., Vol. 20* , pp. 965-971, 1980.
6. S. Nakazawa, J. F. T. Pittman, and O.C. Zienkiewicz, Finite Elements in Fluids, Vol. 4, pp. 251-283, R. H. Gallagher, D. H. Norrie, J.T. Oden and O.C. Zienkiewicz, eds. (New York: John Wiley and Sons), 1982.
7. R. E. Colwell, and K.R. Nicholls, The Screw Extruder, *Ind. Eng. Chem., Vol. 51*, pp. 841-843, 1959.
8. R. M. Griffith, Fully developed flow in single screw extruders, *Ind. Eng. Chem. Fundam., Vol. 1*, pp. 180- 187, 1962.
9. T. H. Kwon, Y. Jaluria, M. V. Karwe, and T. Sastrohartono, *Modeling of Polymer Processing (Recent Developments)*, pp. 77-115, A. I. Isayev (ed.), Hanser Publishers, 1991 .
10. J. C. Heinrich, and O.C. Zienkiewicz, Finite Elements Methods for Convection Dominated Flows, AMD *Vol. 34*, pp. 105-136, T.J.R. Hughes (ed.), ASME Publ., 1979.
11. J. J. Westink, and D. Shea, Consistent Higher Degree Petrov-Galerkin Methods For The Solution Of The Transient Convection-Diffusion Equation, *Int. J. Numer. Methods Eng., Vol. 28* , pp. 1077-1101, 1989.
12. T. J. R. Hughes, and A.N. Brooks, Finite Elements Methods for Convection Dominated Flows, AMD Vol. 34, pp. 19-36, T.J.R. Hughes (ed.), ASME Publ., 1979.
13. A. N. Brooks, and T.J.R. Hughes, Streamline upwind/Petrov-Galerkin Formulations for convection dominated flows with particular emphasis on the incompressible Navier-Stokes equations, *Comp. Methods Appl. Mech. Eng., Vol. 32* , pp. 199- 259, 1982.

14. C. C. Yu, and J.C. Heinrich, Petrov-Galerkin Method for Multidimensional, Time-Dependent, Convective-Diffusion Equations, *Int. J. Num. Methods in Eng., Vol. 24* , pp. 2201- 2215, 1987.
15. S. V. Patankar, and D. B. Spalding, A Calculation Procedure for Heat, Mass and Momentum Transfer in Three-dimensional parabolic Flows, Int. J. Heat and Mass Transfer, *Vol.* 15, pp.1787-1806, 1972.
16. M. Mooney, Explicit Formulas For Slip And Fluidity, *J. Rheology, Vol. 2,* pp. 210- 222, 1931.
17. D. M. Kalyon, P. Yaras, B. Aral, and U. Yilmazer, Rheological behavior of a concentrated suspension: A solid rocket fuel simulant, *J. Rheology, Vol. 37,* pp. 35-53, 1993.
18. Y. Cohen, and A. B. Metzner, Apparent Slip Flow of Polymer Solutions, *J. Rheol., Vol. 25,* pp. 67-102, 1985.
19. A. V. Ramamurthy, Wall slip in Viscous fluids and influence of materials of construction , *J. Rheology, Vol. 30,* pp. 337- 357, 1986.
20. U. Yilmazer, and D. M. Kalyon, Slip effects in Capillary and Parallel disk Torsional flows of Highly Filled Suspensions, *J. Rheol., Vol. 33,* pp. 1197-1212, 1989.
21. S. G. Hatzikiriakos, and J.M. Dealy, Wall slip of molten high density polyethylene. I. Sliding plate rheometer studies, *J. Rheol., Vol. 35,* pp. 497-523, 1991.
22. W. R. Schowalter, The Behavior of Complex Materials at Solid boundaries, *J. Non-Newtonian Fluid Mech., Vol. 29,* pp. 25-36, 1988.
23. W. T. Silliman, and L.E. Scriven, Separating Flow Near a Static Contact Line: Slip at a Wall and Shape of a Free Surface, *J. Comp. Phys., Vol. 34,* pp. 287-313, 1980.
24. Z. Ji, A. D. Gotsis, and D.M. Kalyon, Single Screw Extrusion Processing of Highly Filled Suspensions Including Wall Slip, *SPE ANTEC Technical Papers, Vol. 36,* pp. 160- 163, 1990.
25. T. C. Papanastasiou, Flows of materials with yield, *J. Rheol., Vol. 31,* pp. 385- 404, 1987.
26. T. J. R. Hughes, M. Mallet, and A. Mizukami, A New Finite Element Formulation For Computational Fluid Dynamics: II. Beyond SUPG, *Comp. Methods in Appl. Mech. Eng., Vol. 54,* pp. 341-355, 1986.
27. F. B. Hildebrand, Advanced Calculus for Applications, 2nd edition, Prentice-Hall, Inc., Englewood Cliffs, New Jersey, pp. 105, 1976.

28. O. R. Burggraf, Analytical and numerical studies of the structure of steady separated flows, *J. Fluid Mech., Vol. 24*, pp. 113-151, 1966.
29. S. Gopalakrishna, M. Karwe, and Y. Jaluria, Numerical Methods in Industrial Forming Processes- NUMIFORM 89, Thompson, Zienkiewicz and Samuelson, eds., pp. 265-270, 1989.
30. M. Esseghir, and V. Sernas, A Cam-Driven Probe for Measurement of the Temperature Distribution in an Extruder Channel, *SPE ANTEC Technical Papers, Vol. 37*, pp. 54-57, 1991.
31. M. Esseghir, "An Experimental Investigation of the Transport Phenomena in Single and Twin Screw Extruders," Ph. D. Thesis, Rutgers, The State University of New Jersey, 1991.
32. P. M. Gresho, and R. L. Lee, Finite Elements Methods for Convection Dominated Flows, AMD *Vol. 34*, pp. 37-61, T.J.R. Hughes (ed.), ASME Publ., 1979.
33. Richtmeyer, R.D., and K.W. Morton, Difference Methods for Initial Value Problems, Wiley, New York, 1967.

Table 1

OPERATING CONDITIONS AND PROPERTIES	
$\tau_y^* (\tau_y/(m_o\omega^n)) = 0.05$ (dimensionless)	Radius of barrel (R_s) = 0.025m
$n_b^* (n_b\omega) = 80$ (dimensionless)	Helix angle ø = 17.61°
$\omega = 4.2\ s^{-1}$	$\rho = 1400\ kg/m^3$
$\tau_y = 6{,}650.$ Pa	$C_p = 2000$ J/kgK
$m_o = 35{,}000.$ Pa-s	k = 0.27 W/mK
n = 1.0	$c'(T_b-T_o)=2.0$
Pe = 28,000.	G = 14.51

List of Figures

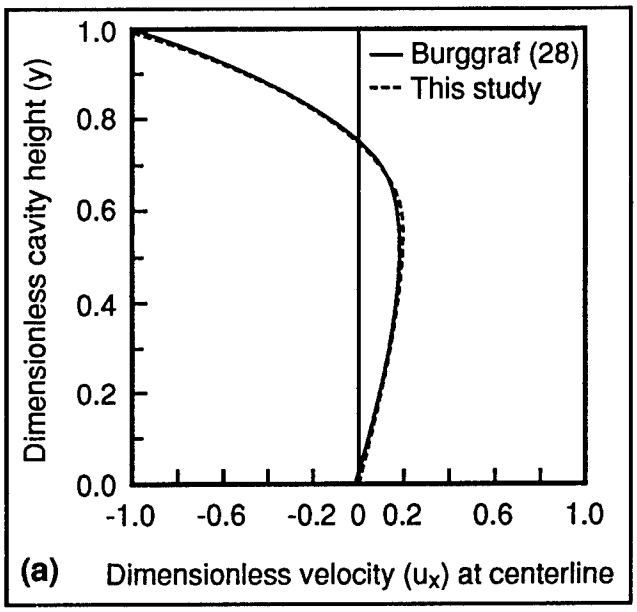
1.0
0.8
0.6
0.4
0.2
0.0
Dimensionless cavity height (y)
— Burggraf (28)
--- This study
-1.0 -0.6 -0.2 0 0.2 0.6 1.0
(a) Dimensionless velocity (u_x) at centerline

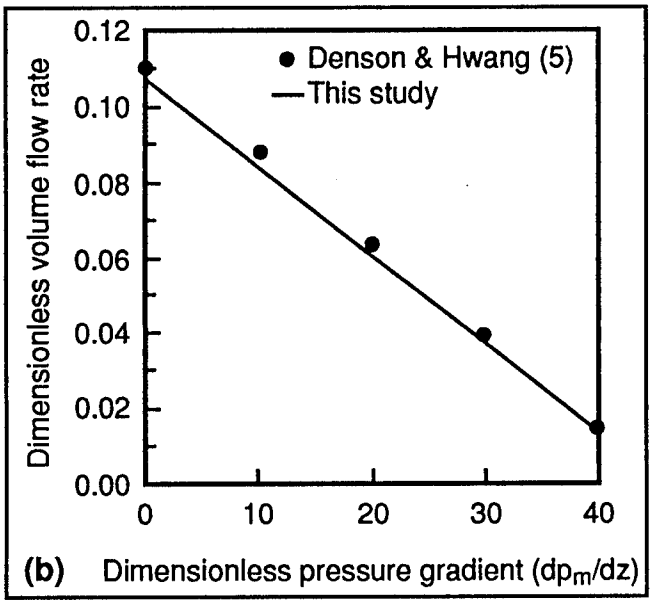
0.12
0.10
0.08
0.06
0.04
0.02
0.00
Dimensionless volume flow rate
● Denson & Hwang (5)
—This study
0 10 20 30 40
(b) Dimensionless pressure gradient (dp_m/dz)

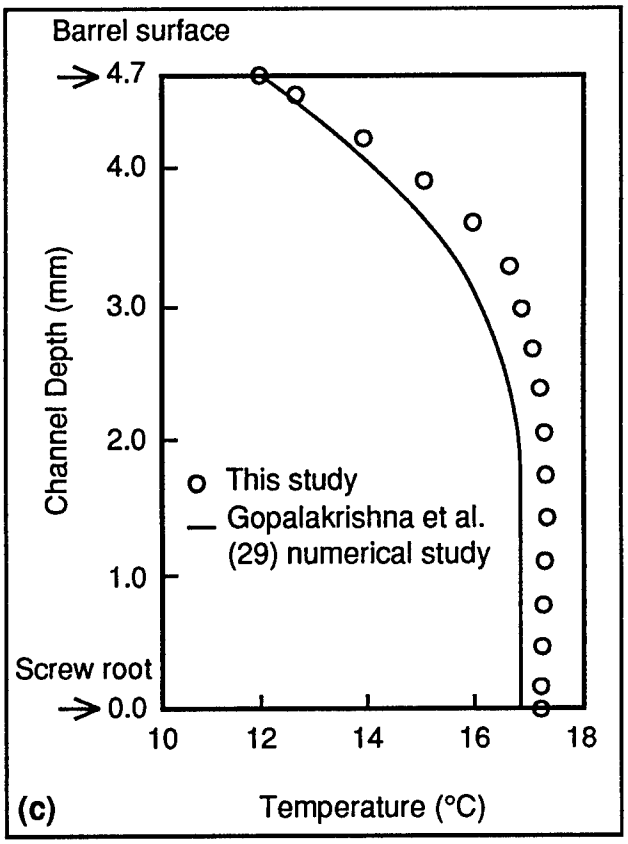
Barrel surface
4.7
4.0
3.0
2.0
1.0
Screw root
0.0
Channel Depth (mm)
o This study
— Gopalakrishna et al. (29) numerical study
10 12 14 16 18
(c) Temperature (°C)

Figure 1

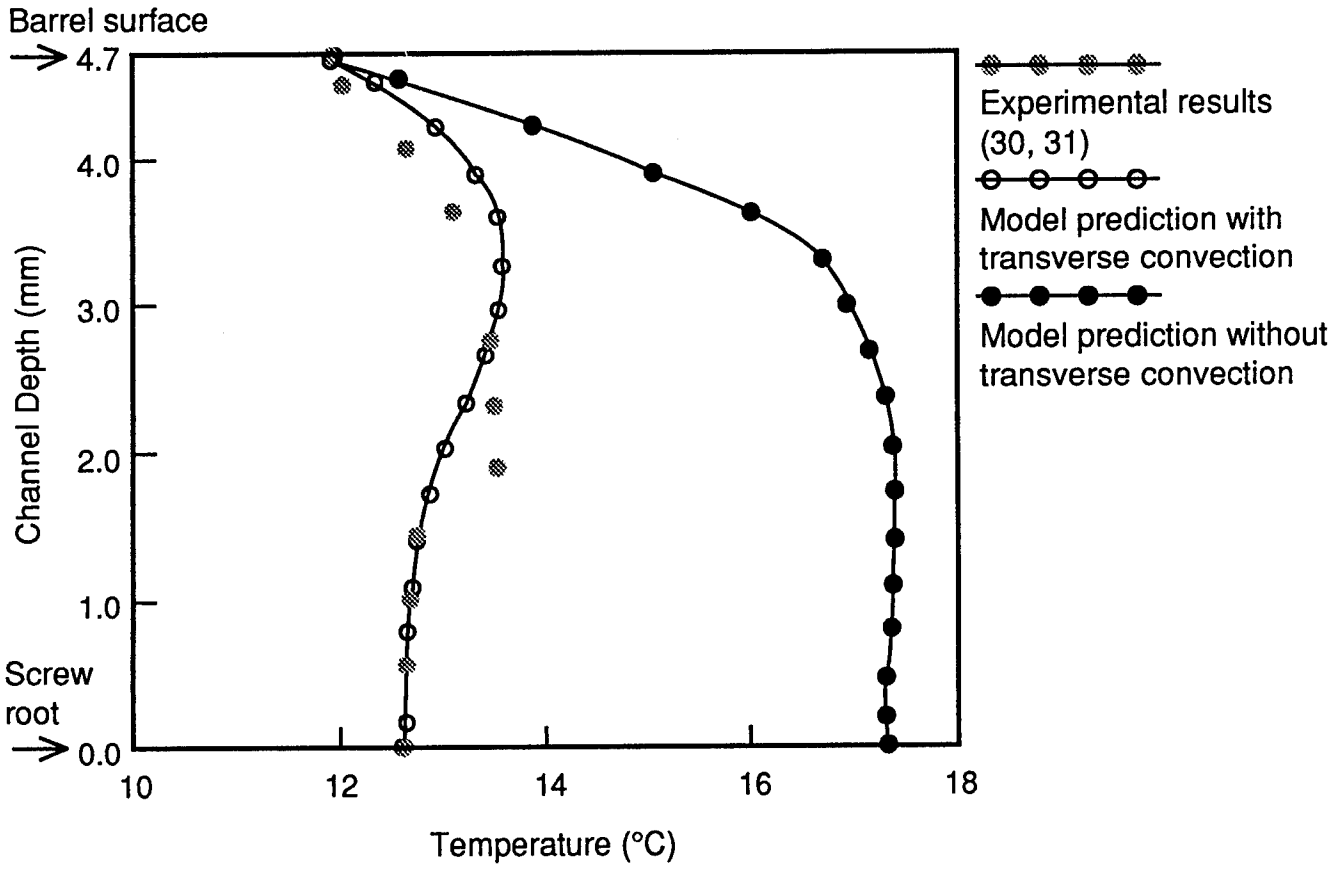
Barrel surface
4.7
4.0
3.0
2.0
1.0
Screw root
0.0
Channel Depth (mm)
10
12
14
16
18
Temperature (°C)
Experimental results (30, 31)
Model prediction with transverse convection
Model prediction without transverse convection

Figure 2

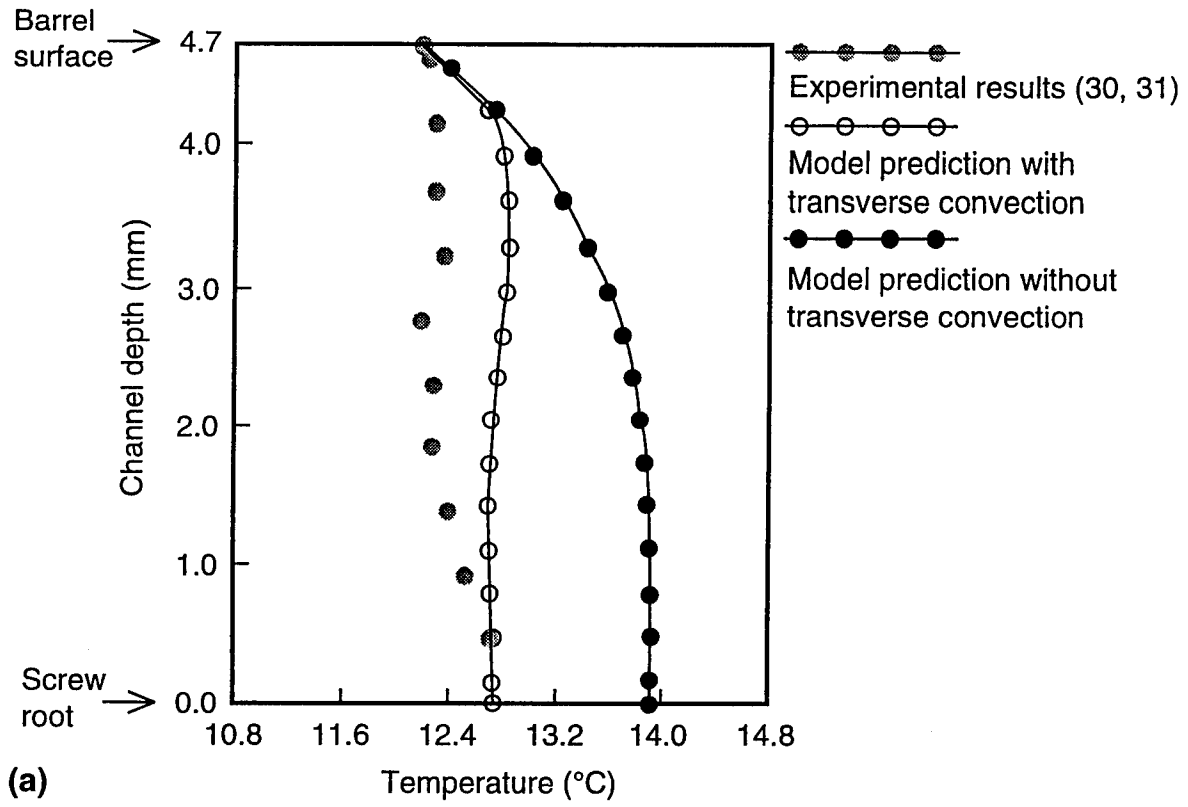
Barrel surface
Screw root
Channel depth (mm)
4.7
4.0
3.0
2.0
1.0
0.0
10.8
11.6
12.4
13.2
14.0
14.8
Temperature (°C)
Experimental results (30, 31)
Model prediction with transverse convection
Model prediction without transverse convection

(a)

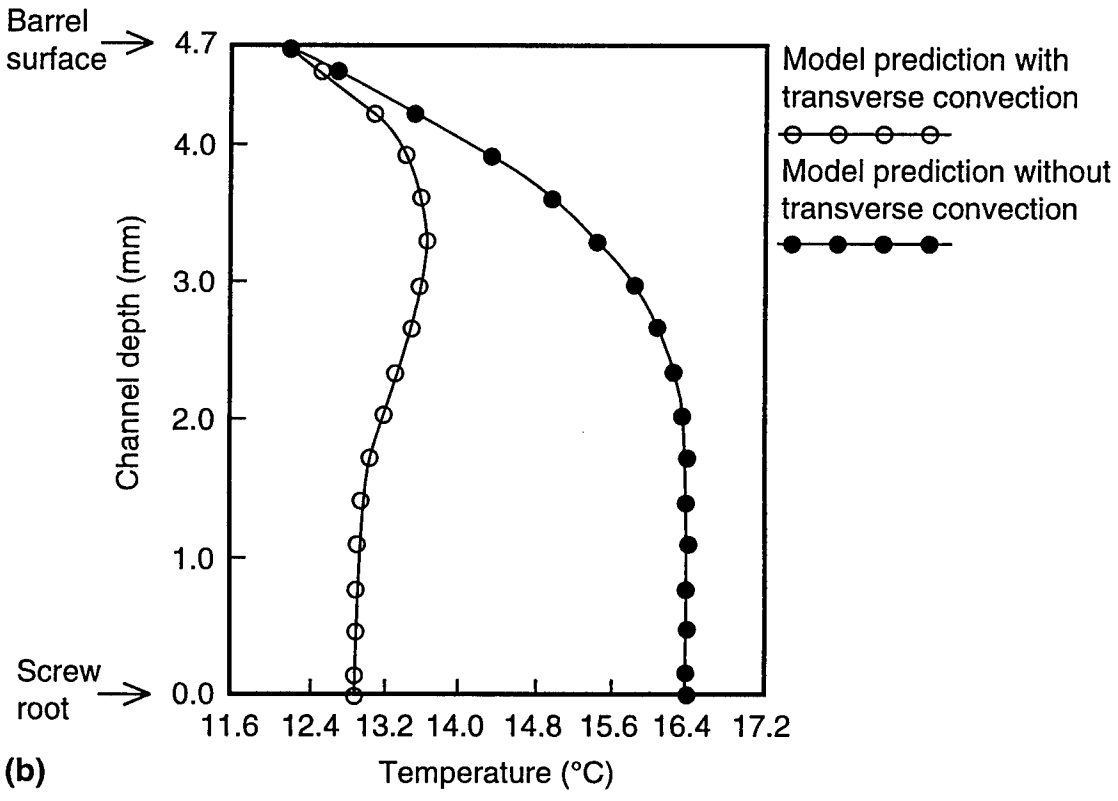
Barrel surface
Screw root
Channel depth (mm)
4.7
4.0
3.0
2.0
1.0
0.0
11.6
12.4
13.2
14.0
14.8
15.6
16.4
17.2
Temperature (°C)
Model prediction with transverse convection
Model prediction without transverse convection

(b)

Figure 3

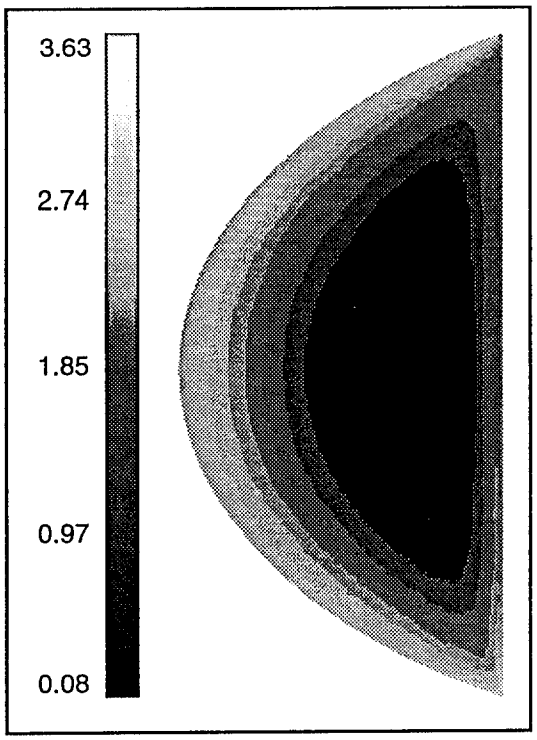

(a)

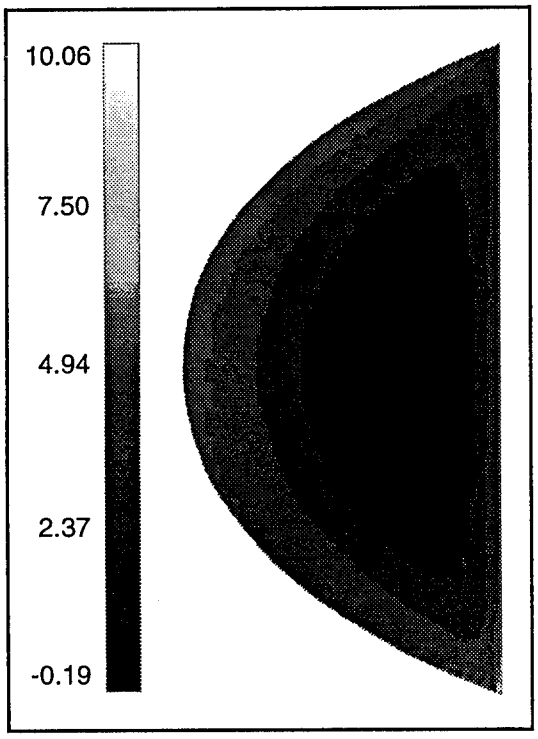

(b)

Figure 4

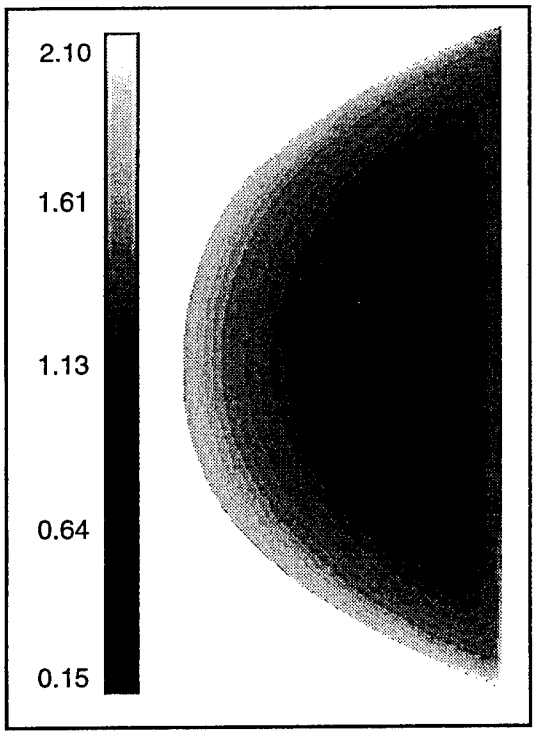

(a)

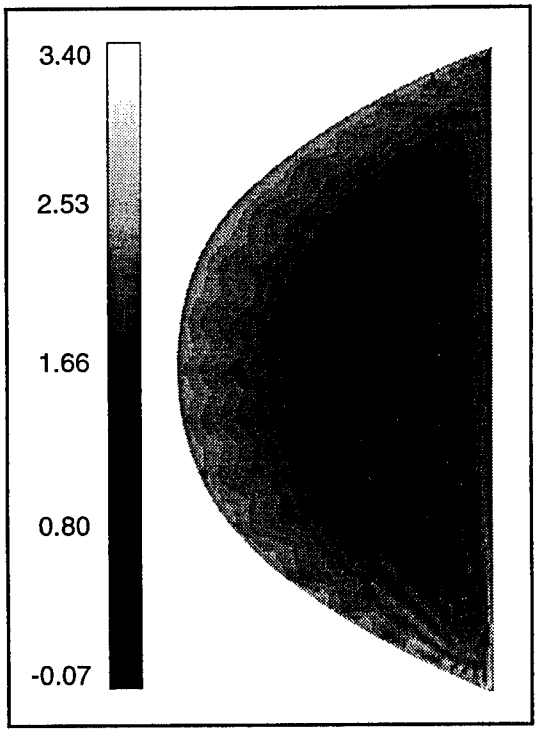

(b)

Figure 5

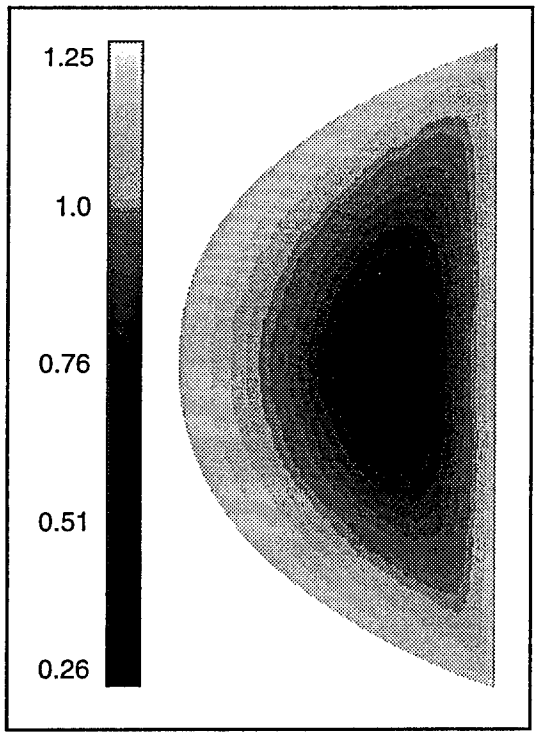

(a)

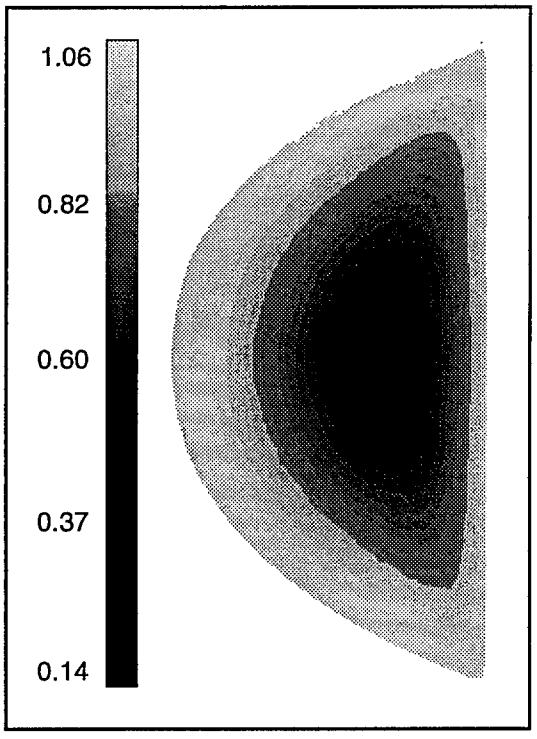

(b)

Figure 6

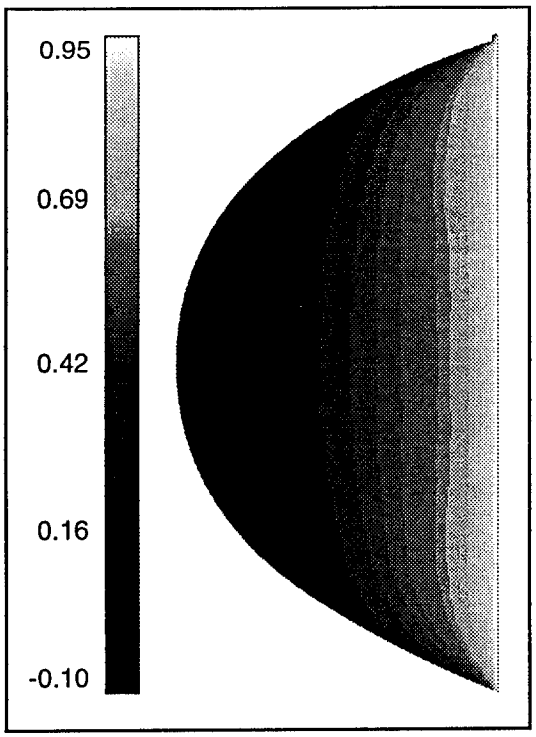

(a)

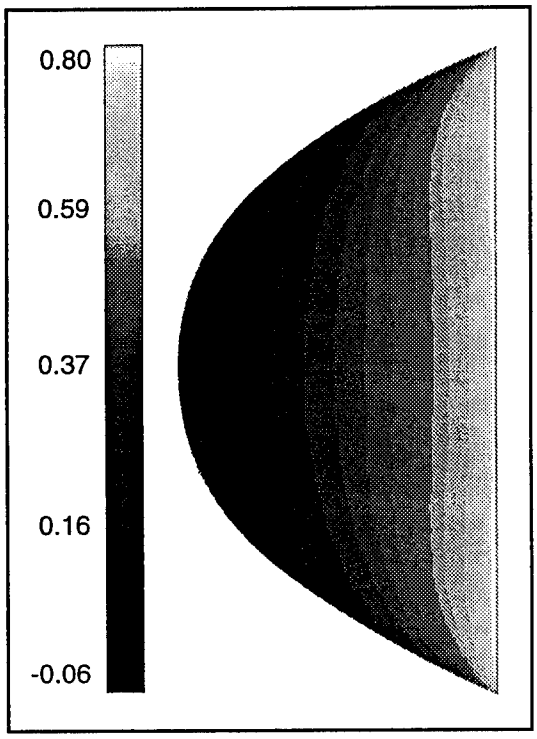

(b)

Figure 7

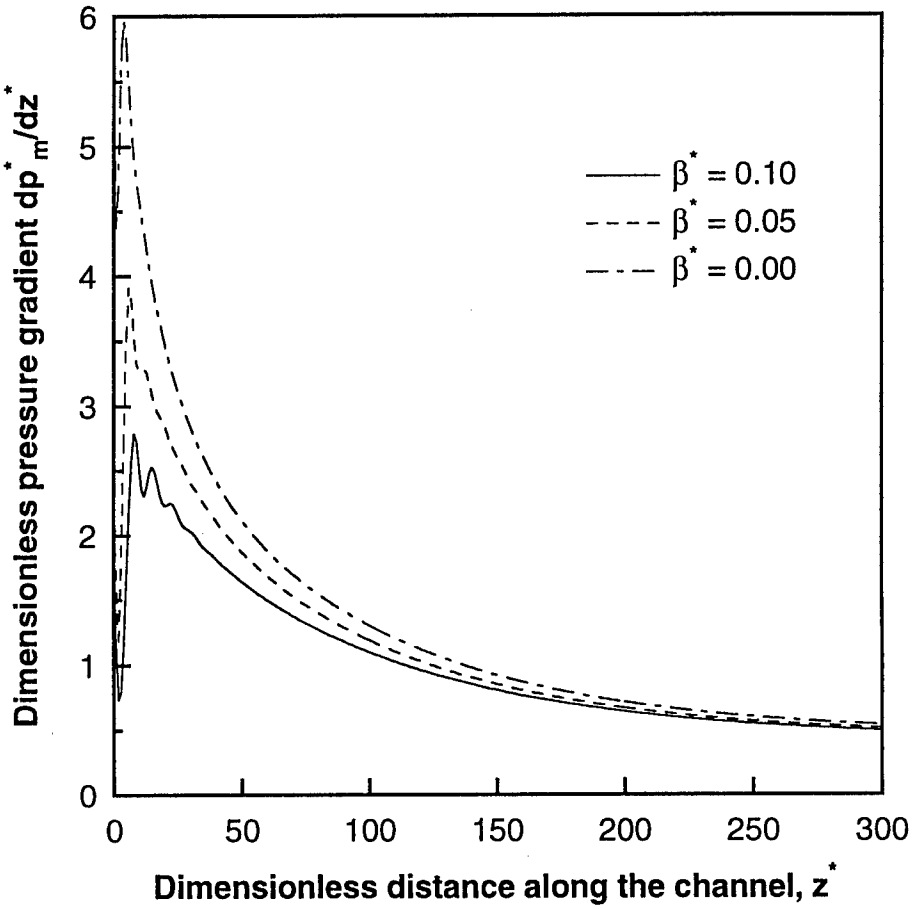
Dimensionless pressure gradient dp^*_m/dz^*
6
5
4
3
2
1
0
0
50
100
150
200
250
300
Dimensionless distance along the channel, z^*
$\beta^* = 0.10$
$\beta^* = 0.05$
$\beta^* = 0.00$

Figure 8

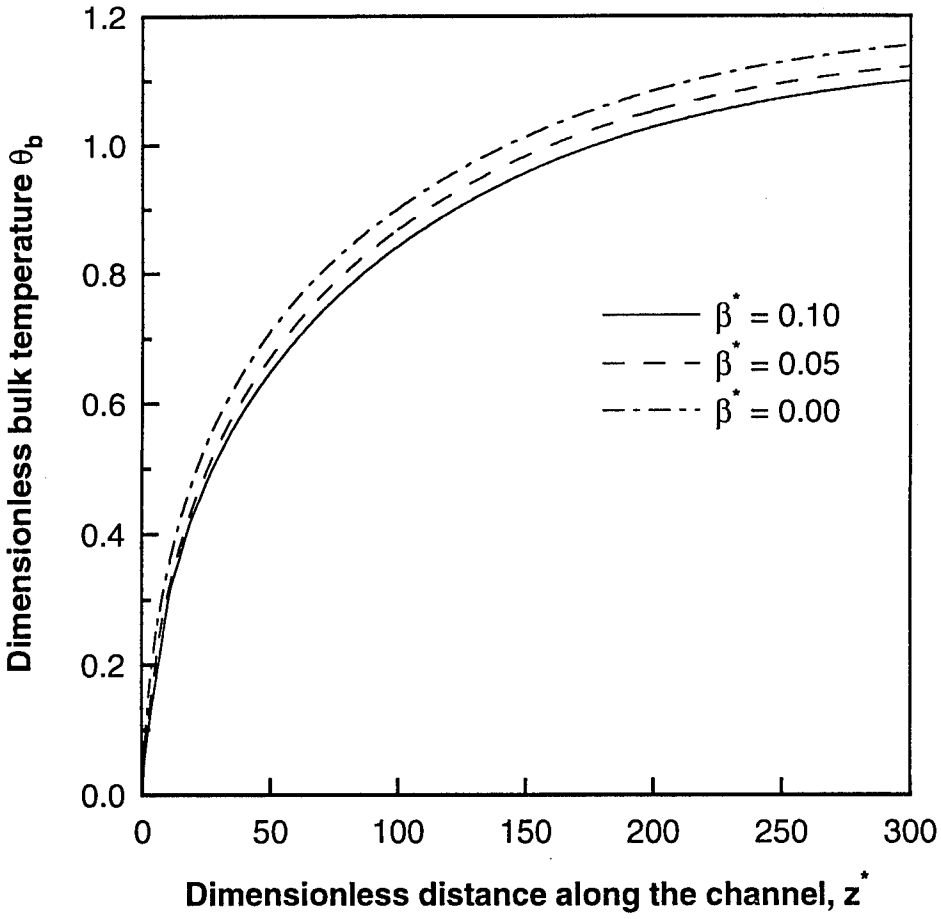
1.2
1.0
0.8
0.6
0.4
0.2
0.0
0
50
100
150
200
250
300
Dimensionless bulk temperature θ_b
Dimensionless distance along the channel, z^*
$\beta^* = 0.10$
$\beta^* = 0.05$
$\beta^* = 0.00$

Figure *9*

DEGREE OF MIXING ANALYSES OF CONCENTRATED SUSPENSIONS BY ELECTRON PROBE AND X-RAY DIFFRACTION

R. YAZICI AND D. M. KALYON

HIGHLY FILLED MATERIALS INSTITUTE, STEVENS INSTITUTE OF TECHNOLOGY, HOBOKEN, NEW JERSEY 07030

INTRODUCTION

One of the most challenging aspects of any mixing operation, where two or more identifiable components are brought together, is the characterization of the state of the mixture *i.e.*, the degree of mixedness or the "goodness" of mixing. In the nondiffusive mixing of a viscous polymeric binder with solid components, the complete description of the state of the mixture would require the specification of the sizes, shapes, orientations and the positions of the ultimate particles of the components.

The techniques applied to characterize the degree of the mixedness of a composite would involve either direct or indirect methods. Indirect methods include the determination of some representative property including transmissive, reflective, resistivity, ultrasound and rheological properties. Such techniques are ideal especially for product quality control, where the relationship between the measured property and the ultimate property of interest is apriori known. However, although such techniques are useful, they offer little insight into the mechanisms and efficiency of the mixing operation.

On the other hand, direct measurement techniques can provide detailed information on the process and the development of the microstructure of the composite. The simplest technique which can be utilized to determine the mechanisms of mixing in a batch or continuous mixer is the injection of a dye into a transparent fluid and then to follow the distribution and the interfacial area growth of the nondiffusive tracer. Such techniques were used by Bigio and Erwin[1] and Bigio *et al.*[2] to analyze the mixing mechanisms occurring in tangential and partially-full co-rotating twin screw extruders. Ottino[3] has employed the flow visualization technique to investigate the mechanisms of mixing in various time dependent flows, which may be governed by chaotic dynamics. On the other hand, Morikawa *et al.*[4] have followed the spatial distribution of color incorporated elastomers to gain insight into the mixing occurring in internal mixers. The dispersive mixing aspects, in conjunction with simple shear flows, where the imposed stresses can be monitored, were also characterized employing the cone and plate flow of a transparent oil containing carbon black agglomerates (Rwei *et al.*[5]).

If the materials of interest are opaque or if transparent barrel sections cannot be built, the mechanisms of mixing can be studied through "post-mortem" analysis. In this technique, generally a distinguishable tracer is added into a mixer in a step or pulse fashion. After a certain duration of mixing, the mixture is systematically removed and sectioned into parts to allow the investigation of distributive and dispersive mixing aspects. David and Tadmor,[6] have used this technique for probing the mechanisms of laminar mixing occurring in co-rotating disk processors and to follow dispersive mixing of rubber and carbon black formulations. Gokbora[7] has utilized pigmented polyethylene granules to investigate the state of mixedness occurring in single screw extrusion processing. Kubota *et al.*[8] have investigated the flow mechanisms and mixing of rubber compounds in single screw extruders based on the post-mortem analysis of tracer incorporated rubber strips upon screw pulling. Kalyon and co-workers[9,10] have employed color incorporated thermoplastic elastomers, followed by computerized image analysis, to investigate the distributive mixing of thermoplastic elastomers in the regular flighted and kneading disc elements of twin screw extruders.

On the other hand, the rapid advent of imaging and sensing technology has facilitated the introduction of various powerful techniques, including the magnetic resonance imaging and x-ray based techniques, to the analyses of opaque mixtures. Kalyon *et al.*[11] have employed magnetic resonance imaging, wide-angle x-ray diffraction and x-ray radioscopy to characterize the amount of air entrained into composite suspensions with elastomeric binders during extrusion processing, which is related principally to the degree of fill profile in the extruder. Techniques such as x-ray computed tomography were applied to the study and the quality control of advanced composites,[12] rocket motors,[13] precision castings,[13-15] ceramics[16] and assembled structures[17] but have not been applied to the study of the state of mixedness. The applications of various nondestructive evaluation techniques in the tire industry are reviewed by Trivisonno.[18] It may be envisioned that such powerful techniques, including magnetic resonance imaging and computed tomography, with three dimensional and real-time analysis capabilities, will be utilized widely for on-line process and product control of various mixing and processing flows in the near future in many industries.

In this study the energy dispersive x-ray and wide angle x-ray diffraction techniques are being introduced into the field of goodness of mixing measurements. The applicability of these two techniques to the quantitative characterization of the distributive mixing occurring in continuous mixers and the scale of examination effects has been demonstrated with a highly filled suspension involving an elastomeric binder, *i.e.*, hydroxyl terminated polybutadiene, mixed with two different solid fillers.

EXPERIMENTAL PROCEDURES

MATERIAL PROCESSING AND SAMPLE PREPARATION

In this study, the concentrated suspension consisted of a polymeric matrix and 76.5 volume percent of solids. The matrix was hydroxyl terminated polybutadiene (HTPB) and an antioxidant. The fillers were aluminum (Al) and ammonium sulfate (AS) in powder form. Mean particle size of aluminum was 20 microns. Ammonium sulfate was bimodal in particle size with 75% coarse particles and 25% fine particles. The mean particle sizes of the coarse and fine fractions of ammonium sulfate were 200 and 20 microns, respectively.

An APV MP50 twin screw extruder with a screw length-to-diameter ratio of 15 was employed for processing of the suspension samples. The extruder was equipped with a Zenith gear pump for feeding of the liquid ingredients, a K-Tron volumetric feeder for the feeding of aluminum and an Acrison loss-in-weight feeder for the feeding of ammonium sulfate. The moisture content of ammonium sulfate was reduced to below 0.1%, before it was placed into the hopper of the loss-in-weight feeder. This feeder was kept sealed at all times. The conditions of the suspension preparation, including screw configuration and screw speed (43 rpm) were kept the same in all of the experiments. A vacuum port was installed and employed in conjunction with specially designed devolatilization elements, "ball wings", to maximize the surface-to-volume ratio of the suspension, for the satisfactory removal of the air entrained at the earlier stages of processing. The devolatilization section was sealed by the die in the upstream direction and a series of reversely configured fully-flighted conveying screw elements in the downstream direction. A Welch Duo-Seal vacuum pump was used to remove the air from the suspension through a vacuum port.

The samples were collected from the exit of the die under steady-state conditions. Sample cups with dimensions of 45 × 15 mm^2 and with 1 mm depth were filled flush, with the suspension. The samples were kept frozen at all times to prevent segregation effects, except during the duration of the microstructural analyses.

CHARACTERIZATION OF MIXING INDICES

Various mixing indices, which characterize the goodness of mixing of the suspension samples, were determined on the basis of the relative volume-fraction measurements of the two filler materials by three principal analytical methods: scanning electron microscopy

(SEM), electron-probe energy-dispersive x-ray analysis (EDX) and wide-angle x-ray diffractometry (XRD). Mixing indices were determined at different scales of examination by varying the sample area through alteration of the size of the electron and x-ray probes by several orders of magnitude. The ratio of the volume fractions of the two fillers, aluminum (Al) and ammonium sulfate (AS), ϕ_{Al}/ϕ_{AS}, was utilized as a measure of degree mixedness of the sample.

In general, the quantitative description of the mixing quality or goodness of mixing of a given mixture can be developed by comparison of the state of the mixture to the most complete mixing state attainable.[19] This *complete mixing* corresponds to statistical randomness of the ultimate particles of the ingredients being mixed.[20]

If one makes N measurements of concentration c_i of one of the components, then the mean concentration may be calculated according to

$$\bar{c} = \frac{1}{N}\sum_{i=1}^{N} c_i, \tag{1}$$

where $\bar{c}$ should not differ significantly from ϕ, the overall concentration of the component, unless a faulty sampling technique is used. The difference between $\bar{c}$ and ϕ decreases as the finite number N, of the characterized samples, is increased. The measured concentration values of the minor component also depend on the sample size. These values approach the overall concentration of the minor component ϕ as the sample size is increased.

A basic measure of the homogeneity of a mixture is the extent to which the concentration values at various regions of the volume of the mixture differ from the mean concentration. The variance s^2, arising from the individual concentration c_i measurements, provides such an index to quantitatively assess the degree of mixedness. The variance is given by

$$s^2 = \frac{1}{(N-1)}\sum_{i=1}^{N} (c_i - \bar{c})^2. \tag{2}$$

A small variance value implies that most of the samples yield concentration c_i values which are close to the mean $\bar{c}$ of all samples, thus suggesting a homogeneous system. The maximum variance occurs if the components are completely segregated. Maximum variance is given by

$$s_0^2 = \bar{c}(1 - \bar{c}). \tag{3}$$

If the variance is normalized to its maximum value, the resulting parameter is called the intensity of segregation, I_{seg}. This is given by

$$I_{seg} = \frac{s^2}{s_0^2} = \frac{s^2}{\bar{c}(1-\bar{c})}. \tag{4}$$

Intensity of segregation I_{seg}, is another important index in evaluating goodness of mixing or distribution. The intensity of segregation ranges from unity, for completely segregated system, to zero, for a homogeneous system.

In this study, the mean, variance and intensity of segregation of the relative concentration fractions of the two fillers (aluminum and ammonium sulfate), ϕ_{Al}/ϕ_{AS}, were determined to assess the goodness of mixing. The overall value of the relative volume concentration fractions of aluminum and ammonium sulfate, ϕ_{Al}/ϕ_{AS}, was 0.20 ± 0.02, as specified during processing.

ANALYTICAL TECHNIQUES

Electron microscopy coupled with energy-dispersive x-ray analysis is a powerful tool in the characterization of the microstructure and the corresponding elemental distributions in multi-phase materials.[21,22] In this study the two techniques were utilized in synergy to obtain both qualitative and quantitative information on the state of mixedness. First the spatial distribution of the filler particles was determined by secondary-electron microscopic analysis. In order to distinguish the aluminum and ammonium sulfate particles from each other, el-

emental mappings of aluminum and sulfur were carried out with energy-dispersive x-ray analysis at the same locations, where the secondary-electron images were taken. The identity of each particle in the SEM images was thus determined for further evaluation.

Chemical analysis of materials in the scanning electron microscope is performed by measuring the energy and intensity distribution of the x-ray signal generated by a focused electron beam. A sufficiently energetic electron beam may eject an inner-shell electron, leaving the atom in an ionized or excited state with a vacancy in one of the shells. During subsequent deexcitation of the atom, electron transition occurs from an outer shell to fill this vacancy. The transition involves a change in energy. The excess energy which the excited atom contains can be released in the form of a photon in the x-ray range of the electromagnetic spectrum. Since the energy of the emitted x-ray is related to the difference in energy between the sharply defined levels of the particular atom, it is referred to as a characteristic x-ray. The specific energies of the characteristic x-ray peaks for each element has been tabulated and can be used to evaluate the unknown materials.

The energy-dispersive x-ray analyzer, shown schematically in Figure 1, employs a solid-state detector to acquire the total spectrum of characteristic x-rays from 0.75 to 20 keV (or more). Large numbers of x-ray photons can be counted at all energy levels with the aid of a multi-channel analyzer. This allows for the rapid evaluation of numerous elements in the sample.[21,22]

The intensity of the characteristic x-radiation is proportional to the concentration of the particular element in the sampling volume. Intensity values, therefore, can be utilized for quantitative analysis. The number of characteristic x-ray photons per second (N_i) detected from an element is given by:

$$N_i = Jk_i\phi_i; \tag{5}$$

where J is the incident electron flux, ϕ_i is the concentration of the element i, k_i is a proportionality factor that includes ionization cross-section, fluorescent yield, and detection efficiency.

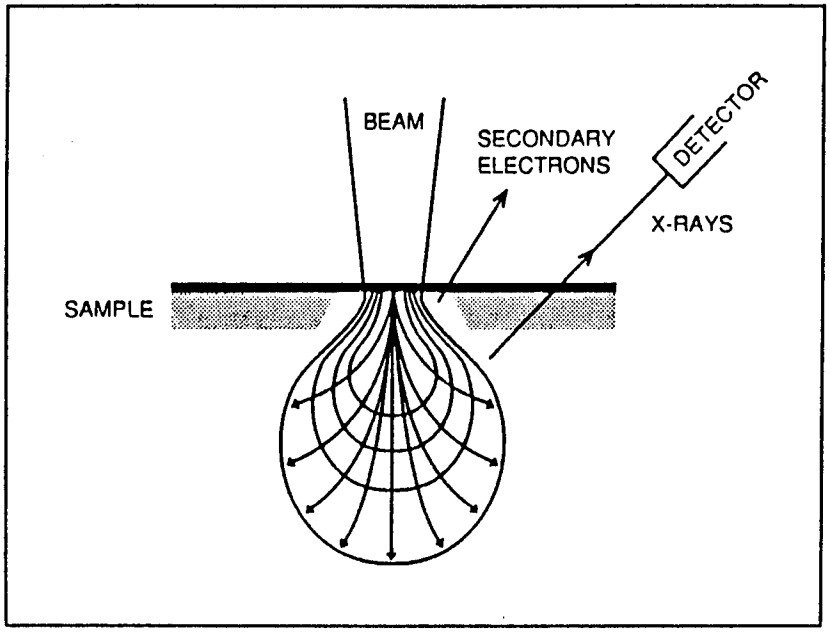

FIG. 1.—Schematic drawing of the excited sample volume under electron beam with secondary electron and x-ray emission.

With computerized modern instruments the k_i values are readily calculated and quantitative analysis, accurate to 0.5 weight percent, is achieved for elements with an atomic number higher than sodium.[21] The absolute determination of the elemental concentration, however, requires calibration with standard samples, especially when light elements are present in the sample. Determination of relative concentrations of two elements in a specimen can be reduced to:

$$\frac{N_1}{N_2} = k_R \phi_1/\phi_2, \tag{6}$$

where k_R is the relative proportionality factor for the two elements in a given mixture.

In this study the relative atomic fractions of the two elements aluminum and sulfur were measured by energy-dispersive x-ray analysis. Variation of the relative atomic fractions of the two elements was utilized to assess the degree of distributive mixedness. In order to calibrate the measured values standard samples were prepared by mixing controlled amounts of aluminum and ammonium sulfate powders. According to this calibration the relative atomic fraction proportionality factor $k_{R.at.}$ was 1.21, *i.e.*,

$$N_{Al}/N_S = 1.21\phi^{at}_{Al}/\phi^{at}_S, \tag{7}$$

where ϕ^{at}_{Al} and ϕ^{at}_S refer to the atomic concentrations of aluminum and sulfur, respectively.

The relative weight fraction and relative volume fraction values for aluminum and ammonium sulfate components were then calculated from the relative atomic fraction of aluminum and sulfur. The conversion factor from relative atomic to relative weight fraction was 4.898 and from relative atomic to relative volume fraction was 7.47. Molecular and crystal structure parameters[23] of the two components were used in determining these conversion factors. Finally, the relative volume fraction proportionality factor $k_{R.vol.}$ was 9.04, *i.e.*,

$$N_{Al}/N_S = 9.04\phi^{vol}_{Al}/\phi^{vol}_{AS}. \tag{8}$$

Energy-dispersive x-ray measurements were carried-out with a series of successively smaller probes at sites chosen systematically, based on a grid system. A JOEL 840 (40 Å resolution) scanning electron microscope with Tractor Northern TN 5500 energy-dispersive x-ray analysis system was used in these studies. Incident beam voltage was set at 15 kV. The take-off angle of the x-rays (the angle of the x-ray detector with respect to the sample surface) was set at 40 degrees. The window thickness was 7.5 microns. Multiple probe sizes were used in these experiments (80 mm^2, 9 mm^2, 1 mm^2, 0.1 mm^2 and 0.01 mm^2) to determine the distributive mixing index, *i.e.*, intensity of segregation, as a function of the scale of examination.

X-ray diffractometry has been successfully applied for both qualitative and quantitative phase analysis in multi-phase materials.[24,25] Upon irradiation with x-rays, a given substance produces a characteristic diffraction pattern. Diffraction is essentially a scattering phenomenon in which a large number of atoms in the crystalline material, arranged periodically on a lattice, scatter the x-rays in phase. These phase relations are such that destructive interference occurs in most directions of scattering; but in a few directions constructive interference takes place and diffracted beams are formed. According to Bragg's Law, the diffracted beams make a 2θ angle with respect to the incident beam, *i.e.*

$$\lambda = 2d \operatorname{Sin} \theta, \tag{9}$$

where λ is the wavelength of the x-rays of the incident beam and d is the spacing between the atomic (lattice) planes of the crystalline material. Since the d-spacings between atomic planes and their distribution in space (the crystal structure) is unique for each material, the angular distribution of the diffraction peaks and their intensities (the diffraction pattern) is also unique for a particular material. Diffraction patterns are obtained with diffractometers equipped with suitable detectors. Qualitative analysis by x-ray diffraction is accomplished

by identification of the particular diffraction pattern of a substance from the standard diffraction tables.[23]

The particular advantage of x-ray diffraction analysis is that it discloses the presence of a substance, as that substance actually exists in the sample, and not in terms of its constituent chemical elements. If the sample contains more than one compound or phase that constitute the same chemical elements, all these compounds are disclosed by diffraction analysis. Quantitative analysis is also possible, because the intensity of the diffraction pattern of a particular phase—in a mixture of phases—depends on the concentration of that phase in the mixture. The relation between the integrated intensity I_x and the volume fraction ϕ_x of a phase is generally nonlinear since diffracted intensity depends strongly on the absorption coefficient of the mixture, μ_m, which itself depends on the concentration. For a two-phase material, (with absorption coefficients μ_1 and μ_2 for the individual phases) the absorption coefficient for the mixture becomes:

$$\mu_m = \phi_1\mu_1 + \phi_2\mu_2. \tag{10}$$

The integrated intensity from phase 1 is then given by[24]:

$$I_1 = K_1\phi_1/\mu_m, \tag{11}$$

where K_1 is a constant that depends on the material and the incident beam used but not on the concentration. The ratio of intensities from phases 1 and 2, however, is independent of μ_m and varies linearly with concentration:

$$I_1/I_2 = (K_1/K_2)\phi_1/\phi_2. \tag{12}$$

In this study the ratio of relative volume fractions of aluminum and ammonium sulfate, ϕ_{Al}/ϕ_{AS}, was calculated from the integrated intensity ratio I_{Al}/I_{AS}. These measurements were carried out utilizing particular crystal-planes of the two filler materials. Relatively high number of crystal-plane reflections were evaluated in order to eliminate texture effects and to increase accuracy. Integrated intensities of the first two reflections (111 and 200) of aluminum and the first five reflections (002, 011, 102, 111 and 200) of ammonium sulfate were utilized for calculations. The value of the K_{Al}/K_{AS} constant was taken as 0.489 for (111) planes. This value was calculated according to the $I/I_{corundum}$ values listed by JCPDS.[23] The contribution of the absorption of the matrix to the absorption coefficient of the mixture was less than 3% and, thus, it was ignored. The relative volume fraction ϕ_{Al}/ϕ_{AS} values were further calibrated with measurements carried-out on standard samples.

An automated GE wide-angle x-ray diffractometer was used for these studies. Nickel filtered Cu K_α radiation at 30 kV and 15 mA was used. The scanning speed was one degree per minute. A 0.2 degree receiving slit was used in all runs. The x-ray probe size was varied by using 3 degree and 0.4 degree primary beam slits and a 8 mm high window. The x-ray probe sizes used were 20 mm × 8 mm (160 mm^2) and 1 mm × 8 mm (8 mm^2), respectively, at a Bragg angle, θ, of 20 degrees.

RESULTS AND DISCUSSION

Typical SEM photomicrographs of the concentrated suspension sample are shown in Figure 2 at two different magnifications. The smaller light-colored particles are aluminum and the larger dark-gray particles are ammonium sulfate. The matrix is the dark colored material found in between the particles. Some regions which are richer in either aluminum or ammonium sulfate can be discerned. However, it is not possible with the available SEM technology to distinguish and quantitatively characterize the concentration of each solid component at a given location. The typical characteristic dimension of grouping/clustering of alike particles is 400 to 600 microns. Pockets of matrix-rich regions are not observed upon microscopic examination.

It is difficult to prepare samples with the image quality as indicated in Figure 2(a and b). As shown in Figure 3 (panel a), usually the matrix covers the surface particles and blurs the images. Removal of the matrix from the surface without disturbing the particle distri-

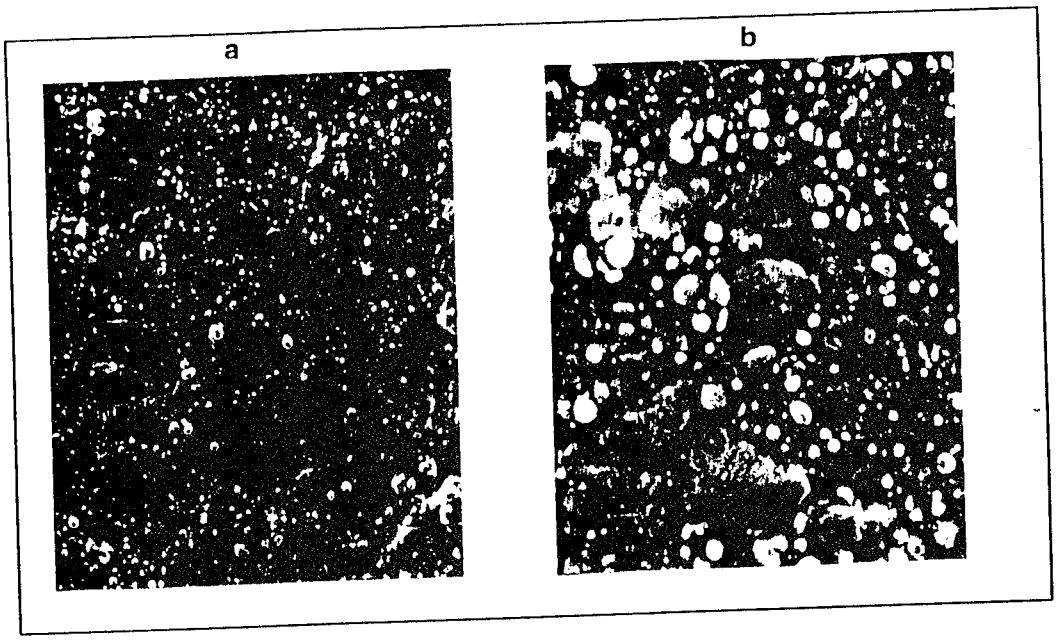

RC+T, Yazici Fig. 2 - 90%

FIG. 2.—Scanning electron micrographs at two magnifications: (a) 60 ×, (b) 200 ×.

bution is not an easy task. Keeping the sample under vacuum for an extended time or selective etching of the matrix works with limited success. In most cases a matrix layer covers the surface and prevents the identification of the location of the particles. In order to identify the aluminum and ammonium sulfate particles and to carry-out the quantitative analysis of mixing indices, the elemental mappings of aluminum and sulfur were carried-out using energy-dispersive x-ray analysis, EDX, at the same locations of the scanning electron micrographs. These elemental mappings are shown in Figure 3, panel b and c, respectively. As shown with connecting arrows in Figure 3, the EDX technique can clearly distinguish ammonium sulfate and aluminum particles.

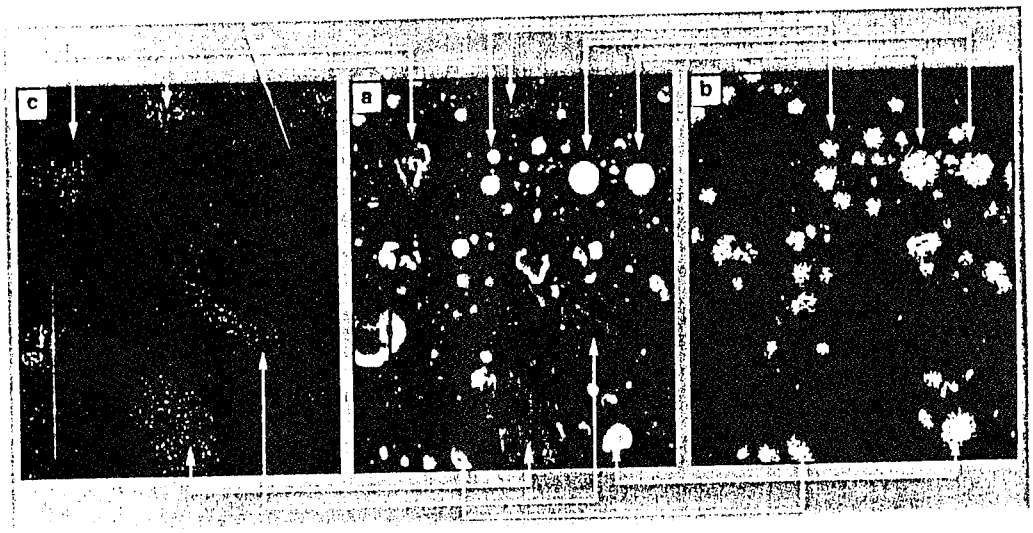

RC+T, Yazici Fig. 3 - 67%

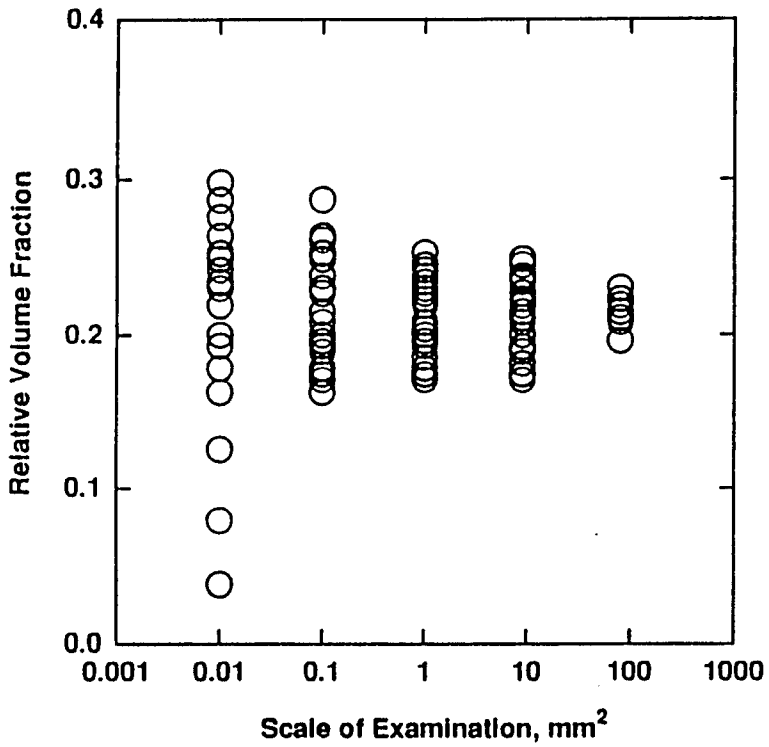

FIG. 4.—Variation of the relative volume fraction of the two solid components, aluminum and ammonium sulfate, at different locations of the mixture as a function of scale of examination of energy-dispersive x-ray analysis.

The results of the quantitative energy-dispersive x-ray analysis of the relative volume fractions of aluminum and ammonium sulfate, ϕ_{Al}/ϕ_{AS}, are given in Figure 4. The statistical analysis of the results are listed in Table I. The variance of the relative volume fraction ϕ_{Al}/ϕ_{AS}, depends on the probe size. The largest probe size, 80 mm² gives rise to the minimum variation in the volumetric ratio as expected. With the moderate probe sizes, 1 mm² to 10 mm² range, the variance of the volume ratio remains the same. At the relatively smaller probe sizes of 0.1 mm² and 0.01 mm², the deviation of the relative volume fraction of the two solid components from the mean increases considerably with decreasing probe size. The marked change in the variance of the relative volume fraction values between probe sizes 0.1 mm² to 1 mm² is in good agreement with the qualitative microstructural features observed in scanning electron microscopy. Clustering of the particles in 300 to 600 micron diameter regions should give rise to the observed scatter in the energy-dispersive x-ray analysis results.

TABLE I

STATISTICAL PARAMETERS OF THE RELATIVE VOLUME FRACTIONS, Φ_{Al}/Φ_{AS}, FOR DIFFERENT EDX PROBE SIZES

Relative volume fraction, Φ_{Al}/Φ_{AS}, parameters	EDX probe size				
	80 mm²	9 mm²	1 mm²	0.1 mm²	0.01 mm²
mean	0.216	0.215	0.217	0.217	0.216
standard deviation	0.007	0.024	0.025	0.034	0.069
99% confidence interval	±0.005	±0.014	±0.013	±0.018	±0.039
intensity of segregation	0.0003	0.0034	0.0037	0.0068	0.0281

Ed: use lowercase phi in tables (to match text)?

Yes Thanks (B)

Probes smaller than 0.01 mm² in size were not used, since they are in the same size range as the particle diameter of ammonium sulfate.

The 99% confidence intervals of the energy-dispersive x-ray analysis data determined according to Student's-t-distribution are also included in Table I. The mean of the data for all probe sizes is around 0.215–0.217. These mean values agree with the input volumetric ratio, thus suggesting the absence of systematic errors. On the other hand, the standard deviation values increase from 0.007 at the probe size of 80 mm² to 0.07 at a probe size of 0.01 mm², indicating that the deviation from the mean increases by about one order of magnitude going from the largest to smallest probe. The confidence intervals again reflect the same observation, with an increasing range around the mean as the probe size is reduced. Obviously, if the probe size is reduced further, one would probe only the completely segregated regions consisting of either aluminum or ammonium sulfate single particles.

Which probe size (scale of examination) should be used for the characterization of the goodness of a given mixture? The scale of examination should be selected depending on the application and the relevant ultimate properties of the mixture. For some applications the sample area may be as large or larger than the maximum probe size used in this analysis, *i.e.*, 80 mm². However, for other applications it may be necessary to achieve a certain degree of mixedness at a smaller scale of examination.

The results of the quantitative x-ray diffraction analysis of relative volume fractions of aluminum and ammonium sulfate, by employing the relative integrated intensities, are given in Figure 5. The statistical analysis of these results are presented in Table II. With x-ray diffractometry, the mean of the relative volume fraction values of aluminum in the solid phase ϕ_{Al}/ϕ_{AS}, was determined to be 0.216. Determination of the relative integrated intensity I_{Al}/I_{AS}, values at the smaller probe size (8 mm²) was found to be complicated by the preferred crystallographic orientation exhibited by the ammonium sulfate particles. This preferred orientation was especially evident with 002, 200, or 202 planes. As seen in Figure 3, the

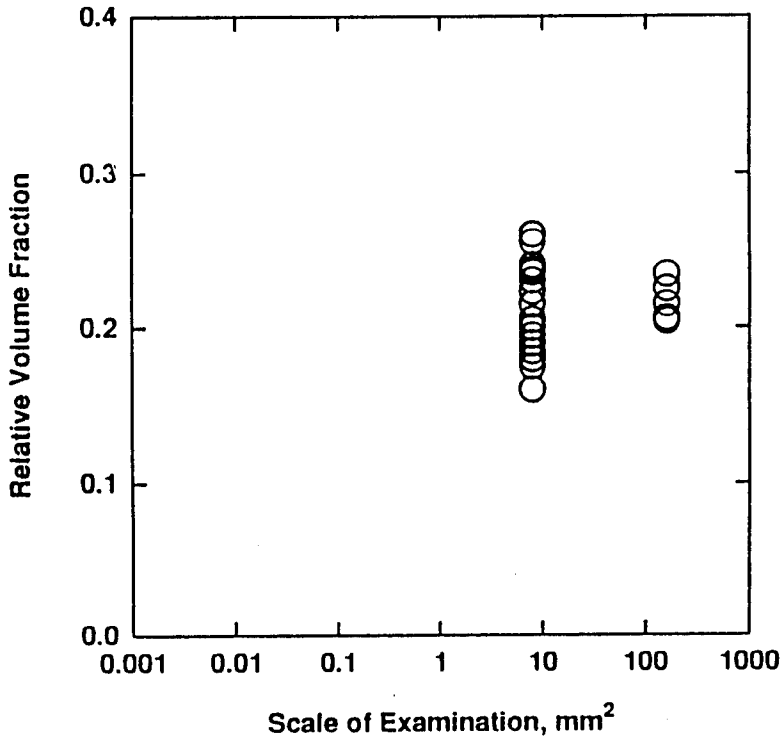

FIG. 5.—Variation of the relative volume fraction of the two solid components, aluminum and ammonium sulfate, at different locations of the mixture as a function of scale of examination of x-ray diffractometry.

TABLE II

STATISTICAL PARAMETERS OF THE RELATIVE VOLUME FRACTIONS, Φ_{Al}/Φ_{AS}, FOR DIFFERENT XRD PROBE SIZES

Relative volume fraction, Φ_{Al}/Φ_{AS}, parameters	XRD probe size	
	160 mm²	8 mm²
mean	0.216	0.216
standard deviation	0.012	0.029
99% confidence interval	±0.012	±0.017
intensity of segregation	0.0009	0.0050

ammonium sulfate particles exhibit relatively flat and angular surfaces, which can be preferentially oriented during processing. Since the samples are taken from random locations and at random orientations from the extruded suspension, a variety of preferred orientation characteristics were observed during x-ray diffractometry.

The x-ray diffractometry analysis also indicates that the various values of deviation from the mean increase with the decreasing scale of examination. However, there are differences between the wide angle x-ray diffraction and energy-dispersive x-ray analysis data that emanate from the applicable depth of penetration. The electron beam used in energy-dispersive x-ray analysis is strongly absorbed at the surface thus the x-ray photons that make it to the detector come mostly from the top few microns depth. This depth is smaller than the particle sizes of both solid components of the formulation. However, in the wide-angle x-ray diffraction measurements 95% of the information is derived from the top 50 to 100 microns of the suspension, depending on the filler type and the diffraction angle θ. The penetration depth can be estimated from:

$$x = 3 \sin \theta / 2\mu_m. \tag{13}$$

The penetration depth obtained with the x-ray diffraction technique is greater than the electron probe measurements and, thus, x-ray diffraction results are more representative of the bulk.

The intensity of segregation index I_{seg} values were determined from the energy-dispersive x-ray and x-ray diffractometry data, as shown in Tables I and II. The intensity of segregation values increase with the decreasing scale of examination in both techniques. The intensity values obtained with energy-dispersive x-ray analysis and x-ray diffraction are close, indicating that both techniques are capable of characterizing the degree of distributive mixedness of the solid ingredients.

It should be noted that the applicabilities of the two techniques to various processes and materials are different. Wide-angle x-ray diffraction may also be suitable for on-line analysis of microstructural distributions and, thus, product quality control. However, the scale of examination cannot be reduced beyond a certain threshold with x-ray diffraction, when preferred orientation effects complicate the intensity ratio measurements. On the other hand, the energy-dispersive x-ray analysis is post-mortem in nature and requires a lengthy analysis and application of vacuum during characterization.

With a conventional EDX detector, as used in this study, the elemental mappings are restricted to elements with atomic numbers above that of sodium. However, with other currently commercially available EDX units, with windowless detectors, elements with atomic numbers greater than or equal to five can also be mapped. On the other hand, the x-ray diffraction technique is applicable to all semi-crystalline ingredients, regardless of their atomic mass.

CONCLUSIONS

Two x-ray based techniques involving energy-dispersive analysis and diffractometry were introduced to the analyses of the degree of mixedness, *i.e.* the "goodness of mixing" of concentrated suspensions. A hydroxyl terminated polybutadene matrix was mixed with aluminum and ammonium sulfate. In the analysis, the ratio of the relative volume fractions of the two solid components was used as the basis of the analytical evaluation. Both characterization techniques are capable of determining the relative volume fraction of the two solid components as a representative measurement of the distributive mixing efficiency and both are sensitive to the scale of examination. The introduced techniques should be useful in the better definition of the degree of mixedness as well as in resolving differences in mixing efficiencies of various mixers used in processing of concentrated suspensions.

ACKNOWLEDGMENTS

This research was supported by federal grants N00014-89-J-3208 and N00014-90-J-4019 as managed by the Office of Naval Research. We are grateful for this support. The content of the information does not necessarily reflect the position or the policy of the Government, and no official endorsement should be inferred.

[*Received November 13, 1992; revised February 5, 1993*]

REFERENCES

[1] D. Bigio and L. Erwin, *Int. Polym. Process.* **4**, 242 (1989).
[2] D. Bigio, K. Cassidy, M. Dellagon, and W. Bain, *Int. Polym. Process.* **7**, 111 (1992).
[3] J. M. Ottino, "The Kinematics of Mixing: Stretching, Chaos and Transport," Cambridge University Press, 1989.
[4] A. Morikawa, K. Min, and J. L. White, *Int. Polym. Process.* **4**, 23 (1989).
[5] S. P. Rwei, I. Manas-Zloczower, and D. F. Feke, *Polym. Eng. Sci.* **30**, 701 (1990).
[6] B. David and Z. Tadmor, *Int. Polym. Process.* **3**, 38 (1988).
[7] M. N. Gokbora, "Mixing in Single Screw Extruders," Ph.D. Thesis, University of Bradford, 1981.
[8] K. Kubota, R. Brzoskowski, J. L. White, F. C. Weissert, N. Nakajima, and K. Min, RUBBER CHEM. TECHNOL. **60**, 924 (1987).
[9] D. M. Kalyon, A. D. Gotsis, U. Yilmazer, C. G. Gogos, H. Sangani, B. Aral, and C. Tsenoglou, *Adv. Polym. Technol.* **8**, 337 (1988).
[10] D. M. Kalyon and H. N. Sangani, *Polym. Eng. Sci.* **29**, 1018 (1989).
[11] D. M. Kalyon, R. Yazici, C. Jacob, B. Aral, and S. W. Sinton, *Polym. Eng. Sci.* **31**, 386 (1991).
[12] R. H. Bosi and G. E. Gergeson, *J.O.M.* **43**(9), 8 (1991).
[13] R. A. Armistead, *Adv. Mater. Processes* **3**, 42 (1988).
[14] P. D. Tonner and G. Tosello, *Mater. Eval.* **44**, 203 (1986).
[15] C. Johns, "Medical CAT-Scanning for Aircraft Engine Components," *The Leading Edge*, 27–31 (Fall, 1987).
[16] T. Taylor, W. A. Ellingson, and W. D. Koenigsberg, *Ceram. Eng. Sci. Proc.* **7**, 772 (1986).
[17] R. H. Bossi, R. J. Kruse, and B. W. Knudson, "Computed Tomography of Electronics," Report WRDC-TR-89-4112 (Dayton, OH: Wright Research and Development Center, Dec. 1989).
[18] N. M. Trivisonno, "Nondestructive Evaluation of Tires," RUBBER CHEM. TECHNOL. **58**, 469 (1985).
[19] D. M. Kalyon, in "Encyclopedia of Fluid Mechanics," Houston, Tx, Gulf Publishing, vol 7, Ch. 28, 887–926 (1988).
[20] W. D. Mohr, "Processing of Thermoplastic Materials," E. Bernhard, Ed., Krieger Publishing Co., Malabar, 1959.
[21] J. I. Goldstein, D. E. Newbury, P. Echlin, D. C. Joy, C. Fiori, and E. Lifshin, "Scanning Electron Microscopy and X-Ray Microanalysis," Plenum Press, New York, 1981.
[22] E. Lifshin, M. F. Ciccarelli, and R. B. Bolon, "X-Ray Spectral Measurements, Practical Scanning Electron Microscopy," Plenum Press, New York, 1975.
[23] International Center for Diffraction Data, JCPDS Files 4-0787 [Al] and 10-343 [$(NH_4)_2SO_4$], Swathsmore, PA (1978).
[24] B. D. Cullity, "Elements of X-Ray Diffraction," Reading, MA, Addison-Wesley Pub., 1986.
[25] L. E. Alexander, "X-Ray Diffraction Methods in Polymer Science," Krieger Publ. Co., Malabar, 1985.